Asiyah Esmail
Bachelor's degree in Biochemistry

Biopolymeric substrates for reconstructed dermis development

Dissertation for the degree of Master's in Biotechnology

Supervisor: Doctor Filomena Freitas, Assistant Professor, UCIBIO, FCT-UNL
Co-supervisor: Doctor Abel Oliva, Senior Researcher, ITQB-UNL

FACULDADE DE CIÊNCIAS E TECNOLOGIA
UNIVERSIDADE NOVA DE LISBOA

September 2019

Asiyah Esmail
Bachelor's degree in Biochemistry

Biopolymeric substrates for reconstructed dermis development

Dissertation for the degree of Master's in Biotechnology

Supervisor: Doctor Filomena Freitas, Assistant Professor, UCBIO, FCT-UNL
Co-supervisor: Doctor Abel Oliva, Senior Researcher, ITQB-UNL

September 2019

Biopolymeric substrates for reconstructed dermis development

Acknowledgements

Firstly, I would like to thank my supervisors, Filomena Freitas and Abel Oliva, for receiving me in their labs, for the guidance, advice and for the shared excitement of this work which motivated me throughout this year.

I want to thank all the people that collaborated in this work, Prof. Cristiana Torres for teaching me about bioreactor operation, Prof. Christian Grandfils (CEIB, Univ. Liège) for the determination of M_w and PDI, Prof. Alexandre Paiva and Liane Meneses (LAQV-FCT/NOVA) for helping me prepare scaffolds with $scCO_2$, Prof. Célia Henriques and Prof. Jorge Carvalho (CEFITEC, FCT/NOVA) for receiving me in their lab and teaching me about electrospinning, Prof. Elvira Fortunato (CENIMAT, FCT/NOVA) for allowing me to use CENIMAT installations, Ana C. Marques and Sara Silvestre for guiding me through surface modification of the scaffolds and Deneb Menda for always making time for a SEM session with me.

I would also like to thank everyone from the labs that hosted me, from the Biomolecular Diagnostic Lab I would like to thank Patricia, Sara and Ricardo for all the patience and for helping me whenever I needed. A big thank you to everyone from the Bioeng group, which welcomed me in for a second time. A special thank you to João, Ana, Patricia F&R, Silvia, Rita and Diana for all the patience, advice and comradery, and to my colleagues, Tatiana, Juliana, Bruno and Mauro for accompanying me in this journey.

For my friends, for the ones that were there since the beginning for the ones that joined me in university, for the ones that are still close by and for the ones that are far only in distance, a huge thank you for putting up with me for all this time.

Last, but definitely not least, I want to thank my parents and brother for all the unconditional love and support, which without this wouldn't be possible.

From the bottom of my heart, thank you to all!

Abstract

The first goal of this thesis was the production of polyhydroxyalkanoates (PHAs) with differing material properties, namely medium-chain-length polyhydroxyalkanoates (mcl-PHAs), elastic and tacky polymers, and short-chain-length polyhydroxyalkanoates (scl-PHAs), specifically P(3HB) and P(HBHV), which are more crystalline and brittle. All three biopolymers were successfully biosynthesised. Glycerol was used for the batch cultivation of *Pseudomonas chlororaphis* DSM 19603 for mcl-PHA production and used cooking oil was employed for the batch fermentation of *Cupriavidus necator* DSM 428 for P(3HB) and P(HBHV) production. Concerning P(HBHV), 3HV (25%) was incorporated into the polymer by means of feeding levulinic acid as co-substrate. mcl-PHA was mainly composed of 3-hydroxydecanoate (64%) and 3-hydroxyoctanoate (16%) and had a molecular weight of 0.69×10^5 Da. It presented a degradation temperature of 292 °C and a crystallinity degree of 3.7%. P(3HB) was obtained with a molecular weight of 5.2×10^5 Da and a crystallinity degree of 41.3%. Moreover, the polymer had melting and thermal degradation temperatures of 175 and 293 °C, respectively. P(HBHV) presented melting and degradation temperatures of 176 and 292 ˚C, respectively, and a crystallinity fraction of 17.8%.

The aim for the second part of this work was to prepare porous/fibrous PHA-based scaffolds, followed by their physical and chemical characterization. Several techniques were employed, namely, solvent casting with particulate leaching (SCPL), supercritical CO_2 ($scCO_2$), emulsion templating and electrospinning. Emulsion templating and electrospinning displayed the most promising results in implementing porosity without compromising the characteristics of the polymer. Electrospinning allowed the fabrication of a P(HBHV)/mcl-PHA blend with enhanced mechanical properties. Furthermore, oxygen plasma and UV/ozone surface modification techniques were tested, and oxygen plasma offered enhanced hydrophilicity while not significantly impacting polymer integrity.

Finally, scaffolds bioactivity was investigated. Human dermal fibroblasts were able to adhere and proliferate in electrospun PHA-based scaffolds, with P(HBHV)/mcl-PHA oxygen plasma-treated showing the most promising results (40% attachment). This work demonstrated the potential of PHAs as materials for the development of new 3D-scaffolds for skin reconstitution.

Keywords: short-chain length polyhydroxyalkanoates (scl-PHA), medium-chain length polyhydroxyalkanoates (mcl-PHA), PHA-based scaffolds, dermis reconstitution.

Resumo

O primeiro objetivo deste trabalho foi a produção de polihidroxialcanoatos (PHAs) com propriedades físico-químicas distintas, nomeadamente polihidroxialcanoatos de cadeia média (mcl-PHA), polímeros elásticos e viscosos, e polihidroxialcanoatos de cadeia curta (scl-PHA), especificamente P(3HB) e P(HBHV), polímeros rígidos e cristalinos. Os três biopolímeros foram biosintetizados com sucesso. O glicerol foi usado na cultivação em *batch* de *Pseudomonas chlororaphis* DSM 19603 para a produção de mcl-PHA e óleo alimentar usado foi implementado para a fermentação em *batch* de *Cupriavidus necator* DSM 428 para produção de P(3HB) e P(HBHV). Relativamente ao P(HBHV), 3HV (25%) foi incorporado no polímero por meios de utilização de ácido levulínico como co-substrato. O mcl-PHA era composto principalmente por 3-hidroxidecanoato (64%) e 3-hidroxioctanoato (16%), e tinha um peso molecular de 0.69×10^5 Da. Apresentou temperatura de degradação de 292 °C e um grau de cristalinidade de 3.7%. O P(3HB) foi obtido com um peso molecular de 5.2×10^5 Da, um grau de cristalinidade de 41.3% e apresentou temperaturas de fusão e de degradação de 175 e 293 °C, respetivamente. O P(HBHV) demonstrou temperaturas de fusão e de degradação de 176 e 292 ˚C, respetivamente, e um grau de cristalinidade de 17.8%.

Numa segunda parte deste trabalho, *scaffolds* baseados nos PHAs produzidos foram preparados, seguidos da sua caracterização física e química. Diversas técnicas foram implementadas, nomeadamente, evaporação de solvente com lixiviação de partículas (SCPL), CO_2 supercrítico ($scCO_2$), emulsões modelo e eletrofiação. Os métodos de emulsões modelo e eletrofiação revelaram os resultados mais promissores, implementando porosidade sem comprometer as características dos polímeros. A eletrofiação permitiu a fabricação de misturas de P(HBHV)/mcl-PHA com propriedades mecânicas melhoradas. Além disso, técnicas de plasma de oxigénio e UV/ozono foram testadas para alteração da superfície dos *scaffolds*, o plasma de oxigénio ofereceu um aumento na hidrofilicidade, sem impactar significantemente a integridade do polímero.

Finalmente, a bioatividade dos *scaffolds* foi investigada. Fibroblastos humanos da derme foram capazes de aderir e proliferar nos *scaffolds* de PHA produzidos por eletrofiação, com a mistura de P(HBHV)/mcl-PHA tratada com plasma a apresentar os resultados mais promissores (adesão de 40%). Este trabalho demonstrou o potencial dos PHAs como materiais para o desenvolvimento de novos *scaffolds* 3D para reconstrução da pele.

Palavras-chave: polihidroxialcanoatos de cadeia curta, polihidroxialcanoatos de cadeia média, *scaffolds* baseados em PHAs, reconstrução da derme

Table of Contents

List of Figures

List of Tables

List of Abbreviations

3HB	3-hydroxybutyrate
3HD	3-hydroxydecanoate
3HDd	3-hydroxydodecanoate
3HHx	3-hydroxyhexanoate
3HO	3-hydroxyoctanoate
2HTd	3-hydroxytetradecanoate
3HV	3-hydroxyvalerate
Mw	Average molecular weight
CDW	Cell dry weight
n.a.	Data Not Available
n.d.	Data Not Detected
DSC	Differential Scanning Calorimetry
GC	Gas Chromatography
HPLC	High-Performance Liquid Chromatography
Kv	Kilovolt
LB	Luria-Bertani
mcl	medium – chain – length
Mpa	Megapascals
Mn	Number –average molecular weight
OD	Optical density
PLGA	Poly lactic-*co*-glycolic acid
P(3HB)	Poly(3-hydroxybutyrate)
P(HBHD)	Poly(3-hydroxybutyrate-*co*-3-hydroxydecanoate)
P(HBHV)	Poly(3-hydroxybutyrate-*co*-3-hydroxyvalerate)
PCL	Polycaprolactone
PDI	Polydispersity index
PGA	Polyglycolide
PHA	Polyhydroxyalkanoate
PLA	Polylactic acid
PS	Polystyrene
rpm	rotation per minute
SEC	Size exclusion chromatography
SEM	Scanning electron microscopy
scl	Short-chain-length

Chapter 1- Introduction and Motivation

1. Introduction

1.1. Biopolymers

In recent years, there has been growing interest in biopolymers, as opposed to fossil-based polymers, due to escalating crude oil prices, depleted petroleum resources and heightened concern for the damages to the environment. Bio-based polymers can be produced from renewable sources and degraded to environmentally friendly constituents, unlike fossil-based polymers that degrade slowly and continue to accumulate at alarming rates.

Biopolymers are chain-like molecules produced by living organisms that composed of carbon-containing repeating chemical blocks (monomers) (Rudin & Choi, 2013). They can have an animal, plant or microbial origin. Lignocellulosic (biofibres), gums and natural rubber are examples of plant-based biopolymers, chitin, chitosan and collagen of animal-derived polymers, whereas polyhydroxyalkanoates (PHAs), bacterial cellulose and xanthan are produced by microorganisms (Terms, 2015). These natural polymers have an enormous range of applications in various sectors, from consumable goods to the biomedical field.

1.2. Bioplastics

Bioplastics are thermoplastic materials that exhibit properties similar to conventional plastics, but that are derived from renewable resources. Bioplastics can fall under two major categories: (1) biodegradable, regarding the life-cycle, where it includes materials that offer degradability in the environment in a sustainable time frame and (2) biopolymers (or bio-based), concerning the origin of the carbon atom constituents, it comprises thermoplastics that are derived fully or in part from biomass. Moreover, the classifications are not mutually exclusive, and a bioplastic can be both biodegradable and bio-based, which is the case for PHAs and polylactic acid (PLA) (Cooper, 2013).

There are three main pathways to produce bioplastics: (1) extraction and modification of natural polymers from biomass, which include examples such as thermoplastic starch and rubber; (2) polymerization of bio-based monomers, the case for PLA, polyamides and polyurethanes and (3) extraction of polymers produced by microorganisms, the method used for production of PHAs (Rudin & Choi, 2013).

Presently, bioplastics represent only one per cent of the 335 million tonnes of plastic produced annually (European Bioplastics, 2018). As per demand continues to rise, the market is expanding rapidly. According to the latest data report by the European Bioplastics in cooperation with the research institute, Nova Institute, it is estimated an increase in the production capacity of bioplastics from around 2.11 million tonnes in 2018 to approximately 2.62 million tonnes in 2023 (Figure 1.1, b). Within bioplastic production, biodegradable plastics cover 43.2% of all bioplastic produced, about the same as reported for 2017 (42.9% (European Bioplastics, 2017b)) but 20% more than of the reported for 2016 (23.2% (European Bioplastics, 2017a)), highlighting that demand has been accentuated in the last few years. PHA represents only 1.4% of the bioplastic

produced in 2018 (Figure 1.1, a), this number is set to quadruple by 2023 due to the increasing interest in this completely biodegradable and highly tailorable bioplastic, as it offers a range of physical and mechanical properties depending on their chemical composition (European Bioplastics, 2018).

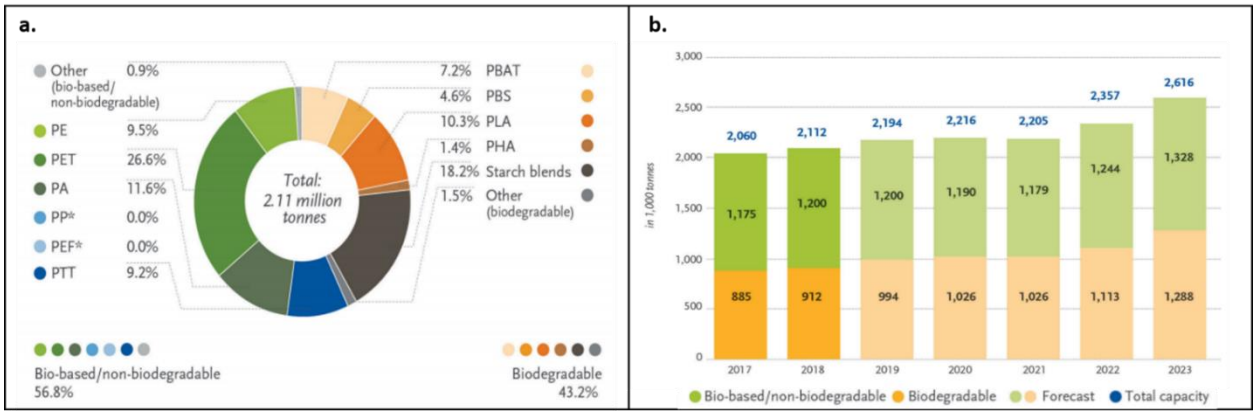

Figure 1.1- (a) Global production capacities of bioplastics in 2018 (by material type). (b) Global production capacities of bioplastics 2018 – 2023. (Adapted (European Bioplastics, 2018)

1.3. Polyhydroxyalkanoates (PHAs)

PHAs are among the most studied biopolymers, considering they are not only biodegradable but also biocompatible (Rathbone et al., 2010; Yan et al., 2011) (they have no adverse effects on biological systems), which broadens their scope of applications. They are a family of biopolyesters that can be synthesized as carbon and energy reserves (Lee, 1996a). PHA biosynthesis can be observed both in bacteria (gram-positive and gram-negative) and plants, however plants can only achieve low production yields (<10% (w/w) of dry weight) (Bohmert et al., 2002), whereas bacterial cells can reach yields up to 90% (w/w) of their dry cell mass (Steinbüchel & Lütke-Eversloh, 2003).

PHA production is generally triggered by environmental stress conditions, such as pH shifts, carbon excess and limiting concentration of essential growth nutrients (e.g. oxygen, nitrogen or phosphate). Since they are water-insoluble, they are stored in the bacterial cytoplasm as granular inclusions (Figure 1.2). When the carbon source is exhausted, the accumulated biopolymers are depolymerised, and their products used as a source of carbon and energy (H. G. Schilegel, 1961; Ciesielski et al., 2010).

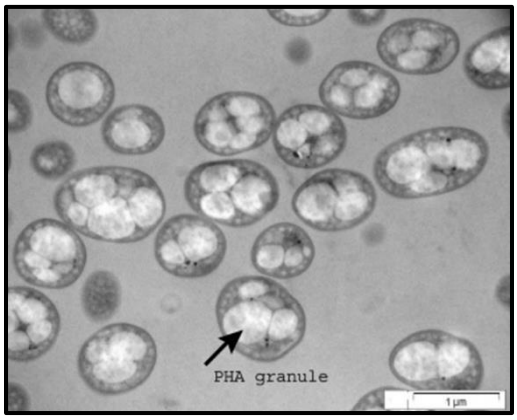

Figure 1.2- Transmission electron micrograph of bacterial cells with PHA granules. Retrieved (Ward et al., 2005).

PHAs can be produced by either mixed microbial cultures (MMC) or pure cultures (Kaur et al., 2017). Each type of fermentation offers different advantages and disadvantages, as summarized in Table 1.1.

Table 1.1- Comparison between pure culture and mixed culture PHA production. Adapted (Kaur et al., 2017).

PHA Production	Pure Culture	Mixed Culture
Substrate Requirements	Pure Carbon Sources Feedstocks	Feedstock Waste Materials
Reactor Configuration	Single Reactor (Batch/Fed-Batch)	Sequential Batch Reactor (SBR)
Advantages	Higher Volumetric Productivity Higher PHA diversity	Production Cost
Disadvantages	Production Cost Aseptic Conditions	Low Volumetric Productivity Low PHA divertisy

The use of a single culture grants a well-defined composition to a biopolymer and high volumetric productivity (up to 80% of cell dry weight) (Salehizadeh & Van Loosdrecht, 2004). Pure culture fermentation is carried out under sterile conditions, and for most bacterial strains (e.g. *Cupriavidus necator* and most *Pseudomonas* species) production occurs in a two-stage process, the first stage is related to biomass growth, where the culture is supplied with nutrients, in the second stage, growth limiting conditions, such as depletion of nutrients, are imposed in order to induce a higher PHA accumulation (Kaur et al., 2017). However, some bacteria (e.g. *Alcaligenes latus* and recombinant *Escherichia coli*) have the capacity to biosynthesize PHAs during their exponential growth phase (growth-associated production) (Lee, 1996b). Although pure carbon sources can be used as substrates, it has been observed that a change in the substrate from pure sugars to carbon-rich agro-industrial residues does not compromise the properties of the PHAs, and feedstocks such as molasses (H. Zhang et al., 1994), cheese whey (Pais et al., 2016), lignocellulosic materials (Bertrand et al., 1990), waste glycerol (Cavalheiro et al., 2009) and used

cooking oil (Cruz et al., 2015), have been successfully employed as substrates for a cheaper and more sustainable alternative to pure carbon sources.

MMC fermentation has the upper hand in terms of cost, since there is no requirement for aseptic conditions, as well as offering the possibility of using various cheap and complex waste feedstocks (Reis et al., 2011). Nevertheless, the productivity reported for this type of fermentation is low in comparison to pure cultures (up to 20% of cell dry weight), there is lacking diversity in the biopolymers obtained, mostly short-chain length PHAs (scl-PHA), and the process cannot be executed in a single reactor (Salehizadeh & Van Loosdrecht, 2004;Serafim et al., 2008). In MMC, there is firstly a selection stage of biomass with high PHA storage ability in a sequencing batch reactor (SBR), the mode of operation of this type of fermentation is called “feast and famine”, on which there is a limitation in the nutrients supplied to the cultures and only the cells that accumulate PHAs survive. Then, there is an accumulation stage carried out in batch mode for PHA production using the selected biomass (Reis et al., 2011).

1.3.1. Structure and Classification of PHAs

Structurally, PHAs are a class of linear polyesters that consist of hydroxy acid monomers (HA) linked by an ester bond. They are a widely diverse group of bio-based polymers, with over 150 structural variations of monomers reported, the most common monomers and general structure of PHAs are represented in Figure 1.3 (Możejko-Ciesielska & Kiewisz, 2016; Tan et al., 2009).

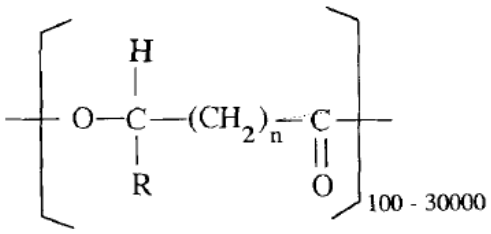

n = 1	R = hydrogen	Poly(3-hydroxypropionate)
	R = methyl	Poly(3-hydroxybutyrate)
	R = ethyl	Poly(3-hydroxyvalerate)
	R = propyl	Poly(3-hydroxyhexanoate)
	R = pentyl	Poly(3-hydroxyoctanoate)
	R = nonyl	Poly(3-hydroxydodecanoate)
n = 2	R = hydrogen	Poly(4-hydroxybutyrate)
n = 3	R = hydrogen	Poly(5-hydroxyvalerate)

Figure 1.3- General Structure of PHAs. Adapted (Kaur et al., 2017).

PHAs molecular weight (Mw) can range from 5 x 10^4 to 2 x 10^7 Da, and they can be classified into two main groups based on the number of carbon atoms in the monomers: (1) short-chain length PHAs (scl-PHAs), consisting of monomers with 3-5 carbon atoms and (2) medium-chain length PHAs (mcl-PHAs), containing monomers from C6 to C14. Furthermore, these biopolymers can also be distinguished as homopolymers, when composed of one type of monomer, or heteropolymers when composed of two or more different monomers (Tan et al., 2016).

1.3.2. Physical Properties of PHAs

In total, there are 14 pathways reported for PHAs biosynthesis, the structural composition of PHAs polymers largely depends on the bacterial strain used, growth conditions (e.g. pH, temperature and oxygen), carbon compound supplied as the growth substrate and its

concentration and fermentation conditions (Możejko-Ciesielska & Kiewisz, 2016). It is possible to obtain polymers with a wide variety of mechanical properties that range from hard crystalline to elastic, thus making them materials that can be tailored for a great range of applications (Anjum et al.,2016).

1.3.2.1 Short-chain length PHAs (scl-PHAs)

Scl-PHAs are stiff, brittle and possess a high degree of crystallinity (60-80%). These characteristics are comparable to those of conventional fossil-derived thermoplastics like polypropylene (PP) or polystyrene (PS) (Anjum et al., 2016). Table 1.2 presents a comparison between these materials and the different types of PHAs.

Poly(3-hydroxybutyrate) (P(3HB)) is a common homopolymer, resistant to hydrolytic degradation, optically pure and highly crystalline due to its stereoregularity, granting it rigidity. Though, it has a subpar mechanical performance compared to PP, as it shows a lower elongation at break, with only 3-8%, versus 500-900% (Anjum et al., 2016). Melting (T_m) and glass transition (T_g) temperatures are important parameters when it comes to any given material since they define lower and upper-temperature limits for numerous applications (Możejko-Ciesielska & Kiewisz, 2016). P(3HB) has a melting temperature between 173 and 180 C˚ and a low glass transition temperature (5-9 C˚). The Mw of P(3HB) produced from wild-type bacteria is usually in the range of 1 x 10^4 to 3 x 10^6 Da, a common wild-type bacterial strain employed for P(3HB) production is *Cupriavidus necator* (Tan et al., 2016; Anjum et al., 2016).

A strategy to improve the properties of PHA is to introduce a secondary HA monomer other than 3HB to produce a copolymer. Poly(3-hydroxybutyrate-*co*-3-hydroxyvalerate(P(HBHV)) is one of the most well-known copolymers. By introducing the 3HV monomer, the material properties of P(3HB) such as crystallinity, melting temperature, stiffness and toughness, are improved (Anjum et al., 2016). P(HBHV) has lower crystallinity, lower melting point (137-170 ˚C), decreased stiffness, increased elongation to break (50%, versus 3-8%), being more flexible than P(3HB). These properties largely depend on mol% of HV that can vary from 0 to 30 mol% (Możejko-Ciesielska & Kiewisz, 2016; Anjum et al., 2016).

1.3.2.2 Medium-chain length PHAs (mcl-PHAs)

Mcl-PHAs are generally composed of one or more types of monomers, the most common are 3-hydroxyhexanoate (3HHx), 3-hydroxyoctanoate (3HO), 3-hydroxydecanoate (3HD), 3-hydroxydodecanoate (3HDd), 3-hydroxytetradecanoate (3HTd). It is also possible to have copolymers of scl-PHA monomers and mcl-PHA monomers combined, a common example is poly(3-hydroxybutyrate-*co*-3-hydroxydecanoate (P(HBHD)). *Pseudomonas* species strains are well-known mcl-PHA producers, some examples include *Pseudomonas oleovorans*, *Pseudomonas putida* and *Pseudomonas chlororaphis* (Tan et al., 2016; Anjum et al., 2016).

In contrast to scl-PHAs, these biopolymers act as elastomers within a very narrow temperature range due to their low melting temperature, they present low crystallinity (25%), low tensile strength, high elongation to break, and T_g below room temperature (Anjum et al., 2016). In Table

1.2 some examples are presented for comparison between the properties of mcl-PHAs, scl-PHAs and a few copolymers. These characteristics attribute more flexibility and elasticity to mcl-PHAs than scl-PHAs, making them suitable for other types of applications, working for example, like glues, rubbers or adhesives (Muhr et al., 2013).

Table 1.2- Comparison between the physical properties of different PHAs and conventional plastics. Adapted (Możejko-Ciesielska & Kiewisz, 2016;Anjum et al., 2016).

Polymer	Melting Temperature (T_m) (˚C)	Glass Transition Temperature (T_g) (˚C)	Tensile Strength (MPa)	Elongation at Break (%)
P(3HB)	173-180	5-9	40	3-8
P(3HB-co-3HV)	137-170	-1	30-37	50
P(3HO)	61	n.a	6-10	300-450
P(3HB-co-3HD)	130	-8	17	680
PP	170-176	-10	29.3-38.6	500-900
PS	80-110	21	50	3-4

PHAs characteristics, such as biocompatibility, mechanical properties comparable to fossil-based materials and customizability, make them suitable to a large array of applications, like environmentally-friendly packaging, novel source of biofuels and as biomedical materials (Tan et al., 2016). This work focused on the latter.

1.4. Human Skin Structure and Function

The skin is our largest organ, it is an essential and complex physical, immunological, and sensory barrier. The skin has several important functions, not only it provides protection against a range of noxious stressors like UV radiation, pathogens and penetration of harmful substances, but also acts as the periphery sensing system of heat, stress and strain (Van den Broek et al., 2017).

The skin structure can be divided into three basic layers: the epidermis, the dermis, and the subcutaneous layer (Van den Broek et al., 2017) (Figure 1.4). The epidermal layer is composed of separate layers, according to the degree of keratinization of the cells. The outermost layer, designated stratum corneum (SC), is made up of denucleated, non-living, flattened cells called corneocytes and acts as the 'first line of defence', protecting our body from the environment (Walters & Brain, 2002). Below the SC, is a layer denominated viable epidermis, that consists of nucleated living cells, namely keratinocytes, melanocytes, Merkle cells (mechanoreceptors) and Langerhans cells (immune cells). The viable epidermis is a key region in drug binding, metabolism and surveillance. The dermal-epidermal junction separates the viable dermis from the subsequent layer, the dermis, which is rich in collagen, is composed mainly of fibroblasts and supplies the epidermis with mechanical support and nutrients (Monteiro-Riviere, 2006). The subcutaneous layer, or hypodermis, consists of fatty connective tissue that connects the dermis to underlying skeletal components (Tobin, 2006).

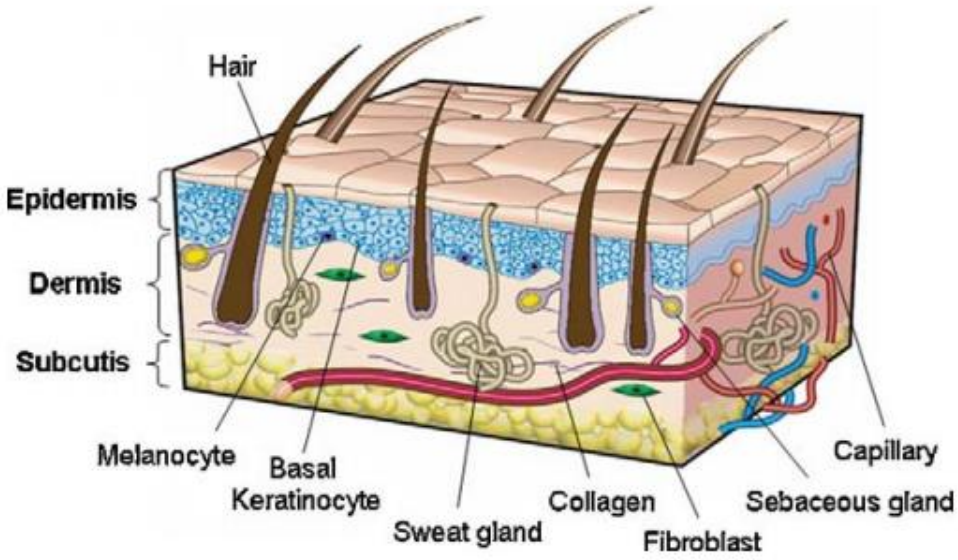

Figure 1.4- The structure of human skin. Retrieved (Böttcher-Haberzeth et al., 2010).

1.4.1. Skin Research Models

The risk assessment and evaluation of percutaneous permeation of a chemical, pharmaceutical or cosmetic, is crucial to the successful development of new formulations intended for human use, thus it is important to have the platforms (healthy and diseased skin models) to do so in many areas of basic and applied research (Abd et al., 2016). Table 1.3 presents different skin models, as well as their advantages and disadvantages.

Nowadays, animal models are mainly used in the preclinical phase of drug development to assess risk and mode of action of drugs. Yet, animal models present significant differences to human skin physiology and immunity (Warren et al., 2015). In addition, since 2009 the use of animals for cosmetic research purposes has been prohibited by the European Union (EU) (European Commission's cosmetics directive (76/768/EEC)), and in March 2013 the import and sale of cosmetics that were tested in animals have been forbidden also (EURL-CVAM Technical Report 2013). This has inevitably forced the cosmetic and pharmaceutical industries to develop alternative test models for the skin.

The gold-standard experimental model is *in vivo* human skin. However, human trials are costly and carry ethical concerns when it comes to substances or materials with potentially toxic effects. Moreover, *in vivo* responses are a challenge to measure and to interpret due to the high variability (Abd et al., 2016). Often, excised human skin (*ex-vivo*), most commonly obtained with consent from plastic surgery or cadavers, is used. Though, there are issues regarding the limitation on the manipulation of experimental variables and the availability, since there are limited quantities of skin, particularly when it comes to diseased skin (Van den Broek et al., 2017). Consequently, these ethical, financial and analytical issues incite the search for reproducible alternatives to *in vivo* and *ex vivo* tests with human and animal skin that will predict human response in a reliable

manner. Accordingly, this shifted focus to the development of *in vitro* artificial or reconstructed skin models.

Two-dimensional (2D) and three-dimensional (3D) skin cell cultures are examples of *in vitro* models. Cell cultures grown in controlled flat environments, for example in a Petri dish, are designated 2D cell cultures. 3D cell cultures combine and shape cells into a 3D form using a scaffold or specialized conditions that help maintain a 3D arrangement (Teimouri et al., 2019).

2D cell cultures have been the main type of cell cultures used in research for a long time, being a low cost and quick method to identify toxic compounds. However, over-time these cultures have proven to offer limitations, 2D cell cultures are restricted to single cell-types and do not consider the impact of other cells as well as the environment. As per result, 2D *in vitro* cell culture studies have not translated to *in vivo* studies, because these simple monolayer models do not recapitulate key functions of the skin, namely barrier function, cell sheeting and layering, immune function, and blood perfusion, therefore presenting an overt lack of physiological relevance (Duval et al., 2017). Henceforth, 3D models have become progressively more popular as they more closely resemble human *in vivo* skin processes.

Table 1.3- Advantages and disadvantages of different skin models. Adapted (Abd et al., 2016; Teimouri et al., 2019).

Skin Model	Advantages	Disadvantages
Animal in vivo skin	Easy to obtain Easy to scale up to humans	Ethical issues Ban on cosmetic use in the EU Different barrier properties than humans
Animal ex vivo skin	Easy to obtain	Different barrier properties than humans
Human in vivo skin	Gold standard	Ethical issues Costly
Human ex vivo skin	Best surrogate for in vivo humans	Availability Variability
2D in vitro skin	Low cost Ease to use	Lacks physiological relevance Inaccurate representation of in vivo processes
3D in vitro skin	Built-in barrier properties Can be engineered to include healthy or diseased features	Current models still exhibit weaker barrier properties than humans

1.4.1.1. 3D-Skin Models

Culturing cells in three dimensions allow for better cell-to-cell contact, increasing intracellular signalling and facilitating cell development, resulting in differentiation into more complex structures. A 3D cell culture provides a suitable micro-environment for ideal cell growth, differentiation and function by permitting individual cells to maintain their normal shape, aiding cells in forming complex interactions with each other and emulating a natural environment to stimulate the creation of a tissue-like construct. There are several types of 3D skin models based on different technologies, they usually fit in one of two categories: scaffold-free or scaffold-based systems (Knight & Przyborski, 2015).

When it comes to scaffold-free systems, the most common are spheroids, multi-cellular aggregates, in which cells can form their own extracellular matrix components usually composed of an inner necrotic layer, an intermediate zone of quiescent cells and an outer stratum of proliferating cells. Spheroids can be produced by the hanging drop method (Keller, 1995) or by using a non-adherent U shape plate(Phung et al., 2011). For skin, this model has not yet been extensively explored, however, there have been successful studies with spheroids that use HaCaT cells (keratinocyte cell line) and fibroblasts co-cultured with melanoma cells for a tumour model (Okochi et al., 2013). This model applied to skin needs optimization but is promising due to its low cost, simplicity and reproducibility.

Scaffold-based methods can use two different main types of materials: synthetic or natural (Knight & Przyborski, 2015). Synthetic materials, like titanium and bioactive glasses, are advantageous for their defined composition, tailorable mechanical properties and degradability, as well as reproducibility, however, they may lack sites for cellular adhesion (Engler et al., 2006; Hayward et al., 2013). On the other hand, natural materials, such as PHAs, gelatine and alginate, offer biocompatibility and cell adhesion sites but fall short on lot-to-lot variability. In terms of the type of scaffold-based methods, they can be broadly divided into hydrogel technology or a solid scaffolds approach (Knight & Przyborski, 2015).

A common choice for 3D cultures is the use of hydrogels, which encapsulates cells in a loose scaffold framework of cross-linked materials, generally of natural bases (e.g. agarose, fibrin and collagen) with high water content (Tibbitt & Anseth, 2009). The cells can be trapped in an artificial extracellular matrix (ECM) protein environment or by migration to the interior of the gel. The encapsulation can be achieved through self-assembly ionic cross-linking or by UV exposure that causes radical polymerizations (Heywood et al., 2004; Topman et al., 2013). The dominant technique when creating an *in vitro* skin model with this method is to use collagen I (ECM protein) as the hydrogel material, serving as a scaffold for dermal fibroblasts to mimic the dermal layer, with subsequent co-culture of keratinocytes on the surface for the epidermal layer (Carlson et al., 2008). Hydrogel skin models have been successfully assembled for healthy skin as well as for diseased skin, specifically psoriasis and skin cancer (Bell et al.,1981; Soboleva et al., 2014; Brohem et al., 2011). Some companies already sell commercial skin models based on this technology, examples include EpiDerm™ (MatTek, Ashland, MA, USA), Episkin™ (L'Oreal; SkinEthic, Nice, France) and Apligraf™ (Organogenesis Inc; Canton, MA, USA). Disadvantages

of hydrogels are the damaging effect on cells when using UV light for encapsulation and the short culture times due to unwanted nutrients diffusion (Jongpaiboonkit et al., 2008).

In this work, we will focus on solid scaffold-based technology, rather than the use of hydrogels. The use of a solid scaffold allows the support of a 3D cell culture, where they can naturally create a tissue-like structure, in a reproducible and controllable fashion. Different types of solid scaffolds can be employed, and there are several technologies for the fabrication of said scaffolds, but most generally they present either a porous or a fibrous structure (Knight & Przyborski, 2015).

1.4.1.2. From 3D Cell Culture to Skin-on-Chip

Although 3D cell-cultures are impressive models with a high level of differentiation, they still fail to fully reconstitute features of living organs that are essential for their function, including tissue-tissue interfaces, spatiotemporal gradients of chemicals and gases, or the mechanical factors of the microenvironment (Huh et al., 2011). However, by culturing skin tissues while incorporating microfabrication technologies and microfluidics, “skin-on-chip”, it’s possible to integrate these features and create an elevated model, which allows the control of physical and biochemical parameters such as medium flow, mechanical force and gradients of the natural human skin, enabling the study of the human physiology in an organ-specific environment (Huh et al., 2011; Zhang et al., 2018).

This is a fairly new area of research, but it is a promising new type of skin model that will in due course lead to the decline of animal experimentation and the acceleration of drug discovery (Zhang et al., 2018).

2. Motivation

Skin is an essential organ that provides a physical, immunological and sensory barrier, offering protection against harmful stressors such as UV radiation, pathogens and dangerous substances (Van den Broek et al., 2017). Thus, it is key for the execution of extensive research on any chemical, cosmetic or pharmaceutical, intended for human use. To do so, models that allow the prediction of *in vivo* human response must be available (Abd et al., 2016). Clinical human trials are expensive and hold ethical concerns, whereas growing awareness towards animal protection impedes the use of *in vivo* animals for cosmetic research purposes. Additionally, animal models can poorly predict human response due to differences in skin physiology and immunity, accentuating the need for artificial skin models skin (van den Broek et al., 2017; Abd et al., 2016).

In recent years, there has been increased interest in the use of 3D cell cultures, stemming from their high degree of differentiation, tissue specialization and protection of in vivo morphology, that yields superior results when compared to 2D models in terms of physiological response, making them suitable replacements of *in vivo* models for drugs and therapies development (Huh et al., 2011).

PHAs have emerged as potentially useful materials in the biomedical field for different applications owing to the versatility of these biopolymers regarding their non-toxic degradation products, biocompatibility, diversity of physical and chemical properties, non-carcinogenicity and cellular support growth (Zubairi et al., 2016).

In the present work, a PHA polymeric scaffold has been developed as a platform for an *in vitro* 3D cell-culture model of reconstructed skin. Predefined porosity and interconnected pores in the scaffold are crucial parameters to assure the attachment and growth of human primary skin cells inside the matrix of a 3D space, imitating tissue growth in normal conditions, and permitting a histological profile that more realistically models the human skin.

The following work was divided into three parts. In the first part, different PHA were obtained by bacterial cultivation using glycerol or used cooking oil as feedstocks to produce mcl-PHA and P(3HB)/P(HBHV) polymers, respectively. The second part of this work consisted of producing porous/fibrous scaffolds using the different types of PHAs obtained on the first part. Several techniques were tested, specifically, solvent casting with NaCl leaching, supercritical CO_2 technology, emulsion templating with water and electrospinning. Moreover, scaffolds were also submitted to oxygen plasma and UV/O_3 surface pre-treatment to evaluate the impacts on the polymeric surface in terms of hydrophilicity, morphology and bioactivity. In the third and final part of this project, the polymeric scaffolds were studied regarding their biological activity promotion, including cytotoxicity, cell attachment and morphology using human fibroblasts. This study aimed to evaluate the feasibility to implement porosity in PHAs with different properties, ranging from elastic (mcl-PHA, P(HBHV)) to brittle (P(3HB)), as well as their bioactive performance, in hopes of creating a suitable scaffold for 3D skin cell culture, that could compete with commercially available scaffolds.

Chapter 2- Production of Polyhydroxyalkanoates

2.1. Introduction

PHA production from several microorganisms (wild-type and engineered bacteria) has been extensively researched (Tan et al., 2016). Moreover, scl-PHA and mcl-PHA have been reported to be produced from many feedstocks, including agro-food and industrial wastes or by-products, which is an auspicious approach for cost-efficient and sustainable biopolymer production (Koller & Marsalek, 2015). Examples of feedstocks include waste glycerol (Basnett et al., 2017), agro-industrial effluents (Lemechko et al., 2019), palm kernel oil (Yun et al., 2003a), camelina oil (Bustamante et al., 2019), among many others.

For mcl-PHA production, the most employed bacteria are the ones from the species of the Genus *Pseudomonas*, such as *Pseudomonas chlororaphis* (Muhr et al., 2013; Yun et al., 2003b), *P. resinovorans* (Cromwick et al., 1996; Cruz et al., 2016) and *P. citronellolis* (Cruz et al., 2016; Muhr et al., 2013). In this work, P. *chlororaphis* will be used to produce mcl-PHA from glycerol. Glycerol has been widely investigated as a feedstock for PHA production since it is one of the by-products of the biodiesel industry and is accepted by PHA-producing microbial strains as carbon- and energy source (Koller & Marsalek, 2015).

Regarding microorganisms able to produce scl-PHA, *Cupriavidus necator* is the most well-known bacterial strain. P(3HB) production by *C. necator* using various feedstocks has been broadly reported in the literature, including spent coffee grounds (Cruz et al; 2014), waste apple pulp (Rebocho et al., 2019) and olive oil distillate (Cruz et al., 2016). In this work, used cooking oil (UCO) was used for P(3HB) production, a food industry waste mainly composed of triglycerides, containing long-chain fatty acids with saturated and/or unsaturated bonds. UCO has been used in previous studies concerning P(3HB) production since it offers higher polymer yields in comparison to productions using sugars (Cruz et al., 2016).

Furthermore, P(3HB) can sometimes fall short on mechanical performance, thus, the incorporation of other monomers, like 3HV, is a strategy to improve the mechanical properties of P(3HB). The production of P(HBHV) copolymers generally involves the use of a main carbon source with a co-substrate that provides precursors for 3HV production, examples of co-substrates are propanol (Obruca et al., 2010a), valeric acid (Lemechko et al., 2019) and avocado oil (Flores-Sánchez et al., 2017). In this study, leuvilinc acid was investigated as a co-substrate to UCO.

In this chapter, bioreactor experiments were performed using glycerol and used cooking oil as the sole carbon source to produce mcl-PHA and P(3HB) polymers, respectively, and used cooking oil with levulinic acid co-substrate to produce P(HBHV). The polymers produced in the batch fermentations were extracted, characterized and subsequently used for the preparation of porous scaffolds (Chapter 3).

2.2. Materials and Methods

2.2.1. Bioreactors Assays

2.2.1.1. Culture Reactivation

The microorganisms used in this study were *Pseudomonas chlororaphis* DSM 19603 and *Cupriavidus necator* DSM 428. The bacterial strains were preserved in glycerol (20%, v/v), as a cryoprotectant agent, at -80 ºC. The reactivation of the cultures was performed by plating a sample of the cryopreserved vials (CHROMagar™ Orientation, Paris) and incubation at 30 ˚C, during 48 h. Subsequently, a single colony of each culture was inoculated into 50 mL liquid Luria Bertani (LB) medium (2.0 g/L bacto tryptone; 1.0 g/L yeast extract; 2.0 g/L NaCl), pH 7.0), in 50 mL baffled shake flasks, and incubated in an orbital shaker at 200 rpm and 30 ˚C, for 24 h. These cultures served as pre-inoculum for the bioreactor assays.

2.2.1.2. *Pseudomonas chlororaphis* Cultivation

2.2.1.2.1. Inoculum

The bacterial culture used in these assays was *P. chlororaphis* DSM 19603. The pre-inoculum (50 mL) was transferred to a 500 mL shake flask with 200 mL LB medium and incubated in an orbital shaker at 200 rpm and 30 ˚C, for 24 h.

2.2.1.2.2. Batch Fermentation for mcl-PHA production

Batch fermentation was performed in a BioStat®B-Plus bioreactor (Sartorius, Germany) with a working volume of 2 L. The cultivation medium was composed of Medium E* ($(NH_4)_2HPO_4$, 11 g/L; KH_2O_4P, 58 g/L; KH_2PO_4, 37 g/L), glycerol at a concentration of 40 g/L as the sole carbon source, 20 mL of 100 mM $MgSO_4$ solution and 20 mL of the micronutrients solution (containing the following, per liter of 1 N HCl: $FeSO_4.7H_2O$, 2.78 g; $MnCl_2.4H_2O$, 1.98 g; $CoSO_4.7H_2O$, 2.81 g; $CaCl_2.2H_2O$, 1.67 g; $CuCl_2.2H_2O$, 0.17 g; $ZnSO_4.7H_2O$, 0.29 g). A 10% (v/v) inoculum (200 mL), prepared as described above, was used. The temperature and the pH were kept at 30 ± 0.1˚C and 7.0 ± 0.1, respectively. The pH was controlled by the automatic addition of 5 M NaOH and 2 M HCl solutions. A constant aeration rate (4 L/min) was kept during all experiments. The dissolved oxygen concentration (DO) was controlled at 30% of the air saturation by automatically adjusting the stirring speed between 300 and 800 rpm. Foam formation was automatically suppressed by addition of Antifoam A (Sigma/VWR).

Samples (6 mL) were periodically taken from the bioreactor and centrifuged. for quantification of the cell dry weight (CDW), PHA, ammonia and glycerol. The supernatant was recovered for glycerol and ammonia quantification, and the pellet was lyophilized for biomass and mcl-PHA quantification.

2.2.1.3. *Cupriavidus necator* Cultivation

2.2.1.3.1. Inoculum

The bacterial culture used in these assays was *C. necator* DSM 428. The pre-inoculum (2x 40 mL) was transferred to two 500 mL shake flask with 2x 200 mL LB medium and incubated in an orbital shaker at 200 rpm and 30 ˚C, for 24 h.

2.2.1.3.2. Batch Fermentation for P(3HB) production

The batch fermentation assay was performed in a BioStat®B-Plus 10 L bioreactor (Sartorius, Germany). The inoculum was 10% (v/v) of the initial 8 L working volume (800 mL). The cultivation medium was composed of Medium E* (composition previously described), supplemented with used cooking oil (UCO) at a concentration of 20 g/L as the sole carbon source. The temperature was maintained at 30 ± 0.1◦C and the pH was controlled at 6.80 ± 0.05 by addition of NaOH 5 M. The airflow rate was kept constant (4 L/min) and the dissolved oxygen concentration (DO) was maintained at 30% of air saturation by the automatic adjustment of the stirring rate (300–1200 rpm). Antifoam A (Sigma/VWR) was added in the bioreactor to control foam formation.

Broth samples (15 mL) were periodically taken from the bioreactor for quantification of cell dry weight, P(3HB), ammonia and UCO. For quantification of the cell dry weight (CDW), cultivation broth samples (6 mL) were centrifuged in duplicate, the supernatant was recovered for glycerol and ammonia quantification and the pellet was lyophilized for biomass and P(3HB) quantification.

2.2.1.3.3. Fed-Batch Fermentation for P(HBHV) production

The fed-batch fermentation assay was performed under the same conditions as described in section 2.2.1.3.2. However, after 21 h of cultivation, levulinic acid (300 g/L) was fed as a co-substrate at a rate of 5 mL/h. Broth samples (15 mL) were periodically taken from the bioreactor for quantification of cell dry weight, P(HBHV), ammonia and UCO. For quantification of the cell dry weight (CDW), cultivation broth samples (6 mL) were centrifuged in duplicate, the supernatant was recovered for glycerol and ammonia quantification and the pellet was lyophilized for biomass and P(HBHV) quantification.

2.2.2. Analytical Techniques

2.2.2.1. Cellular Growth

Cellular growth was monitored during the experiment by measuring the optical density of the cultivation broth at 600 nm (OD600nm) with a dilution necessary for the OD600 to be below 0.3 with deionised water as zero reference. All measurements were done in duplicate.

2.2.2.2. Biomass Quantification

Cell growth was determined by quantification of the cell dry weight (CDW) of each sample. The cell pellet was used for the gravimetric determination of the CDW, after washing once with

deionized water (resuspension in water, and centrifugation at 8000 rpm, for 15 to 20 minutes at 10 ˚C) the pellet was freeze-dried (ScanVac CoolSafeTM, LaboGene), at -110˚C for 48 h**.** All measurements were done in duplicate.

2.2.2.3. Glycerol Quantification

The cell-free supernatant was diluted (1:50) in sulphuric acid (SIGMA-ALDRICH) (H_2SO_4 0.01 N) and filtered with Vectra Spin Micro Polysulfone filters (0.2 µm) (Whatman), at 3000 rpm for 10 minutes. Glycerol concentration was determined by high-performance liquid chromatography (HPLC) with a VARIAN Metacarb column (BioRad) coupled to a refractive index (RI) detector. The analyses were performed at 50 ˚C, with sulphuric acid (H_2SO_4 0.01 N) as eluent at a flow rate of 0.6 mL/min. Glycerol (ReagentPlus 86-88% w/w Scharlau) standards were prepared at a concentration of 1 g/L successively diluting them to the concentrations of 0.5 g/L, 0.1 g/L, 0.05 g/L and 0.01 g/L.

2.2.2.4. Used Cooking Oil Quantification

UCO quantification was performed as previously described by Cruz et al. (2015). Broth samples (4 mL) were mixed with hexane (4 mL) with the aid of a vortex mixer (VWR International) for one minute. The mixture was left to rest until there was a visible phase separation. The upper oil-containing phase was collected to pre-weighed tubes, and the solvent was evaporated in the fume hood. The remaining oil was gravimetrically quantified. All measurements were done in duplicate.

2.2.2.5. Ammonium Quantification

Ammonium concentration was determined by colourimetry, as implemented in a flow segmented analyser (Skalar 5100, Skalar Analytical, The Netherlands). Ammonium chloride (Sigma) was used as a standard at concentrations between 5 and 20 mg L^{-1}.

The cell-free supernatant was diluted (1:200) in deionized water and analysed.

2.2.2.6. Nile Blue Staining

In an Eppendorf tube, 0.5 µL of Nile Blue was added to 0.5 mL of cultivation broth retrieved from the bioreactor, covered with aluminium foil and placed in an oven at 70 °C for 10 minutes. After this time, slides were prepared and observed under the microscope (Olympus BX51 epifluorescence) under contrast light and fluorescent light, with a magnification of 100x.

2.2.2.7. PHA Concentration and Composition

PHA content and composition were determined after hydrolysis of dried cell samples (5 to 10 mg) in 2 mL 20% (v/v) sulphuric acid (SIGMA-ALDRICH) in methanol (Fisher Chemical) and 2 mL of benzoic acid in chloroform (1 g/L) (SIGMA-ALDRICH), on oil bath at 100˚C, for 4 h. Then, 1 mL of water was added, and the organic phase was recovered and analysed by GC (430-GC, Bruker) with a Restek column of 60m, 0.53 mmID, 1 µM df, Crossbond, Stabilwax. The injection

volume was 2.0 µL, with a running time of 32 min, constant pressure of 14.50 psi and helium as the carrier gas. The heating ramp was 0 to 3 min a rate of 20˚C/min until 100˚C, 3 to 21 min a rate of 3˚C/min until 155˚C and 21 to 32 min a rate of 20˚C/min until 220˚C.

For mcl-PHA content and composition determination, standards were prepared using mcl-PHA with 3wt% 3-hydroxyhexanoate (3HHx), 17wt% 3-hydroxyoctanoate (3HO), 57wt% 3-hydroxydecanoate (3HD), 11wt% 3-hydroxydodecanoate (3HDd) and 12wt% 3-hydroxytetradecanoate (3HTd) in concentrations ranging from 0.1 to 2.0 g/L. For P(3HB) and P(HBHV) calibration curves, P(3HB-co-3HV) (Sigma-Aldrich, 88 mol% 3HB, 12 mol% 3HV) acted as standards in concentrations ranging from 0.4 to 8.0 g/L.

2.2.3. Calculations

The residual biomass (X_t) was calculated by subtracting the concentration of polymer at time t (PHA_t, g/L) from the cell dry weight at time t (CDW, g/L):

$$\mathrm{X_t} = \mathrm{CDW_t} - \mathrm{PHA_t} \quad (1)$$

The maximum specific cell growth rate (μmax, h^{-1}) was determined from the linear regression slope of the exponential phase of Ln X_t versus time.

The volumetric productivity (r_p, g/L.h) was obtained by dividing the final PHA concentration (P, g/L) for the total time of fermentation (Δt, h):

$$r_p = \frac{P}{\Delta t} \quad (2)$$

The active biomass yield on substrate basis (*Y*x/s, gx/gs) was calculated by dividing the active biomass (ΔX, g/L) by the total substrate consumed during the cultivation (ΔS, g/L):

$$y_{x/s} = \frac{\Delta X}{\Delta S} \quad (3)$$

The polymer yield on substrate basis (*Y*p/s, gp/gs) was calculated by dividing the PHA produced (ΔP, g/L) by the total substrate consumed during the cultivation (ΔS, g/L):

$$y_{p/s} = \frac{\Delta P}{\Delta S} \quad (4)$$

2.2.4. Polymer extraction and characterization

The cultivation broth recovered from the bioreactor experiments was subjected to centrifugation (8000 rpm, 15 minutes at 4 ˚C), and the resulting pellets were lyophilized and weighted. Soxhlet extraction of the biomass was performed with chloroform (250 mL) (SIGMA-ALDRICH), at 80˚C, for 24 - 48 h. The extracted PHA was resolubilized in chloroform and precipitated in ice-cold ethanol (Carlos Erba Reagents) (chloroform/ethanol 1:10). The precipitate was then recovered in a pre-weighed flask and left at room temperature, in a fume hood, for solvent evaporation.

2.2.4.1 Molecular Mass Distribution

A sample (15 mg) of each polymer was dissolved in 3 mL of chloroform, for 18 h at room temperature. Then, the solution was filtered with a glass fibre filter 47 mm (PALL) and analysed by a Size Exclusion Chromatography (SEC) System (Waters Millenium) with support SEC: PLgel 5 µm Guard; Polymer Laboratories; 50×7.5 mm, PLgel 5 µm 10^4 Å; Polymer Laboratories; 300×7.5 mm, PLgel 5 µm 500 Å; Polymer Laboratories; 300×7.5 mm. Using a temperature of equilibration of 30˚C, with a flow rate of 1 mL/min, degazing and chloroform as the mobile phase. Samples were stored at 4 ˚C before injecting 100 µL in the SEC circuit. A RI detector (Waters 2410) was adopted for polymer detection using the sensitivity 512 and a collect duration of 25 min.

2.2.4.2 Thermal Properties

Thermogravimetric Analysis (TGA) was performed using a thermogravimetric equipment Labsys EVO (Setaram Instrumentation, France). Samples were placed in aluminium crucibles and analysed in the temperature range between 25 and 500 °C, at 10 °C/min.

Differential Scanning Calorimetry (DSC) analysis was achieved using a differential scanning calorimeter DSC 131 (Setaram Instrumentation, France). The samples were placed in aluminium crucibles and analysed in the temperature range between -130 and 320 °C, with heating and cooling speeds of 10 °C/min.

The melting temperature (*Tm*, ºC) was determined at the minimum of the exothermic peak. The degree of crystallinity (*Xc*) was calculated by the ratio between the area of the melting peak (∆Hm, J/g) and the melting enthalpy of 100% crystalline P(3HB) (∆Hm100%), considered as 146 J/g (Morais et al., 2014).

$$X_c = \frac{\Delta \mathrm{Hm}}{\Delta \mathrm{Hm}100\%} \times 100 \quad (5)$$

2.2.4.3 X-Ray Diffraction

The structural analysis of the samples was performed by X-ray diffraction (XRD) using a Benchtop X-Ray Diffractometer (RIGAKU, MiniFlex II), equipped with a Cu X-ray tube (30KV/15 mA). The 2θ scans were performed from 10˚ to 60˚, with a step size of 0.02˚.

2.3. Results and Discussion

2.3.1. mcl-PHA and scl-PHA Production

In order to obtain PHAs with different chemical and physical properties, mcl-PHAs and scl-PHAs, more specifically P(3HB) and P(HBHV), were produced by *P. chlororaphis* DSM 19603 and *C. necator* DSM 428, respectively.

2.3.1.1. mcl-PHA Production by *Pseudomonas chlororaphis* DSM 19603

Figure 2.1. presents the cultivation profile of the batch cultivation of *P. chlororaphis* using glycerol as the sole substrate.

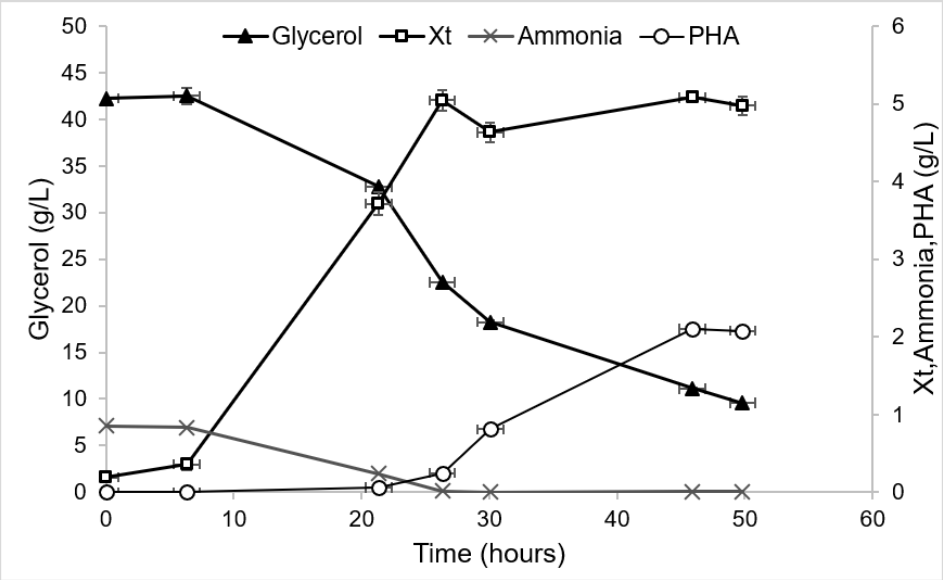

Figure 2.1- Cultivation profile of *P. chlororaphis* using glycerol as the sole carbon source.

There was a lag phase of approximately 6 hours, subsequently, the culture entered the cell growth phase, which lasted for 20 hours. The culture grew with a maximum specific cell growth rate (μ_{max}) of 0.14 h^{-1} (Table 2.1), a value in the range or slightly higher than the ones reported for cultivation of *P. chlororaphis* DSM 50083 in a fed-batch bioreactor run using saturated biodiesel fractions (0.08-0.13 h^{-1}) (Muhr et al., 2013), confirming that glycerol is an appropriate carbon source for this culture. During the exponential growth phase, while the available ammonia was being consumed, the active biomass reached a peak concentration of 5.0 g/L within 26 hours of cultivation. The growth-limiting factor in this experiment was nitrogen, as it is known that nitrogen limitation with excess carbon triggers PHA production (Khanna & Srivastava, 2005). Ammonia was exhausted rapidly within the first 26 hours, reducing from its original value of 0.86 g/L to 0.01 g/L, which was accompanied by a decrease in the cell growth rate and increase in PHA production (Figure 2.1). At the end of the assay (45 hours), a maximum PHA concentration of 2.1 g/L was reached (Table 2.1). This corresponds to an overall volumetric productivity of 0.05 g/L.h, this value is lower than the reported for *P. chlororaphis* DSM 50083 grown in saturated biodiesel fractions (0.07 g/L.h) (Muhr et al., 2013) wherein a higher CDW was reached. Nevertheless, the

value is higher than that of *P. citronellolis* NRRL B-2504 grown in waste apple pulp (0.03 g/L.h) (Rebocho et al., 2019). Glycerol concentration decreased from its initial concentration of 42.2 g/L to 9.6 g/L by the end of the fermentation, not being completely consumed. The PHA content in the biomass was of 29 wt% (Table 2.1), a value comparable to the reported for *P. citronellolis* NRRL B-2504 grown in apple pulp waste (30 wt%) (Rebocho et al., 2019) and *P. citronellolis* DSM 50332 grown in tallow-based biodiesel (20-27 wt%) (Muhr et al., 2013), moreover, the polymer content was higher than the displayed by *P. chlororaphis* DSM-50083 grown in saturated biodiesel fractions (12 wt%) (Muhr et al., 2013). The corresponding growth and polymer yield on glycerol were 0.16 g_x/g_s and 0.07 g_p/g_s, respectively. The growth yield on the substrate was lower than those reported for other studies concerning *P. chlororaphis* strains grown in other feedstocks, such as palm kernel oil (0.62 g_x/g_s) (Yun et al., 2003) and saturated biodiesel fractions (0.62 g_x/g_s) (Muhr et al; 2013), still the polymer yield was on par with the reported for saturated biodiesel fractions (0.08 g_p/g_s) (Muhr et al., 2013), indicating that glycerol is an appropriate substrate for mcl-PHA production purposes.

Table 2.1- Kinetic and stoichiometric parameters for mcl-PHA production by *P. chlororaphis* from glycerol and of other *mcl*-PHA produced by different bacterial strains found in literature using several wastes and by-products as feedstocks (μ_{max}, maximum specific cell growth rate; CDW, cell dry weight; X, active biomass; rp, volumetric productivity; $Y_{x/s}$, active biomass yield on a substrate; $Y_{p/s}$, polymer yield on a substrate basis; n.a; data not available; values with * where estimated based on the values given in the literature).

Feedstock	Bacterial Strain	Cultivation Mode	μmax (h^{-1})	CDW (g/L)	X (g/L)	PHA (g/L)	PHA (wt.%)	rp (g/L.h)	$Y_{x/s}$ (g_x/g_s)	$Y_{p/s}$ (g_p/g_s)	Reference
Glycerol	*P.chlororaphis* DSM-19603	Batch bioreactor	0.14	7.2	5.1	2.1	29	0.05	0.16	0.07	This Study
Apple pulp waste	*P. citronellolis* NRRL B-2504	Batch bioreactor	0.24	4	2.8	1.2	30	0.03*	0.27	0.12	(Rebocho et al., 2019)
Tallow-based biodiesel	*P. citronellolis* DSM 50332	Fed-batch bioreactor	0.08-0.10	11.2-14.1	8.4-11.2	2.8-2.9	20-27	0.07-0.1	n.a	n.a	(Muhr et al., 2013)
Palm kernel oil	*P.chlororaphis* HS21	Batch bioreactor	n.a	3.3	1.81*	1.49	45	n.a	0.62	n.a	(Yun et al., 2003)
Saturated biodiesel fractions	*P.chlororaphis* DSM-50083	Fed-batch bioreactor	0.08-0.13	30	26.4*	3.57*	12	0.07*	0.62	0.08	(Muhr et al., 2013)

2.3.1.2. scl-PHA Production by *Cupriavidus necator* DSM 428

Figure 2.2. presents the cultivation profile of the batch/fed-batch cultivation of *C.necator* using used cooking oil as the sole substrate for P(3HB) production (figure 2.2, a) and used cooking oil with levulinic acid as a co-substrate for P(HBHV) production (figure 2.2, b).

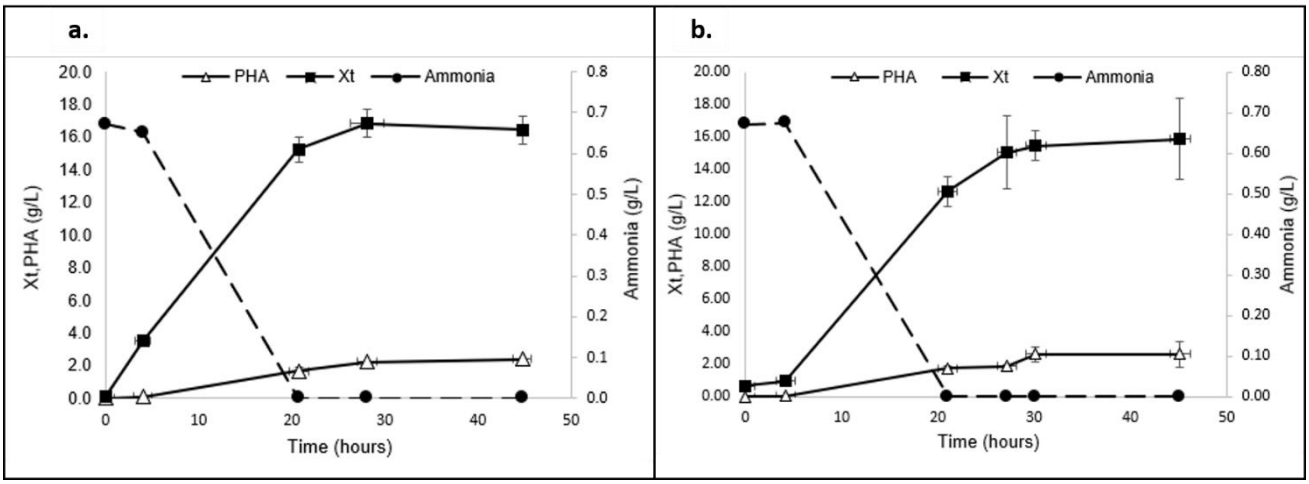

Figure 2.2- Cultivation profile of C.necator using (a) used cooking oil as the sole substrate for P(3HB) production and (b) used cooking oil with levulinic acid as a co-substrate for P(HBHV) production.

In the batch fermentation for P(3HB) production (Figure 2.2, a) ammonium started being consumed straight away, with no detectable lag phase. However, for the fed-batch fermentation for P(HBHV) production (Figure 2.2, b) there was a short lag phase of roughly 4 hours, where an adaptation required for bacterial cells to begin to exploit new environmental conditions might have occurred (Madigan et al., 2000). Still, in both assays, the available ammonium was exhausted within 21 hours, but cellular growth did not cease indicating that there still might have been nitrogen available. Polymer accumulation started at around 4 h for both cultivations runs, attaining final concentrations of 2.2 g/L for P (3HB) and 2.6 g/L for P(HBHV) with the polymer in biomass contents of 13 and 16 wt%, respectively. These values indicate low accumulation of P(3HB) and P(HBHV) when compared to previous studies that employed *C. necator.* For instance, prior work using the same carbon source for P(3HB) production (UCO) showed PHA content of 63 wt% (Cruz et al., 2015), and other carbon sources also demonstrated high accumulations, such as jatropha oil (87 wt%) (Ng et al., 2010) and spent coffee grounds (78.4 wt%) (Cruz et al; 2014). Furthermore, P(HBHV) also has reports of high PHA accumulation by *C. necator* using carbon sources like waste rapeseed oil and propanol (76 wt%) (Obruca et al., 2010), or waste glycerol and valeric acid (71%) (Gahlawat & Soni et al., 2017). These differences may be due to the variability on the fatty acid composition of the oil-containing substrates. Besides, used cooking oils can absorb diverse food compounds, such as vitamins and liposoluble nutrients, during the cooking procedure, impacting the microorganism's fermentation process (Cruz et al., 2015).

P(3HB) and P(HBHV) exhibited volumetric productivity values of 0.08 g/L.h and 0.09 g/L.h (Table 2.2), respectively. The volumetric productivity for P(3HB) was lower than that previously reported by Cruz et al., (2015) for cultivation of *C. necator* on used cooking oil (0.15 g/L.h) as well as for spent coffee grounds oil (0.19 g/L.h) (Cruz et al., 2014), but higher than what was

demonstrated for jatropha oil (0.01 g/L.h) (Ng et al., 2010). For P(HBHV), the volumetric productivity was slightly higher than that reported for fructose with avocado oil as co-substrate (0.05-0.07 g/L.h) (Flores-Sánchez et al., 2017), but lower than for waste glycerol with valeric acid as co-substrate (0.12 g/L.h) (Gahlawat & Soni et al., 2017), as well as for waste rapeseed oil with propanol as co-substrate (1.46 g/L.h) (Obruca et al., 2010). Both fermentations had similar cultivation profiles, presenting significantly close values for CDW, active biomass and volumetric productivity, demonstrating that adding levulinic acid as a co-substrate did not greatly impact the growth or the productivity of the fermentation of *C. necator* with UCO.

Unfortunately, the gravimetric quantification of the used cooking oil was inconclusive, and the calculation of active biomass and polymer yields on the substrate was not conceivable.

Table 2.2- Kinetic and stoichiometric parameters for P(3HB) and P(HBHV) production by C. necator from UCO and UCO/levulinic acid and of P(3HB)/P(HBHV) produced using several wastes and by-products as feedstocks found in literature (CDW, cell dry weight; X, active biomass; r_p, volumetric productivity; n.a; data not available; values with * where estimated based on the values given in the literature).

Feedstock	Cultivation Mode	Polymer	CDW (g/L)	X (g/L)	PHA (wt%)	PHA (g/L)	rp (g/L.h)	Reference
Used cooking oil	Batch bioreactor	P(3HB)	19.1	16.9	12	2.2	0.08	This study
Used cooking oil	Batch bioreactor	P(3HB)	10.4	6.6	63	3.8	0.15*	(Cruz et al., 2015)
Spent coffee grounds	Fed-Batch bioreactor	P(3HB)	16.7	3.6*	78.4	13.1	0.19	(Cruz et al., 2014)
Jatropha oil	Fed-Batch bioreactor	P(3HB)	13.1	1.7*	87	11.4	0.01	(Ng et al., 2010)
Used cooking oil + levulinic acid	Fed-Batch bioreactor	P(HBHV)	18.1	15.5	16	2.6	0.09	This study
Waste rapeseed oil + propanol	Fed-Batch bioreactor	P(HBHV)	138	33*	76	105	1.46	(Obruca et al., 2010)
Fructose + avocado oil	Fed-Batch bioreactor	P(HBHV)	4.45-4.91	1.43-1.81*	59-70	2.64-3.48	0.05-0.07	(Flores-Sánchez et al., 2017)
Waste Glycerol + valeric acid	Batch	P(HBHV)	6.76	1.92	71	4.84	0.12	(Gahlawat & Soni et al., 2017)

2.3.2. PHA composition

The mcl-PHA produced in the assay using *P. chlororaphis* and the P(3HB) /P(HBHV) produced by *C. necator* were characterized in order to identify their monomeric composition. The assay using *P. chlororaphis* with glycerol produced mcl-PHA, which was mainly composed of 3HD (64 wt%), 3HO (16 wt%) and 3HDd (12 wt%). It also had minor contents of 3HTd (7 wt%), while only traces of 3HHx (1 wt%), were detected (Table 2.3). The same monomers were reported for other mcl-PHA synthesized by *P. chlororaphis*, yet their relative content was different. 3HD and 3HO remain the main monomers in other studies, but 3HD was the major component in the mcl-PHA produced in this study, while 3HO was dominant for mcl-PHA produced using saturated biodiesel fractions (Muhr et al., 2013), as well as for palm kernel oil, which that also presented two additional monomers, 3-hydroxytetradecenoate (C14:1), 8%, and 3-hydroxytetradecadienoate (C14:2), 3% (Yun et al., 2003). This difference may be related to the use of different substrates, since glycerol is a sugar-based carbon source, and biodiesel fractions or palm kernel oil are richer in fatty acids, they can trigger different metabolic pathways for PHA production (Gao et al., 2013). For example, the mcl-PHA produced by *P. citronellolis* from waste apple pulp rich in sugars resulted in a monomer composition comparable to the one produced in this work (Rebocho et al., 2019). Moreover, it was demonstrated by Sharma et al. (2012) that the composition of the PHA produced by *P. putida* LS46 cultivated on glycerol with fatty acids slightly differed from that of PHAs produced on fatty acids alone.

The polymer produced by *C. necator* with UCO was a homopolymer composed by 3-hydroxybutyrate (3HB). The composition is very similar to the ones obtained for the same strain using several different feedstocks, such as, spent coffee grounds oil (Cruz et al; 2014), jatropha oil (Ng et al., 2010), fatty acids by-product (Cruz et al., 2016), olive oil distillate (Cruz et al., 2016) and margarine waste (Morais et al., 2014), where the polymers obtained from these productions were also homopolymers, P(3HB). *C. necator* has a Type I synthase, hence it is only able to synthesize two monomers, 3HB and 3HV (Cruz et al., 2016).

The polymer recovered from the biomass produced by *C. necator* cultivated in UCO with levulinic acid as co-substrate was composed of 75 wt% 3HB and 25 wt% 3-hydroxyvalerate (3HV) (Table 2.3). *C. necator* produces P(3HB) regardless of the substrate unless it is supplied with precursors for 3HV incorporation (Cruz et al., 2016). In this work, levulinic acid was used, which successfully introduced 25 wt% of 3HV, producing a P(HBHV) copolymer. Other precursors were reported in the literature, namely, propanol (Obruca et al., 2010), avocado oil (Flores-Sánchez et al., 2017) and valeric acid (Gahlawat & Soni, 2017). Levulinic acid's performance as a precursor is comparable to that of valeric acid, which also displayed a 25 wt% of 3HV, but yielded higher 3HV content than using propanol (8 wt%) (Obruca et al., 2010) or avocado oil (1-7 wt%) (Gahlawat & Soni, 2017), demonstrating to be an effective co-substrate to produce a P(HBHV) copolymer.

Table 2.3- Composition (wt%), Molecular weight (Mw), Molecular number (Mn) and polydispersity index (PDI) of mcl-PHA, P(3HB) and P(3HBHV) produced in this work and of other PHAs found in the literature; n.a- data not available.

		Composition (wt%)							Mw	Mn	PDI	Reference
Bacterial Strain	**Feedstock**	**HB**	**HV**	**HHx**	**HO**	**HD**	**HDd**	**HTd**	**x10^5 Da**	**x10^5 Da**		
***P. chlororaphis* DSM 19603**	Glycerol	-	-	1	16	64	12	7	0.69	0.46	1.5	This study
***P. chlororaphis* DSM 50083**	Saturated biodiesel fractions	-	-	15	51	26	5	n.d	0.66	0.35	1.9	(Muhr et al., 2013)
P. chlororaphis* HS21	Palm kernel oil	-	-	5	40	37	2	5	0.83	n.a	1.5	(Yun et al., 2003)
***P. citronellolis* NRRL B-2504**	Waste apple pulp	-	-	1	22	68	5	4	3.7	1.7	2.1	(Rebocho et al., 2019)
***P. resinovorans* NRRL B-2649**	UCO	-	-	11	43	33	12	1	0.4	0.3	1.3	(Cruz et al., 2016)
***C. necator* DSM428**	UCO	100	-	-	-	-	-	-	5.2	2.9	1.8	This study
***C. necator* DSM428**	UCO	100	-	-	-	-	-	-	1.7	1.1	1.5	(Cruz et al., 2016)
***C. necator* DSM428**	Waste apple pulp	100	-	-	-	-	-	-	5.0	2.5	2.0	(Rebocho, 2018)
***C. necator* DSM428**	Spent coffee grounds	100	-	-	-	-	-	-	2.3	1.9	1.2	(Cruz et al., 2014)
***C. necator* DSM428**	UCO/ Levulinic acid	75	25	-	-	-	-	-	5.6	3.5	1.6	This study
***C. necator* DSM545**	Waste Glycerol/ Valeric acid	75	25	-	-	-	-	-	1.2	n.a	4.3	(Gahlawat & Soni, 2017)
***C. necator* H16 (CCM 3726)**	Waste rapeseed oil/ Propanol	92	8	-	-	-	-	-	n.a	n.a	n.a	(Obruca et al., 2010)
***C. necator* H16 (ATCC 17699)**	Fructose/ Avocado oil	99-93	1-7	-	-	-	-	-	n.a	n.a	n.a	(Flores-Sánchez et al., 2017)
***Comamonas sp*. EB172**	Volatile fatty acids	94-92	6-8	-	-	-	-	-	n.a	8.4	1.8	(Zakaria et al., 2013)
***Haloferax mediterranei* ATCC 33500**	Cheese whey	98.5	1.5	-	-	-	-	-	4.4	n.a	1.5	(Pais et al., 2016)

2.3.3. Molecular Mass Distribution

SEC analysis (Figure A in appendices) revealed that the mcl-PHA synthesized by *P. chlororaphis* had an average molecular weight (M_w) of 0.69 x 10^5 Da, with a polydispersity index (PDI) of 1.5 (Table 2.3). The M_w obtained is among the values reported for other *P. chlororaphis* strains using different carbon sources, such as saturated biodiesel fractions (0.66 x 10^5 Da) (Muhr et al., 2013) and palm kernel oil (0.83 x 10^5 Da) (Yun et al., 2003), higher than the M_w displayed by mcl-PHA grown in UCO with *P. resinovorans* (0.4 x 10^5 Da) (Cruz et al., 2016), but lower than the M_w demonstrated by. *P. citronellolis* cultivated in waste apple pulp (3.7 x 10^5 Da) (Rebocho et al., 2019). These variations between mcl-PHAs may be related to the different production conditions, including the bacterial strain, substrate composition, cultivation mode and cells' stage of growth upon harvesting (Cromwick et al., 1996).

The P(3HB) homopolymer recovered from *C. necator* biomass by Soxhlet extraction with chloroform presented an M_w of 5.2 x 10^5 Da (Figure B in Appendices) and a PDI of 1.8 (Table 2.3). The M_w and PDI are high compared to those reported for P(3HB) synthesized using the same strain and feedstock, used cooking oil, (1.7 x 10^5 Da and 1.5, respectively) (Cruz et al., 2016) , as well as the values presented for spent coffee grounds oil (2.3 x 10^5 Da and 1.2, respectively) (Cruz et al., 2014). However, both the M_w and the PDI were similar to the values obtained for P(3HB) production from waste apple pulp (5 x 10^5 Da and 2.0, respectively) (Rebocho, 2018). This may occur due to the difference of the extraction process that impacted the polymers macromolecules, for instance, in this study Soxhlet extraction was used, but for the P(3HB) produced with coffee grounds oil simple solvent extraction with chloroform mas performed.

The M_w of the P(HBHV) synthesized by C*. necator* grown in UCO with levulinic acid as a co-substrate had an average molecular weight of 5.6 x 10^5 Da and a PDI of 1.6 (Figure C in Appendices) (Table 2.3), these values were comparable to the ones reported for the P(3HB) produced in this work using solely UCO, indicating that adding a co-substrate does not significantly affect these parameters. The average molecular is higher than the value reported for P(HBHV) presenting equal HV wt%, synthesized by *C. necator* grown in waste glycerol with valeric acid (1.2 x 10^5 Da) (Gahlawat & Soni, 2017), which again can be correlated to the different extraction techniques. The PDI was among the values reported for *Comamonas sp*. (1.8) (Zakaria et al., 2013) and *Haloferax mediterranei* (1.5) (Pais et al., 2016), but lower than was exhibited by the polymer produced by *C. necator* grown in waste glycerol with valeric acid (4.3) (Gahlawat & Soni, 2017), demonstrating a more homogenous molecular mass distribution.

2.3.4. Thermal Properties of the biopolymers

The mcl-PHA produced by *P. chlororaphis* from glycerol did not present a noticeable melting temperature, however melting temperatures of mcl-PHAs are usually around 40-50 ˚C, for example, mcl-PHA produced by *P. citronellolis* from apple pulp waste reported a melting temperature (T_m) of 53 °C (Rebocho et al; 2019) and the mcl-PHAs produced from UCO by *P. resinovorans* showed melting peaks in the range of 35.6 – 43.3 °C (Cruz et al., 2016). The mcl-PHA produced in this study demonstrated to be quite amorphous, with a meting enthalpy (ΔH_m) of 5.3 J/g and a crystallinity fraction (X_c) of 3.7% (Table 2.4). These values are lower than those of the mcl-PHA produced by *P. chlororaphis* grown in palm kernel oil, for which a X_c of 27% was reported (Yun et al., 2003), indicating that the substrate has a major effect in crystallinity. Regarding the mcl-PHA's thermal stability, the thermogravimetric curve (Figure D in Appendices) shows that the decomposition of the polymer involved a two-step process. Its decomposition showed two weight loss events. In the first event, occurred most of the weight loss, of approximately 77%, which had a maximum degradation rate (T_{deg}) at 292 ˚C (Table 2.4). There was, however, a second weight loss of 12% at 370 ˚C. The T_{deg} was among the values reported in the literature for other mcl-PHAs, such as mcl-PHA produced by *P. chlororaphis* grown in palm kernel oil (T_{deg}=288 ˚C) (Yun et al., 2003) and by *P. citronellolis* from apple pulp waste (T_{deg}=296 ˚C) (Rebocho et al., 2019).

As for the P(3HB) produced by *C. necator* from used cooking oil, it presented a melting temperature of 175°C (Table 2.4). When compared to other P(3HB) produced by the same bacterial strain and substrate, it was similar to the temperature reported by Martino et al. (2014) (T_m = 172 °C) , and slightly higher then what was demonstrated by Cruz et al. (2016), T_m of 169 °C. The polymer presented an enthalpy melting of 60.3 J/g (Table 2.4), these values are below those attained for other P(3HB) produced by the same strain and substrate demonstrated by Cruz et al. (2016), which were 78.1 J/g. However, it was higher than the value presented by *P. oleovorans* grown in olive oil distillate, which reported a ΔHm of 36 J/g (Cruz et al., 2016). In respect to the decomposition of the P(3HB), it involved a fast one-step process, presenting a single weight loss of approximately 97%, with a maximum degradation temperature (T_{deg}) at 293 °C (Table 2.4) (Figure E in Appendices). Such value is higher than the one obtained for the P(3HB) production by the same strain and substrate reported by Martino et al. (2014) of 266 °C.

Concerning the P(HBHV) copolymer produced by *C. necator* from used cooking oil and levulinic acid, it demonstrated a melting temperature of 176 ˚C (Table 2.4), this value was close the ones reported in the literature for *C. necator* cultivated with fructose and avocado oil (T_m of 164-173 ˚C and 1-7 wt% of 3HV content) (Flores-Sànchez et al., 2014) but higher than what was demonstrated for P(HBHV) produced by *Brevibacillus invocatus* grown in glucose, acetate and propionate (T_m = 143 ˚C) that presented a lower 3HV content than the produced in this work (19 wt%) (Sankhla et al., 2010). This is against the expected since there is a correlation between 3HV content and T_m, more specifically, the higher the 3HV wt.%, the steeper the decline in T_m. It has been reported that P(HBHV) with the 3HV content varying on or after 5-70 wt.% has the T_m decreasing from 170 to 87 ˚C, respectively (Singh et al., 2015). Also, although only one melting

peak was observed, it is possible to have two melting temperatures, which is the case for the P(HBHV) produced by *Halomonas sp*. from agro-industrial wastes, that displayed a lower melting temperature (155 ˚C) and a higher one, more comparable to the one attained in this study (170 ˚C) (Lemechko et al., 2019).

The copolymer produced in this work presented an enthalpy melting of 26 J/g and a crystalline fraction of 17.8 % (Table 2.4). The degree of crystallinity tends to decrease with increasing 3HV content (Singh et al., 2015), for instance, the P(HBHV) with similar 3HV content (27 wt%) produced by *Halomonas sp*. from agro-industrial wastes displayed an enthalpy melting of 27 J/g (Lemechko et al., 2019) , comparable to the polymer produced in this work, but the P(HBHV) produced by *C. necator* from fructose and avocado oil with lower 3HV content (1-7 wt%) demonstrated an enthalpy melting in the range of 53 and 57 J/g (Flores-Sànchez et al., 2014), which correlates to a more crystalline polymer. Moreover, when compared to the P(3HB) produced in this study by *C. necator* with only used cooking oil, P(HBHV) is proven to be significantly less crystalline, meaning that adding a levulinic co-substrate to increase 3HV content is an adequate strategy to tailor for more elastic polymers, when such characteristic is intended. When it comes to P(HBHV) degradation, the decomposition was a fast process, similar of P(3HB), where it involved a one-step process, demonstrating a single weight loss of approximately 97%, with a maximum degradation temperature of 292 ˚C (Table 2.4) (Figure F in Appendices).

Table 2.4- Thermal properties and degree of crystallinity of the mcl-PHA produced from *P.chlororaphis* DSM 19603 and of P(3HB) and P(HBHV) from *C. necator DSM 428*, as well as other PHA obtained from different bacterial strain (T_m, melting temperature; T_{deg}, degradation temperature; X_c, crystallinity fraction; ΔHm, melting enthalpy; n. a. data not available; n. d; not detected).

Polymer	Feedstock	Bacterial Strain	T_m (˚C)	T_{deg} (˚C)	X_c (%)	ΔH_m (J g^{-1})	References
mcl-PHA	Glycerol	*P.chlororaphis* DSM 19603	n.o	292	3.7	5.3	This study
	Palm kernel oil	*P.chlororaphis* HS21	n.o	288	27	n.a	(Yun et al., 2003)
	Waste apple pulp	*P. citronellolis* NRRL B-2504	53	296	15	21.3	(Rebocho et al., 2019)
	UCO	*P.resinovorans* NRRL B-2649	35.6 – 43.3	n.a	6-7	8.3-9.9	(Cruz et al., 2016)
P(3HB)	UCO	*C. necator* DSM428	175	293	41.3	60.3	This study
	UCO	*C. necator* DSM428	169	n.a	53	78.1	(Cruz et al., 2016)
	Olive oil distillate	*P. oleovorans* NRRL B-14682	157	n.a	36	52.5	(Cruz et al., 2016)
	UCO	*C. necator* DSM428	172	266	n.a	n.a	(Martino et al., 2014)
P(HBHV)							
25 wt% HV	UCO	*C. necator* DSM428	176	292	17.8	26	This study
1-7 wt% HV	Fructose/ Avocado oil	*C. necator* H16 (ATCC 17699)	164-173	n.a	n.a	53-57	(Flores-Sànchez et al., 2014)
19 wt% HV	Glucose/ Acetate/ Propionate	*Brevibacillus invocatus* MTCC 9039	143	n.a	48	n.a	(Sankhla et al., 2010)
27 wt% HV	Agro-industrial wastes	*Halomonas sp.* SF2003	155 and 170	n.a	n.a	27	(Lemechko et al., 2019)

2.3.5. X-Ray Diffraction

The structural analysis by XRD allowed the determination of the degree of crystallinity of the mcl-PHA, P(3HB) and P(HBHV) produced in this work. The x-ray diffractograms of all three polymers are presented in Figure 2.3. Concerning the mcl-PHA, the polymer exhibited a pattern of diffraction that is characteristic of amorphous polymers (Sánchez et al., 2003), presenting a broad hump within the 2Θ=18˚ region. However, it exhibited some degree of crystallinity (Xc=3.7%) (Table 2.4), confirmed by a small peak in the crystalline zone near 22˚. The mcl-PHA produced by *P. chlororaphis* in this study, due to its Xc value (3.7%) (Table 2.4) can be considered quite amorphous when compared to other mcl-PHAs from the literature, such as mcl-PHA produced by *P. citronellolis* in waste apple pulp *(*X_c=21.3%) (Rebocho et al., 2019) and by *P.resinovorans* in UCO *(*X_c of 6-7%) (Cruz et al., 2016).

Regarding P(3HB), the x-ray diffractogram for the polymer (Figure 2.3) exhibited all main reflections of the x-ray diffraction pattern of crystalline P(3HB), presenting typical peaks for the crystalline phase, specifically two narrow humps located at 2θ = 14 and 17˚, while the amorphous phase showed a representing broad hump at around 2θ = 22˚ and 26˚. The polymer presented a crystalline fraction of 41.3% (Table 2.4), this value is below those attained for other P(3HB) produced by the same strain and substrate demonstrated by Cruz et al. (2016), which showed a crystalline fraction of 53% (Cruz et al., 2016). However, it was higher than the value presented by *P. oleovorans* grown in olive oil distillate, which reported a crystalline fraction of 52.5% (Cruz et al., 2016).

The P(HBHV) produced in this study had a similar profile as P(3HB) (Figure 2.3), it exhibited the expected reflections for the crystalline phase, with two peaks located at 2θ = 14 and 17˚, as well as an amorphous phase represented by a broad hump at around 2θ = 22˚ and 26˚. However, the crystalline fraction (X_c= 17.8%) (Table 2.4) was much lower than what displayed by P(3HB), which is observable by the differences in the height of the peaks, in which the crystalline phase peaks for P(3HB) show greater intensity than of those by P(HBHV).

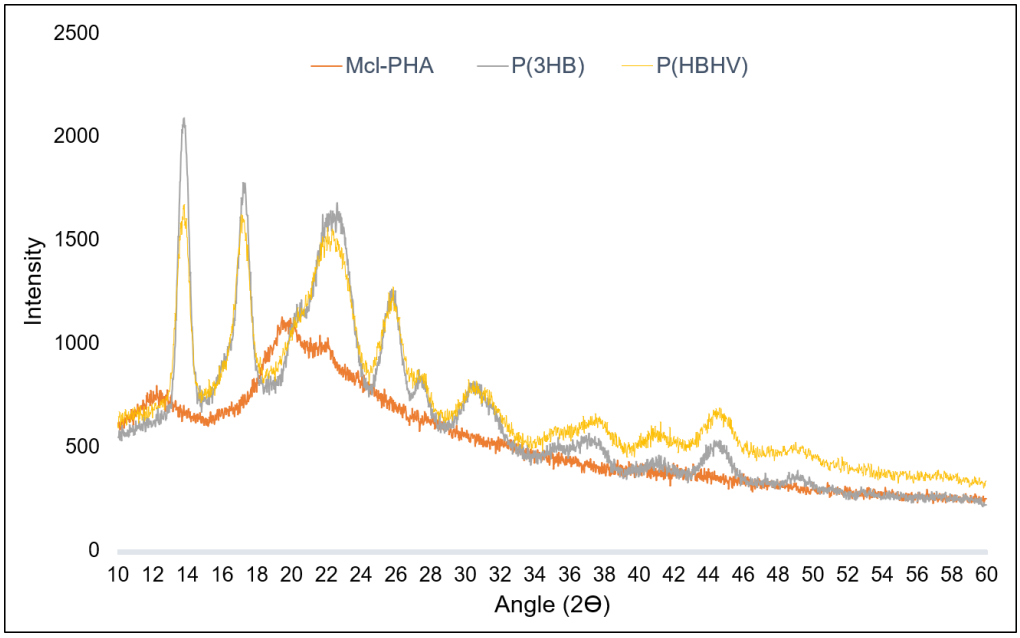

Figure 2.3 - X-ray diffractogram of the , mcl-PHA) produced by *P. chlororaphis* from glycerol and P(3HB), and P(HBHV) produced by C. necator from UCO and UCO/levulinic acid.

2.3.6. mcl-PHA, P(3HB) and P(HBHV) Comparison

Overall, in this work, it was possible to obtain three polymers of the polyhydroxyalkanoate family with varying characteristics. The mcl-PHA produced by *P. chlororaphis*, and P(3HB) and P(HBHV) produced by *C. necator* presented a set of physical-chemical properties similar to other polymers that were produced by other strains with a variety of feedstocks as their carbon sources.

Concerning the average molecular weight, the mcl-PHA presented the lowest value (0.69 x 10^5 Da), and P(3HB) and P(HBHV) had similar values with M_w of 5.2 x 10^5 Da and 5.6 x 10^5 Da, respectively (Table 2.5), meaning that P(HBHV) presents the highest average molecular weight among all polymers. The polydispersity index does not vary significantly between mcl-PHA and P(HBHV), with values of 1.5 and 1.6, respectively, and P(3HB) shows the highest PDI (1.8) (Table 2.5).

P(3HB) and P(HBHV) displayed high melting temperatures within comparable values of 175 and 176 ˚C, respectively (Table 2.5). Degradation temperature for all three polymers is also high and in the range of 292-293 ˚C (Table 2.5), which demonstrates that they hold a big window for processability.

Between all the polymers produced, P(3HB) revealed the highest crystallinity (41.3%), followed by P(HBHV) (17.8%), and then mcl-PHA (3.7%) (Table 2.5), the most amorphous, these values were expected since they reflect the monomer composition of these polymers. mcl-PHAs monomers present a high number of carbons which makes difficult the building of organized polymeric structures, resulting in a more elastic material, yet P(3HB) is composed of just 3HB, conferring it stereoregularity and thus, crystallinity, thus, by adding the 3HV monomer, it is possible to reduce the crystallinity and the stiffness (Singh et al., 2015).

Table 2.5- Composition and physical-chemical properties of the polymers obtained from apple pulp waste (HB, 3-hydroxybutyrate; HV, 3-hydroxyvalerate; HHx, 3-hydroxyhexanoate; HO, 3-hydroxyoctanoate; HD, 3-hydroxydecanoate; HDd, 3-hydroxydodecanoate; HTd, 3-hydroxytetradecanoate; M_w, molecular weight; PDI, polydispersity index; T_m, melting temperature; T_{deg}, degradation temperature; X_c, crystallinity degree: n.o; not observed).

Culture	Polymer	Monomer Composition	T_m (˚C)	T_{deg} (˚C)	M_w (x 10^5 Da)	PDI	X_c (%)
P.chlororaphis DSM 19603	mcl-PHA	HHx-HO-HD-HDd-HTd	n.o	292	0.69	1.5	3.7
C. necator DSM428	P(3HB)	HB	175	293	5.2	1.8	41.3
C. necator DSM428	P(HVHV)	HB-HV	176	292	5.6	1.6	17.8

2.4. Conclusions

In this work, different PHAs were obtained in batch fermentation using glycerol and used cooking oil as the sole carbon source to produce mcl-PHA and P(3HB) polymers, respectively, and used cooking oil with levulinic acid co-substrate to produce P(HBHV). It was possible to obtain three polymers with contrasting physical and chemical properties, which were characterized.

mcl-PHA, composed of 3HHx, 3HO, 3HD, 3HDd and 3HTd (with the monomers 3HO and 3HD in the majority), proved to be a highly amorphous PHA with low crystalline factor (3.7%) and high degradation temperature (292 ˚C). In contrast, the P(3HB) homopolymer proved to be a crystalline polymer (X_c=41.3%), with high melting and degradation temperature (175 ˚C and 293 ˚C, respectively).

Concerning P(HBHV), 3HV was successfully incorporated into the polymer (25 %wt) by means of feeding levulinic acid as co-substrate, it presented a similar melting and degradation temperature (176 ˚C and 292 ˚C, respectively) to P(3HB), however, it also demonstrated to possess a lower degree of crystallinity (X_c=17.8%), proving that adding a co-substrate highly influences the monomer composition, and thus, physical properties of the polymer.

This study demonstrated the extent of how tailorable PHAs really are, whereby choosing appropriate feedstock and bacterial strain we can produce a polymer with physical and chemical properties that fit our needs, from a rubbery and elastic mcl-PHA to a stiff and crystalline P(3HB). Taking into consideration the polymers obtained and the potentialities of the characteristics of each one, their application as biomedical materials for scaffold production will be explored in the following chapters.

Chapter 3- Fabrication and Characterization of PHA-based Scaffolds

3.1. Introduction

Solid scaffolds allow the genesis of a tissue-like structure that is physiologically relevant. There are, however, key rules to take in consideration when designing a 3D solid scaffold (Zubairi et al., 2016):

1. The materials used in the scaffold must be non-immunogenic, non-toxic, biocompatible and have a simple manufacturing process;
2. The macrostructure and microstructure must allow cell survival, signalling, growth and reorganization, whilst maintaining the natural 3D cell shape;
3. Scaffolds should present interconnect open-pore geometry, and spread porosity to allow cell adhesion, growth and reorganization, as well as the diffusion of nutrients and gases;
4. Scaffolds must present appropriate surface properties, such as morphology, hydrophilicity, surface energy and charge;
5. The scaffold should possess mechanical strength to sustain the structure required for cell ingrowth and matrix formation.

There are different types of solid scaffolds, as well as several technologies for the fabrication of said scaffolds, but most generally they present either a porous or a fibrous structure (Knight & Przyborski, 2015).

Regarding fibrous scaffolds, they are mainly produced by a process designated electrospinning, that uses an electric field to control the formation and deposition of polymer fibres onto a grounded surface. This method allows the fabrication of polymer fibres from the microscale to the nanoscale (Xu, Inai, Kotaki, & Ramakrishna, 2004). A unique feature of this technique is the ability to form aligned fibres, which enables cells to adhere and elongate along the fibres, inducing cell alignment and directionality to the cultures (Baker & Mauck, 2007). Materials that have been reported for fibrous scaffolds production include PGA and PLA (Ouyang, Goh, Thambyah, Teoh, & Lee, 2003). In addition, it's possible to co-spin polymers with additives or other biomaterials, improving their functionality and biocompatibility (Saraf, Baggett, Raphael, Kasper, & Mikos, 2010).

Porous scaffolds create a 3D microenvironment that enables cells to enter and not flatten out as in 2D cell cultures. As mentioned, pore dimensions and interconnectivity must allow cells to form contacts and interactions within the 3D space, for them to fill the voids, bridge gaps and create a 3D mass of cells (Knight & Przyborski, 2015). Common methods for 3D porous scaffolds fabrication are solvent casting with particulate leaching, emulsion templating and supercritical CO_2 technology (Zubairi et al., 2016).

Particulate leaching encompasses the casting of a polymer around particulates of a leachable porogen (e.g. salt particles, sugar and paraffin spheres). When the porogen is leached out it leaves behind a network of interconnected pores (Ma & Choi, 2001). However, it’s possible to produce pores that do not communicate with other adjacent spaces, leading to a heterogeneous cell culture, where there are isolated cells within the 3D space. PLA and PLGA are polymers

reported to use this technique to form porous scaffolds intended for human embryonic stem cell culture (Levenberg et al., 2003). Emulsion templating is an alternative to particulate leaching that involves mixing an immiscible liquid with the polymer solution, creating an emulsion that will form connecting voids, resulting in a highly porous, but more homogenous material (Cameron, 2005).

Finally, supercritical fluid technology, or gas foaming, is also a sustainable alternative which allows the production of highly porous scaffolds without the use of any organic solvents that could also leave residues and cause *in vitro* toxicity (Zubairi et al., 2016). This process consists of the saturation of the polymer mix with gas at critical temperatures and pressures. When thermodynamic instability is introduced by decreasing pressure or temperature, nucleation is stimulated, and foaming occurs leading to the growth of pores. The pore size is tailorable by altering temperature and pressure, as well as rates of parameter reduction. Yet, the scaffolds produced with this method generally present poor interconnectivity (Liu, Xia, & Czernuszka, 2007).

There are many commercially available solid scaffolds, such as Alvatex™ (ReproCell, Glasgow, Scotland) and 3D Biotek 3D Insert™ (Merck, NJ, USA), which allow more reproducible studies, as they are produced according to strict quality control procedures that minimize batch to batch variation. PS is the most common material for these scaffolds, as it is inert, which is advantageous when continuous cell culturing conditions are required, though, it is also stiff and lacks biomechanical properties found in soft tissues, such as skin (Knight & Przyborski, 2015).

3.1.1. PHAs Processing

Although PHAs are highly diverse and tailorable, they still suffer from a few limitations. On one hand, the high production cost and poor mechanical properties hinder their use in industrial applications, and on the other hand, their intrinsic hydrophobic characteristics make them hard to employ in the biomedical field. For them to be direct substitutes of plastics, there has been a focus on research to improve less desirable qualities of PHAs, prevalent examples include physical blending with other materials and surface modification (Ke, Liu, Zhang, Xiao, & Wu, 2017; Z. Li, Yang, & Loh, 2016).

3.1.1.1. Blending

Blending is an effective method to improve a polymeric material. When blending a PHA with another biodegradable polymer, we can tune the mechanical properties, while maintaining full biodegradability and biocompatibility. Materials that have been successfully blended with PHAs are starch, cellulose derivatives, PLA and polycaprolactone (PCL) (Del Gaudio et al., 2012; Gerard & Budtova, 2012; Godbole et al., 2003; Wang et al., 2015). Moreover, as previously stated, PHAs properties vary depending on their monomer composition, and we can have rigid polymers such as P(3HB) or elastic polymers like P(HBHD). Hence, a common approach is blending different types of PHAs towards alternating their properties and enabling not only better mechanical performance, but also better bioactive behaviour. For instance, P(3HB)/P(HBHHx)

blends revealed significant improvement in rabbit bone marrow cells growth compared to their pure P(3HB) counterpart (Chen et al., 2009).

3.1.1.2. Surface Modification

Another method to modify PHAs features is by treatments that introduce a reactive functional group, also known as a surface chemical modification. This tactic allows the alteration of the chemical functionality, charge, wettability, and/or morphology of the surface, without influencing the bulk properties (Ke et al., 2017).

A treatment that is widely used, and that is included in this work, is plasma treatment, which relies on the use of ionized gaseous mixture (plasma) to modify surface properties, such as roughness, adhesion, penetrability, wettability, and biocompatibility, important features for biomedical applications (Ke et al., 2017). Here, electrical discharges in low-pressure gases result in excited species through energetic collision, that initiate etching, crosslinking and incorporation of new functional groups. Plasma treatment provides manifold possibilities by adjusting the type of gas used (O_2, N_2, CO_2, air plasma, etc.), and effectiveness greatly depends on parameters like gas flow, power, pressure and treatment time (Denes & Manolache, 2004). O_2 plasma, specifically, introduces oxygen atoms by grafted ester, carboxyl, or carbonyl groups, enhancing surface energy and hydrophilicity. P(HBHV) treated with O_2 plasma reported increased hydrophilicity (but maintained only 3–4 months) and augmented roughness, additionally, it was shown to improve bioactive behaviour, such as greater alkaline phosphatase (ALP) activity of osteoblasts (Köse et al ., 2003; Mas et al., 1997).

Alternatively, ultraviolet/ozone (UV/O_3) surface pre-treatment also allows the creation of carboxyl groups at the surface of a polymer to enhance hydrophilicity. Yet, opposed to plasma treatment, it is cost-effective and involves only a simple apparatus with no requirement of vacuum. UV/O_3 treated PCL showed enhanced attachment and growth kinetics for HaCaT skin keratinocyte cells when compared to untreated PCL (Ke et al., 2017; Samsudin et al., 2017).

3.2. Materials and Methods

3.2.1. Scaffold Fabrication

3.2.1.1. Films Preparation

Polymer solutions (4% (w/v)) with either P(3HB), P(HBHV) or mcl-PHA were prepared using chloroform (Sigma-Aldrich). To obtain homogenous solutions, an oil bath at 60˚ C with continuous stirring was used overnight. The solutions were transferred to glass Petri dishes (5 cm diameter) and placed in a desiccator, in the fume hood, where they were kept at room temperature until complete solvent evaporation. Figure 3.1 shows a schematic representation of the film fabrication procedure.

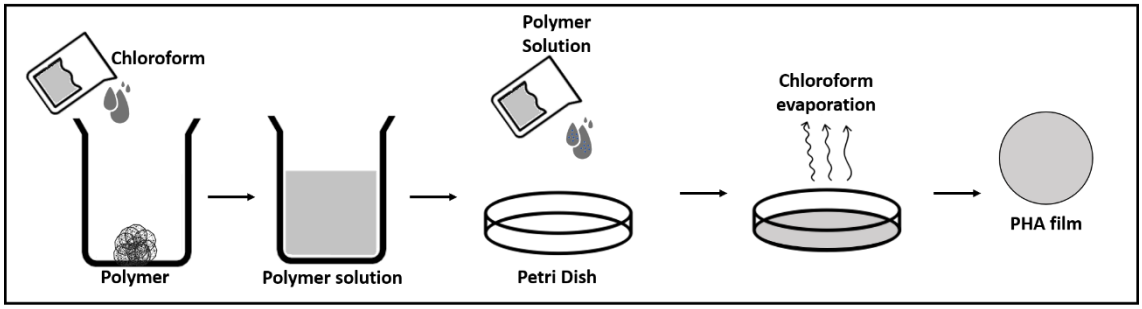

Figure 3.1- Schematic representation of PHA film preparation.

3.2.1.2. Solvent Casting with Particulate Leaching (SCPL)

A polymer solution was prepared using chloroform at a concentration of 4% w/v for P(3HB) and P(HBHV) and 50% (w/v) for mcl-PHA, as described in section 3.2.1.1. The particles chosen for this work were sodium chloride (NaCl) (Sigma-Aldrich). NaCl crystals were firstly ground with a mortar and pestle and then passed through a molecular sieve (106 µm void). The incorporation of particles was achieved by two different techniques, the NaCl particles were either added into the polymer solution with continuous stirring until the solution became pasty, thick and packed and then transferred to a petri dish (5 cm diameter) (Figure 3.2, A), or the polymer solution was poured to a petri dish containing NaCl crystals spread evenly (Figure 3.2, B). In both methods the solvent was evaporated completely in a desiccator kept at room temperature in a fume hood. The particulate leaching was performed using an ultrasonic bath for salt dissolution (Figure 3.2, C), using 100 mL of distilled water, each scaffold was washed three times, and between each wash samples of the water were taken, and conductivity was measured to guarantee elimination of the salt (Mettler Toledo Fiveeasy conductivity).

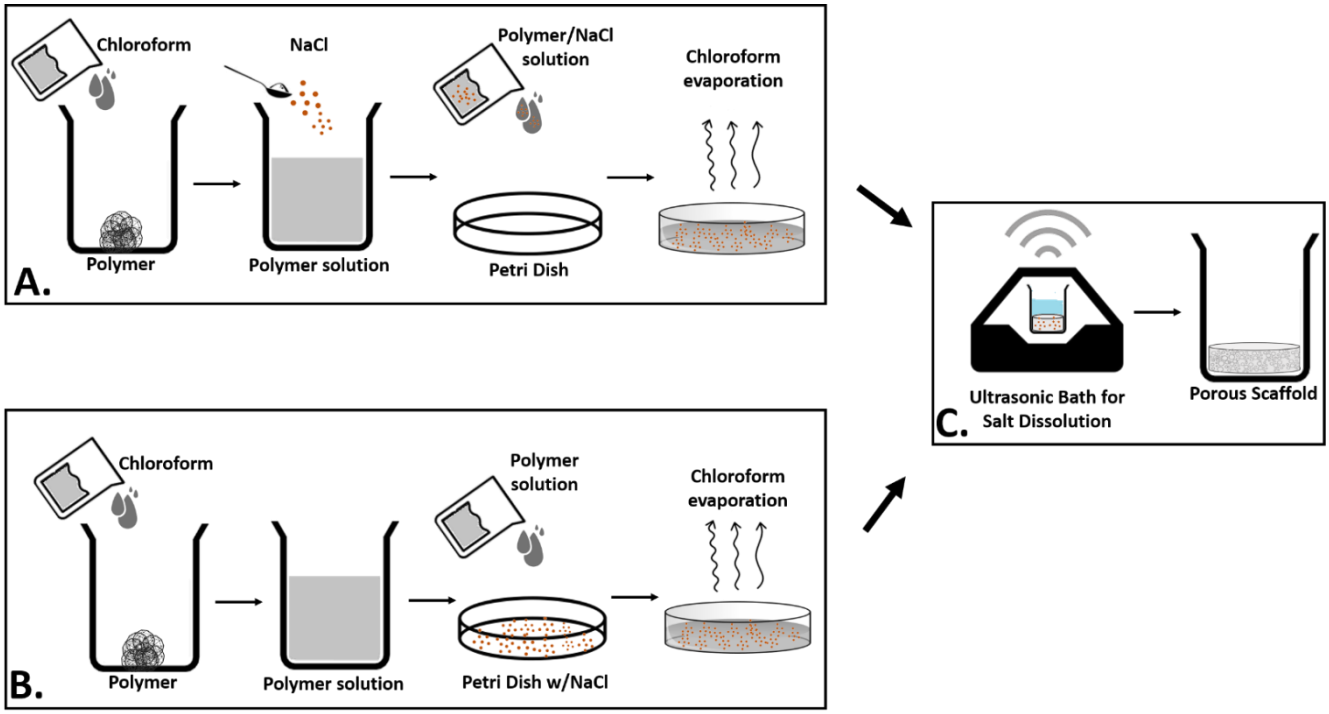

Figure 3.2- Schematic representations of the Solvent-Casting with Particulate Leaching.

3.2.1.3. Supercritical CO_2

The preparation of porous PHA scaffolds using sc-CO_2 was performed in a batch apparatus. P(HBHV) films were produced as described in section 3.2.1.1. and cut into circles with 1.5 cm diameter. The samples were loaded into the high-pressure vessel and then heated in a bath up to 40 °C. CO_2 was liquefied in a cooling bath containing water/ethylene glycol solution and then pumped with a pneumatic metering pump (Williams, V series), to the desired pressure. The pressure inside the vessel was controlled using a pressure transducer. The tests were performed at two different pressures, 200 and 280 bar, and soaking times, 1 and 6 hours. The system was closed in order to promote the foaming of the matrixes. Afterwards, the system was slowly depressurized. Figure 3.3 shows a schematic representation of the system used for the assays.

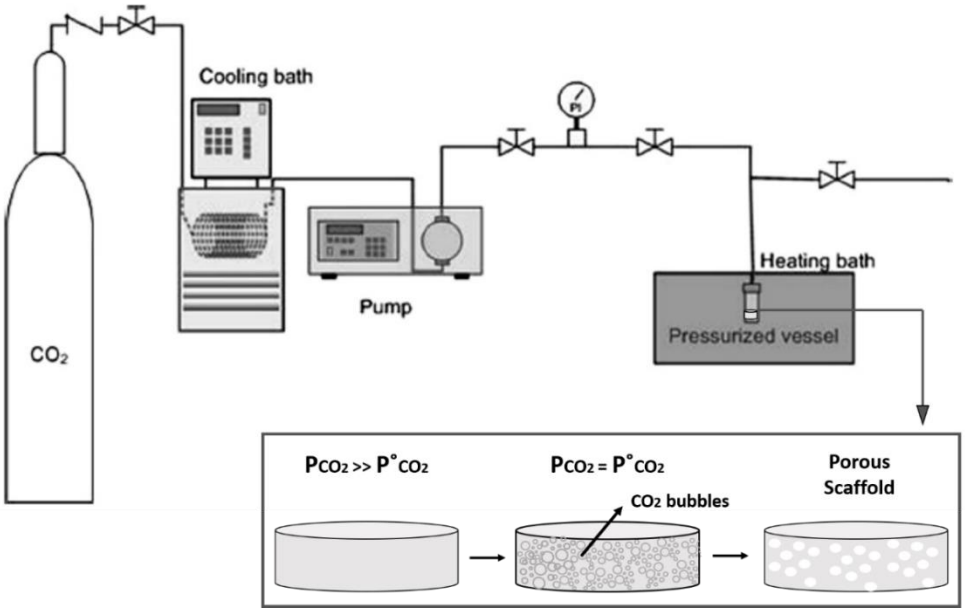

Figure 3.3- Schematic representation of the system used in super-critical foaming. Adapted (Martins, Craveiro, Paiva, Duarte, & Reis, 2014).

3.2.1.4. Water Emulsion Templating in Chloroform

Polymer solutions (4% w/v) of P(3HB), P(HBHV) and mcl-PHA were prepared using the same method as described in section 3.2.1.1. Once cooled, deionized water was added (1 mL), and the resulting solution was shaken until an emulsion was formed (no visible phase separation was observed). The emulsion was transferred to a glass petri dish (5 cm diameter) and the solvents (water and chloroform) were evaporated completely in a desiccator, in the fume hood, at room temperature. Figure 3.4 shows a schematic representation of the procedure.

For mechanical testing, films were produced using the same procedure, however, the volume of the solution was of 25 mL and it was transferred to a larger petri dish (10 cm diameter).

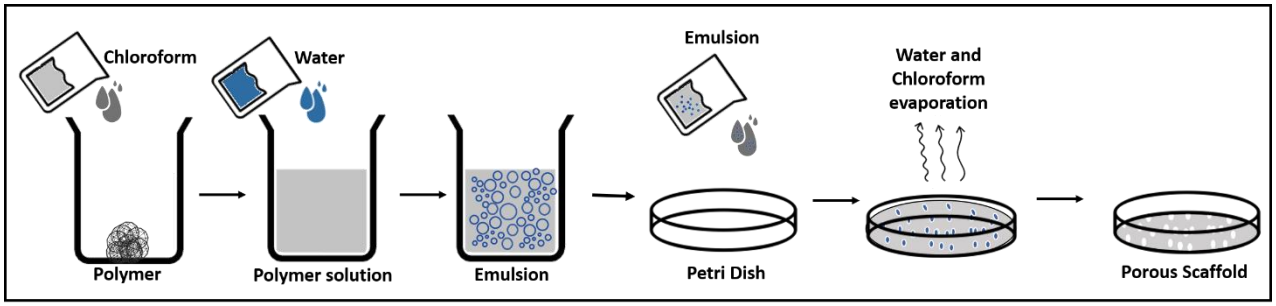

Figure 3.4- Schematic representation of the water emulsion in chloroform technique.

3.2.1.5. Electrospinning

All spinning solutions were prepared in chloroform. P(3HB) and P(HBHV) were dissolved at concentrations of 4% (w/w). mcl-PHA solutions were prepared at a concentration of 12% (w/w) and 25% (w/w). Blends of mcl-PHA with both P(3HB) and P(HBHV) were produced at a 4% (w/w) concentration, the weight compositional ratios between P(3HB)/P(HBHV) and mcl-PHA in the blend solutions were 50/50, 60/40 and 70/30. The solutions were mixed with a magnetic stirrer overnight.

The electrospinning apparatus consisted of a syringe pump (NE-1000 Programmable Single Syringe Pump, New Era PumpSystemsInc, USA), a high-voltage power supply (T1CP300304p, ISEG, Germany) and a homemade grounded rotating collector. Figure 3.5. shows a schematic representation of the system used.

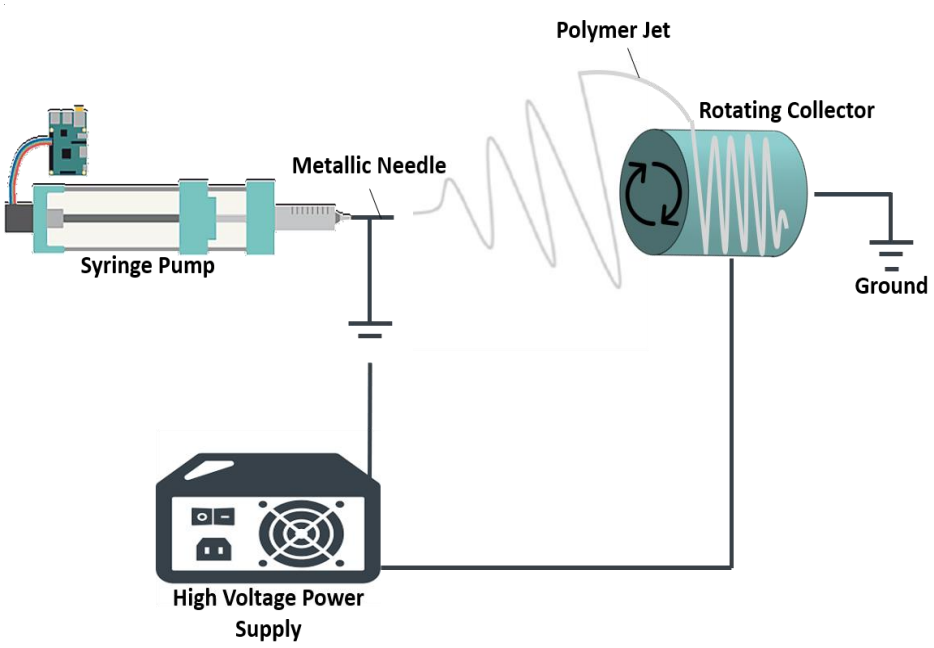

Figure 3.5- Schematic representation of the electrospinning setup used in the experiments.

A 5 mL syringe containing the polymer solution was loaded into the syringe pump, and a nozzle with an inner diameter of 0.508 mm was attached to the syringe. The electric field was applied by means of a high voltage supply. The electrospun mats were collected onto a grounded rotating collector. Different parameters were studied, namely, the effects of polymer concentration, applied voltage (8 Kv, 10 Kv, 12 Kv and 15 Kv) between nozzle tip and collector, polymer solution feeding rate (0.5 ml/h and 1 ml/h) and tip-to-collector distance (20 and 25 cm). The polymer jet was collected onto a glass slide for approximately 5 seconds and observed under an optical microscope (Visiscope TL524PI, VWR) equipped with a camera (Visicam3.0, VWR).The experiments were performed at room temperature.

3.2.2. Scaffolds Characterization

3.2.2.1. Scanning Electron Microscopy (SEM)

Scaffold morphology was assessed by Scanning Electron Microscopy (SEM). The samples were prepared for observation by freezing in liquid nitrogen, followed by the fracturing of the scaffolds to obtain smaller pieces. The samples were analysed using a bench scanning electron microscope (TM3030 Plus +Quantax 70, Hitachi, Japan) with an acceleration voltage of 15 kV. Images of the surface and cross-section were obtained. SEM images were processed by an imaging processing program (ImageJ).

3.2.2.2. Water Contact Angle

The surface wettability of the films was characterized by contact angle measurement by the sessile drop method. A drop of distilled water was manually deposited on the sample's surface with a small syringe. The software acquired ten images per sample and the tangent of each drop was determined by fitting its shape to a known mathematical function. Multiple replicates were performed, and the mean angle was determined. All images were acquired by CAM2008 (KSV Instruments Ltd, Finland).

3.2.2.3. Swelling in Water

Scaffold samples with a size of 1.0×1.0 cm^2 were weighted and their thickness was measured with a micrometre (Elcometer, England). The samples were immersed in 15 mL deionized water, in a closed vial, and kept at 30 ºC during 24 h. The swelling degree of the samples was calculated with the following equation:

$$\text{Swelling Degree}\ (\%) = \frac{X2 - X1}{X1} \times 100 \quad (6)$$

where X1 and X2 are, respectively, initial and final mass (g), respectively, of the samples measured at a different time period. The samples thickness after immersion was also measured.

3.2.2.4. Mechanical Tests

Scaffolds produced by emulsion and electrospinning were cut into rectangular-shaped strips (~30×15 mm) and the average thickness was measured. Tensile tests were performed at ambient temperature (22 °C) using a texture analyser (Food Technology Corporation, England) equipped with a 50 N load cell. The strips were attached on tensile grips A/TG and stretched with a crosshead speed of a 100 mm/min in tension mode until break. The stiffness of the membranes was determined by measuring the Young modulus (MPa), determined as the slope of the linear initial section of the stress-strain curve. The tensile stress at break (MPa) was calculated as the ratio of the maximum force to the films initial cross-sectional area. The elongation (strain) at break (%) was determined as the ratio of the extension of the sample upon rupture by the initial gage length. These properties were determined using four replicas throughout the experiment

3.2.2.5. Molecular Mass Distribution

SEC analysis was performed to scaffolds produced by emulsion and electrospinning as previously described in section 2.2.4.1.

3.2.2.6. Thermal Properties

DSC and TG analysis were performed to scaffolds produced by emulsion and electrospinning as previously described in section 2.2.4.2.

3.2.2.7. X-Ray Diffraction

X-ray diffraction analysis was performed to scaffolds produced by emulsion and electrospinning as previously described in section 2.2.4.3.

3.2.3. Scaffolds Surface Modification

3.2.3.1. Ozone and UV Radiation Treatment (UV – O_3)

Non-porous films were used to test optimal exposure time, films produced as described in section 3.2.1.1. were submitted to 15,30,60 and 120 minutes of treatment (Novascan PSD Pro Series (Novascan Technologies, Inc. EUA)). The water contact angle was measured before and after treatment and the decrease in water contact angle was calculated using the following equation:

$$\text{Water Contact Angle Decrease } (\%) = \frac{\theta 1 - \theta 2}{\theta 1} \times 100 \quad (7)$$

Where Θ1 is the water contact angle before UV/ozone and Θ2 is the water contact angle after UV/ozone treatment.

Scaffolds produced with the water emulsion technique were also tested, the samples were submitted to 120 minutes of treatment and SEM images of the scaffolds were taken to assess changes in morphology.

3.2.3.2. Oxygen (O_2) Plasma Treatment

Emulsion produced scaffolds were used to test optimal exposure time to oxygen plasma, other parameters were fixed, such as pressure (100 mTorr) and O_2 flow rate (10 sccm). The samples we submitted to 5,7 and 12 minutes of treatment (Alcatel GIR300 Reactive Ion Etching). To study the effects of the treatment, the water contact angle was measured, SEM images of the scaffolds were taken to assess changes in morphology and molecular mass distribution was studied by SEC.

3.3. Results and Discussion

3.3.1. PHA films

The biopolymers, namely mcl-PHA, P(3HB) and P(HBHV), produced previously were used to prepare films using the solvent casting method for the purpose of investigating the behaviour of non-porous films. In order to prevent the formation of cracks in the films, slow solvent evaporation was employed in a saturated chloroform environment inside a desiccator.

3.1.1. Morphology of PHA films

The PHA films that were obtained exhibited distinguishable characteristics. The mcl-PHA film was orange-tinted, flexible and displayed 69 µm in thickness (Figure 3.6, a.), the colour can be attributed to the presence of phenazines, orange-coloured pigments proved to be produced by *P. chlororaphis* (Laursen & Nielsen, 2004). P(3HB) films were 160 µm thick, compact, transparent and offered some degree of flexibility (Figure 3.6, d.). The P(HBHV) films were 190 µm thick and as compact as P(3HB), however, they presented an opaque white colour and displayed a higher degree of flexibility, (Figure 3.6, g.).

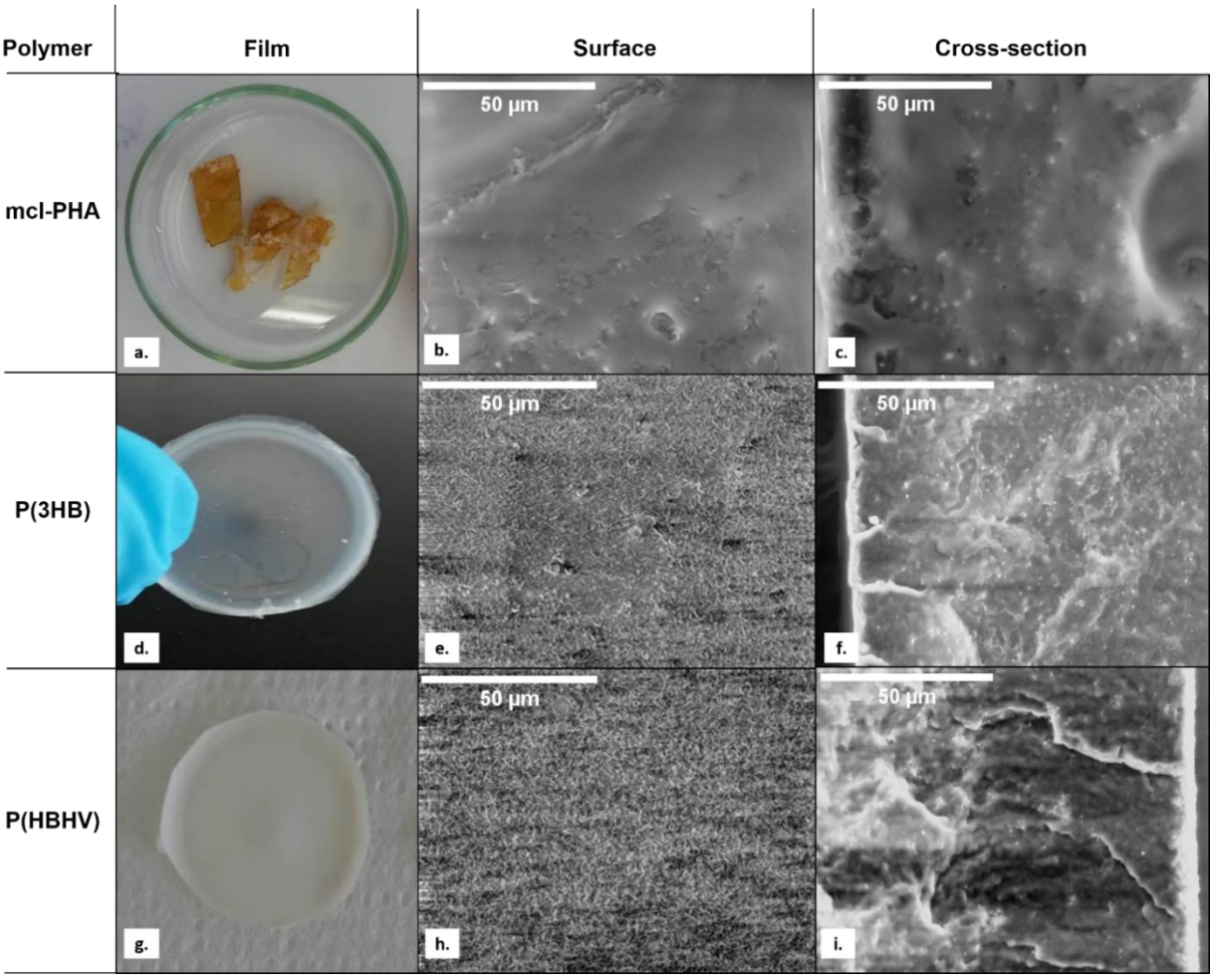

Figure 3.6- Macroscopic images of mcl-PHA (a), P(3HB) and P(HBHV) films produced by solvent casting; Surface (b, e, h) and cross-section (c, f, i) amplified 1500x images obtained by Scanning Electron Microscopy (SEM) analysis of the prepared PHA based films

The films obtained by solvent casting were studied using scanning electron microscopy (SEM) in order to evaluate their morphology (Figure 3.6). The mcl-PHA film presented a mainly homogenous and rough surface, it was not possible to observe any cracks in the film's surface and cross-section (Figure 3.6, b and c). However, there were some imperfections, such as small holes, that may be related to impurities in the polymer solution. The morphology of the mcl-PHA film produced in this film resembled others using polymers with similar composition found in the literature (Rebocho et al., 2019). The P(3HB) film showed an irregular surface, exhibiting a degree of rugosity that may be due to its intrinsic crystallinity (Figure 3.6, e), the cross-section demonstrated to have some texture, still it did not show significant porosity, which can be explained by the slow evaporation process. The structure was similar to other reported P(3HB) films morphology (Bergstrand et al., 2012; Bergstrand et al., 2014). The P(HBHV) copolymer films revealed an analogous structure to the P(3HB) films (Figure 3.6, i and j), presenting a rough surface with rugosity and a cross-section with no observable porosity, the morphology was also similar to other P(HBHV) films reported in the literature (Degeratu et al., 2010).

3.3.1.2. Water Contact Angle and Swelling in Water

With the aim of evaluating the hygroscopic and hydrophobic capacities of the PHA films that were produced, their swelling behaviour (or water uptake) and water contact angles were studied. For water uptake evaluation, a sample of a film of each polymer, mcl-PHA, P(3HB) and P(HBHV), was immersed in deionized water, at 30 ˚C for 24 h. The mcl-PHA, P(3HB) and P(HBHV) showed a negligible swelling degree of approximately, 2.6%, 2.1% and 1.4%, respectively, exhibiting no significant change in the mass or in the volume of the films after immersion. These results indicate that non-porous PHA films produced by solvent casting do not offer high interaction with water, which is undesirable for the application in question.

The water contact angle is an indicator of the wettability of a surface, measuring its degree of hydrophobicity or hydrophilicity. It depends on several factors including surface roughness, preparation and cleanliness. The smaller the contact angle, the larger the wetting tendency is, and a water contact angle higher than 90° is considered hydrophobic (Dwivedi et al., 2017; Jung & Bhushan, 2006).The surface water contact angles attained for the PHA films are presented in Table 3.1. The mcl-PHA films presented a surface contact angle (θ) of 89 ± 6˚ (Table 3.1), which can be considered hydrophobic. This value is lower than the reported in the literature for other mcl-PHAs, such as PHO (θ = 98˚) (Mauclaire et al., 2010) and mcl-PHAs with similar composition, like the one produced by *P. citronellolis* from waste apple waste that has the monomeric composition of HHx (2%), HO (22%), HD (68%), HDd (5%) and HTd (4%) with a water contact angle of 101˚(Rebocho et al., 2019), therefore, meaning that the mcl-PHA film produced in this work presents higher hydrophilicity than other reported mcl-PHAs. Factors such as surface roughness and cleanliness may be at fault.

The P(3HB) films presented a water contact of 81 ± 0.75˚ (Table 3.1), although considered hydrophilic, it is a higher value than what was demonstrated by other P(3HB) that display measurements in the range of 63-68.5˚ (Rathbone et al., 2010; Zhang et al., 2000 ; Misra et al., 2006), this may be to the roughness exhibited by these films (observed in the previous section regarding morphology) that contributes to a greater solid-liquid interface and leads to an increase of the surface contact comparatively to other P(3HB) films (Burton & Bhushan, 2005).

As for P(HBHV), the films showed the lowest water contact angle with θ = 78 ± 0.4˚ (Table 3.1), this measurement was also lower than reported for other P(HBHV) films, for instance different studies concerning P(HBHV) films with 8 wt% of 3HV presented a water contact angle of 84˚ and 95˚ (Rathbone et al., 2010; Degeratu et al., 2010), the higher hydrophobicity is probably correlated to the lower 3HV content than the P(HBHV) used in the films produced in this work (25 wt%). P(HBHV) also demonstrated higher hydrophilicity than the P(3HB) films proving that the addition of 3HV in P(3HB) results in lowering the water contact angle and consequently in the increase of hydrophilicity.

When compared to other materials commonly used in the biomedical field, specifically PLA, PCL and PLGA (Zubairi et al., 2016), all the films produced in this study exhibit higher hydrophilicity than PCL and PLGA that show water contact angles of 113˚ and 106˚, respectively

(Xia et al., 2013; Ajalloueian et al., 2014), yet PLA remains the most hydrophilic (θ = 65˚) (Tham et al., 2014).

Table 3.1- Water contact angles for the PHA films prepared with mcl-PHA, P(3HB) and P(HBHV) and comparison with values reported in the literature for different materials (PLA, polylactic acid; PCL, Polycaprolactone and PLGA, poly**(**lactic**-***co***-**glycolic acid)).

Material	Water Contact Angle (Θ)	Reference
mcl-PHA	89 ± 6	This study
	101 ± 0.9	(Rebocho et al.,2019)
	98 ± 2	(Mauclaire et al., 2010)
P(3HB)	81 ± 0.75	This study
	63	(Rathbone et al., 2010)
	68.5	(Zhang et al., 2000)
	66	(Misra et al., 2006)
P(HBHV)	78 ± 0.4	This study
	84	(Rathbone et al., 2010)
	95	(Degeratu et al., 2010)
PLA	65	(Tham et al., 2014)
PCL	113	(Xia et al., 2013)
PLGA	106 ± 5.2	(Ajalloueian et al., 2014)

3.3.2. Solvent-Casting with Particulate Leaching (SCPL) Scaffolds

With the purpose of producing porous scaffolds using the polymers produced in this work, mcl-PHA, P(3HB) and P(HBHV), the solvent-casting procedure with particulate leaching (SCPL) was performed. This technique allows the incorporation of particles of a leachable porogen, in this case, sodium chloride (NaCl), into the polymer solution forming a thick paste that is left in a desiccator for solvent evaporation.

3.3.2.1. Scaffold Morphology

In this study, two techniques of particulate incorporation were investigated: (A) mixing the polymer solution with NaCl and (B) pouring the polymer solution over a layer of the porogen.

Regarding technique A, macroscopically all polymers produced homogenous scaffolds (Figure 3.7). mcl-PHA scaffolds were 280 µm thick and maintained the polymer's orange tint, transparency and elastic properties (Figure 3.7, a.), however when examining the scaffold using scanning electron microscopy (SEM) in order to evaluate their morphology (Figure 3.7, b. and c.), it was possible to determine that the technique was not successful in implementing porosity, as images of the surface and cross-section present no visible pores, and bear a resemblance to mcl-PHA non-porous films.

Fabrication with P(3HB) gave origin to homogenous scaffolds with a thickness of 190 µm (Figure 3.7, d), In contrast to non-porous films they presented an opaquer white colour. Unfortunately, when analysing SEM imaging of the scaffold, it seems to not present any pores in the surface (Figure 3.7, e), while displaying a level of roughness compared to non-porous P(3HB) films, still, in the cross-section rounded structures can be observed that may be due to the leaching of NaCl (Figure 3.7, f).

Concerning P(HBHV) scaffolds, they were similar to P(3HB) films macroscopically (Figure 3.2, g), presenting a 180 µm thick, homogenous, white and opaque scaffold. Though, when examining the scaffold using SEM, it proved to be more porous on the surface (Figure 3.7, h) relatively to the other materials scaffolds, although the pores were very small. Moreover, the cross-section also showed to hold a degree of porosity (Figure 3.7, i).

Solvent casting with particulate leaching with technique B led to scaffolds with different characteristics than the ones fabricated with the previous technique. The mcl-PHA scaffolds were 180 µm thick and presented a white colour, with a slight orange tint, much less evident than with the scaffold produced with technique A (Figure 3.8, a). SEM imaging showed no noticeable pores on the surface (Figure 3.8, b), but the cross-section presented a few large pores that can be related to the leaching of NaCl (Figure 3.8, c). In addition, with this technique a few scaffolds were not able to withstand the ultrasonic bath without disintegrating, this might have been due to the use of excessive salt. Nonetheless, mcl-PHA does not seem an appropriate polymer to be employed with this technique since it was not able to produce homogeneously porous scaffolds.

Furthermore, employing technique B for P(3HB) scaffolds gave origin to white, opaque, foam-like scaffolds with a thickness of 470 µm (Figure 3.8, d), moreover, they were also highly brittle and would easily crack. The investigation through SEM demonstrated a somewhat porous surface

when compared to the previous technique (Figure 3.8, e), and the cross-section revealed to a layered and porous morphology (Figure 3.8, f), that may be responsible for the foam-like structure of the scaffold.

The use of the P(HBHV) polymer with this second technique allowed the fabrication of white, opaque, foam-like, 340 µm thick scaffolds (Figure 3.8, g), similarly to P(3HB), but with less fragility which may be linked to the higher flexibility of the polymer. When examining the scaffold using SEM in order to evaluate its morphology, a visible porous surface can be observed, comparable to the one exhibited by the P(HBHV) scaffold using the previous technique (Figure 3.8, h). The cross-section showed a layered porous structure, comparable to a P(HBHHx)/P(3HB) blend scaffold produced with solvent casting with particulate leaching reported in the literature (Zhao et al., 2003).

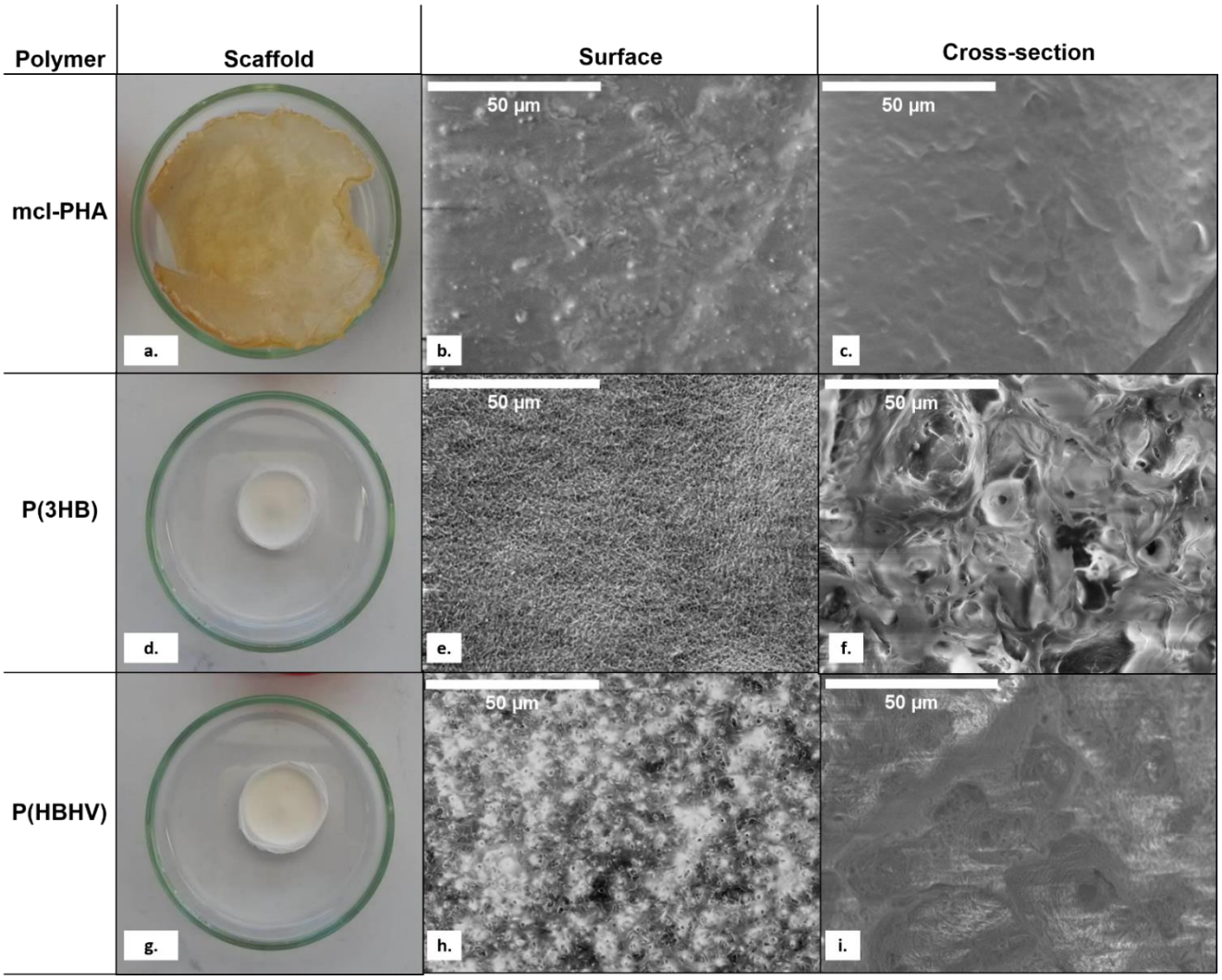

Figure 3.7- Macroscopic images of mcl-PHA (a.), P(3HB) (d.) and P(HBHV) (g.) scaffolds produced with solvent casting with particulate leaching with polymer solution and porogen mixing; Surface (b, e, h) and cross-section (c, f, i) amplified 1500x images obtained by Scanning Electron Microscopy (SEM) analysis of the prepared PHA based scaffolds.

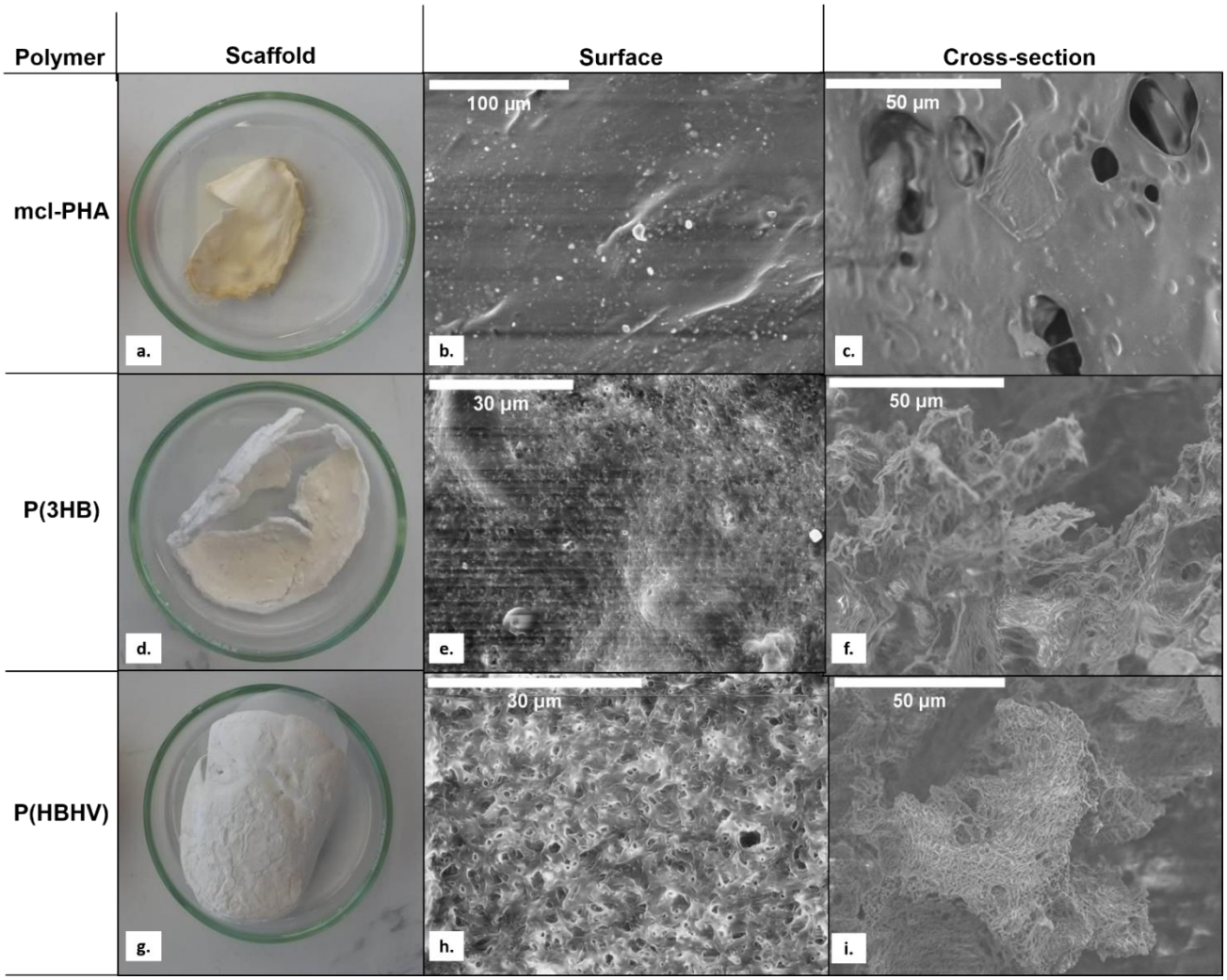

Figure 3.8 - Macroscopic images of mcl-PHA (a.), P(3HB) (d.) and P(HBHV) (g.) scaffolds produced with solvent casting with particulate leaching with polymer solution poured onto porogen; Surface (b, e, h) and cross-section (c, f, i) amplified 1500x images obtained by Scanning Electron Microscopy (SEM) analysis of the prepared PHA based scaffolds.

3.3.2.2. Water Contact Angle and Swelling in Water

Swelling in water and water contact angle were measured for the scaffolds fabricated through SCPL. Concerning mcl-PHA based scaffolds, the water contact angle measured at 99.2 ± 5˚ using the technique A (mixing the porogen onto the polymer solution) and 89 ± 0.2˚ when using the technique B (pouring the polymer solution onto the NaCl) (Table 3.2). The value for technique A is higher than for non-porous mcl-PHA films, probably due the increased roughness of salt particles that were not completely leached out, on the other hand the value for technique B is the same as for non-porous films, indicating that this technique does not highly affect the water contact angle of mcl-PHA based scaffolds. Regarding water uptake, there was negligible swelling using technique A (0.63%), however, there was a higher swelling percentage when technique B was implemented (54.5%) (Table 3.2), proving that this technique can improve the penetration of water into mcl-PHA scaffolds. Even so, this value is lower than what is reported for other biomaterials, such as PLA (75-290%) (Choudhury et al., 2015) and PLGA (630%) (Pamua et al., 2004).

P(3HB) based scaffolds presented a water contact angle of 84.7 ± 0.4˚ and 72 ± 1.2˚ for techniques A and B, respectively (Table 3.2). Again, as for mcl-PHA, the value is higher for technique A than for B, which may be correlated to roughness associated with undissolved NaCl, although considered hydrophilic, these values were below the reported for other materials, such as PLA (68.7˚) (Zhu et al., 2015). The swelling degree was 76.6% for technique A and 175% for technique B (Table 3.2), which are considerably divergent values that imply that the second technique is much more effective in increasing water uptake of a scaffold. These values are in the range of what was reports for PLA (75-290%) (Choudhury et al., 2015), although lower than what is reported for PLGA (630%) (Pamua et al., 2004).

Scaffolds fabricated using P(HBHV) measured water contact angles of 70 ± 0.3˚ and 80.2 ± 1.1˚ for techniques A and B, respectively (Table 3.2), in contrast to the other polymers the hydrophilicity was higher for technique A, with a water contact angle among the reported for PLA (68.7˚). In respect to water uptake, similarly to P(3HB), the swelling was much more significant with technique B (181%) than with technique A (48.3%) (Table 3.2).

These results indicate that between the A and B, the ladder seems to be the most promising method for scaffold fabrication, as it allowed for mostly higher swelling in water and lower water contact angles. Moreover, P(3HB) and P(HBHV) are more suitable materials to use with this technique, as mcl-PHA did not yield satisfactory results, yet, all the scaffolds produced did not offer the pore size and distribution desired for the final application, however, this could be overcome by the use of other porogens, as well as their size optimization. For instance, P(HBHV) porous scaffolds fabricated trough particulate leaching reported pores of larger dimensions using gelatine (200-300 μm) than with sodium chloride (5-25 μm) (Degeratu et al., 2010). In addition, one of the disadvantages using the SCPL technique is the existence of porogen residual, this can also be resolved by using more effective leaching techniques, such as dialysis, opposed to an ultrasonic bath (Zubairi, 2015).

Table 3.2- Water contact angles for the PHA scaffolds prepared with mcl-PHA, P(3HB) and P(HBHV) by solvent casting with particulate leaching and comparison with values reported for different materials (PLA, polylactic acid; PCL, Polycaprolactone and PLGA, poly(lactic-*co*-glycolic acid)).

Technique	Polymer	Water Contact Angle (Θ)	Swelling in Water (%)	References
A	mcl-PHA	99.2 ± 5	0.63	This study
	P(3HB)	84.7 ± 0.4	76.6	
	P(HBHV)	70.0 ± 0.3	48.3	
B	mcl-PHA	89.1 ± 0.2	54.5	This study
	P(3HB)	72.0 ± 1.2	175	
	P(HBHV)	80.2 ± 1.1	181	
A	PLA	n.a	75-290	(Choudhury et al., 2015)
B	PLA	68.7 ± 2.3	n.a	(Zhu et al., 2015)
A	PCL	135	n.a	(Limpanuphap et al., 2007)
A	PLGA	n.a	630	(Pamua et al., 2004)

3.3.3. Supercritical CO_2 Scaffold Fabrication

Supercritical CO_2 as a foaming agent for porous scaffold fabrication was investigated using P(HBHV). The studies were performed at two different pressures, 200 and 280 bar, and soaking times, 1 and 6 hours.

3.3.3.1. Scaffold Morphology

Macroscopically, the P(HBHV) film did not present any significant difference after the foaming procedure, regardless of soaking time, indicating immediately that the polymer had a low affinity for CO_2, hindering the process, since the main requirement of the CO_2 foaming process is that CO_2 can be dissolved in a sufficient amount in the polymer (Duarte et al., 2009).

The scaffold obtained with the higher soaking time (6 hours) was examined using scanning electron microscopy (SEM). The surface of the scaffold presented a certain degree of porosity (Figure 3.9, a, b), however, the pores showed very small dimensions. The cross-section also displays observable porosity at high image amplification (Figure 3.9, d), but there is no communication or interconnectivity. These images confirm that, although some CO_2 was dissolved, causing a small degree of porosity, the solubility of CO_2 is not high in P(HBHV).

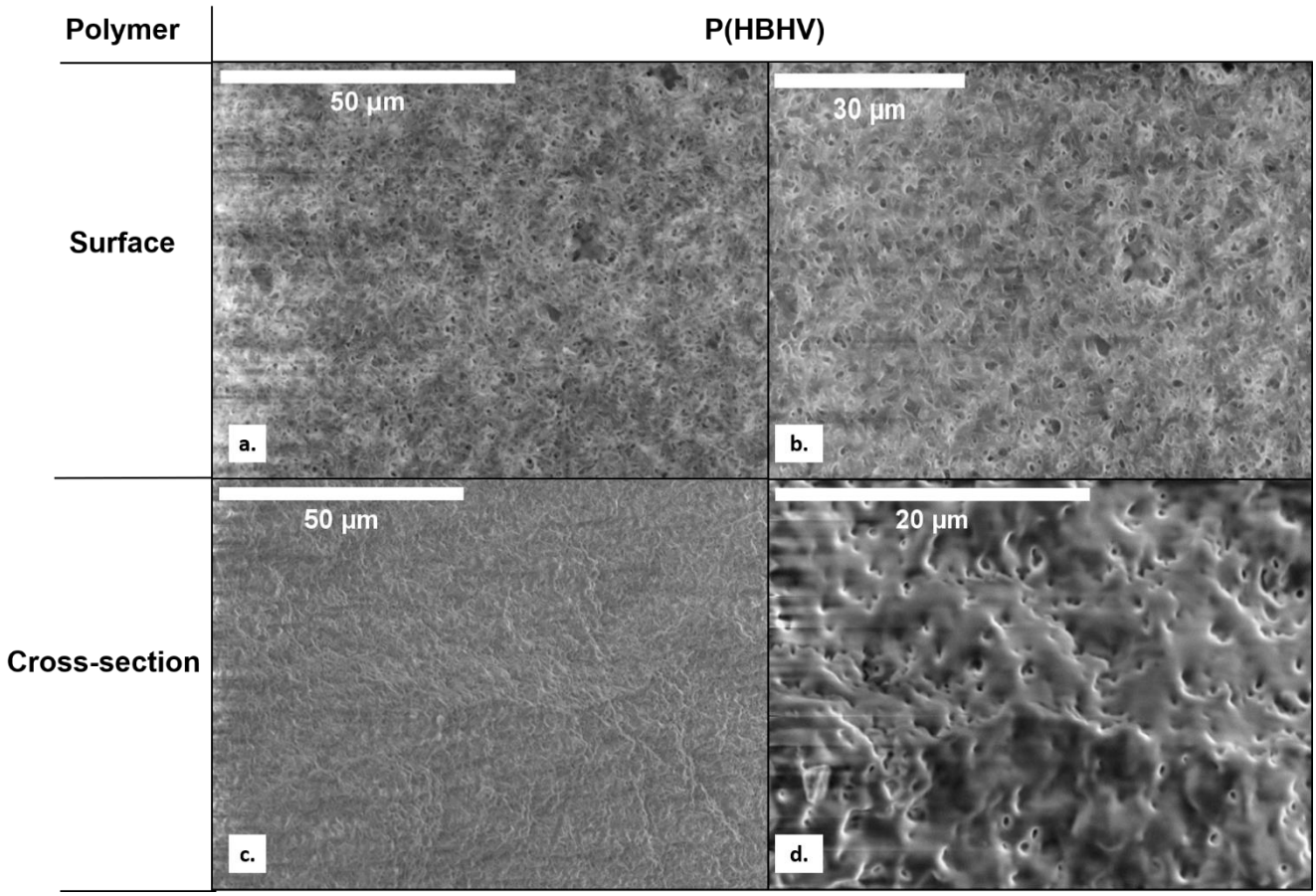

Figure 3.9 - Images obtained by Scanning Electron Microscopy (SEM) analysis of P(HBHV) scaffold fabricated by supercritical CO_2 foaming; a. surface amplified x 1.8k; b. surface amplified x 2k; c. cross-section amplified x 1.5k; d. cross-section amplified x 5k.

3.3.3.2. Water Contact Angle and Swelling in Water

Two different types of scaffolds fabricated trough supercritical CO_2 were studied regarding water contact angle and swelling in water: scaffolds processed in milder conditions with a pressure of 200 bar and soaking time of one hour, and scaffolds processed under harsher conditions with pressure and soaking time of 280 bar and 6 hours, respectively.

The water contact angles for the scaffolds processed in milder and harsher conditions, presented similar values of 96.4 ± 2.13˚ and 96.5 ± 0.18˚, respectively. Both measurements are higher than 90˚, which means that the surface of the scaffolds can be considered hydrophobic. These values are higher than the water contact angle for films prior to soaking, which might be related to increased surface roughness after the foaming procedure.

Concerning water uptake, the scaffolds processed in harsher conditions demonstrated a higher water uptake (18.5%) than the ones processed in mild conditions, which displayed swelling of 4.8%, that can be considered negligible. The value for scaffolds processed in higher pressure and soaking time proves that foaming was successful to a degree of increasing water uptake, however, the value is still considerably low.

CO_2 has plasticising properties that work by reducing the glass transition temperature, which means that this technique may not be favourably used in polymers with high crystallinity or high glass transition temperatures and is more commonly applied to semi-crystalline or amorphous polymers (Duarte et al., 2009). scl-PHAs offer low glass transition temperature (5-9 ˚C) (Tan et al., 2016), similar to other materials that have been successfully foamed using this process, such as PLGA (T_g = 36˚C) that generated interconnected pores and porosities as high as 89% using supercritical CO_2 (L. Singh et al., 2004), however the PLGA used in that study was amorphous when compared to the P(HBHV) used in this work, which could be the reason why the process was not as successful. This might indicate that scl-PHAs present an intrinsic difficulty to be foamed owing to their higher crystallinity, however, adding chain extender additives has been demonstrated to improve foamability in biopolyesters (Ventura et al ., 2016). Moreover, using mcl-PHA which is much more amorphous than P(HBHV) or P(3HB), while presenting a low glass transition temperature, maybe a good strategy, nevertheless, due to time constraints such was not possible to be investigated. Other than the material that is employed, the processing conditions like pressure, temperature and soaking time may need tuning as they are of utmost importance in controlling the pore size and structure of the scaffolds (Tai et al., 2007).

3.3.4. Water Emulsion Templating for Scaffold Fabrication

Water-in-chloroform emulsion template combined with solvent casting was studied as a method to produce porous scaffolds using the polymers produced in this work, namely, mcl-PHA, P(3HB) and P(HBHV).

3.3.4.1. Scaffold Morphology

The scaffolds obtained by emulsion templating demonstrated distinct characteristics. mcl-PHA water-in-chloroform emulsions were not successfully able to template porosity onto the scaffolds. Macroscopically (Figure 3.10, a) we can observe a typical PHA film, comparable to the ones produced by solvent casting, furthermore, there is a hole in the film that was due to the water that did not mix with the chloroform. SEM imaging confirms that the process was ineffective in introducing porosity in mcl-PHA, surface and cross-section images (Figure 3.10, b and c) demonstrate a homogenous film opposed to a porous scaffold.

P(3HB) emulsion templated scaffolds demonstrated a thickness of 479 ± 29 µm and an opaque white colour (Figure 3.10, d), the solvent evaporation occurred extremely fast, even when the samples were placed in the desiccator, leading to shrinking and curling of the scaffold. When observed under SEM, the P(3HB) scaffolds demonstrated some roughness in the surface (Figure 3.10, e), still, no discernible porosity was displayed, likely due to the quick evaporation on the scaffold surface. Nonetheless, the cross-sections revealed distinguishable porosity, with spherical pores of various sizes that appear to be interconnected by windows, which is the typical morphology for an emulsion templated scaffold (Cameron, 2005). The size of the pores was estimated using imaging software and they are mainly in the 0.78-3.58 µm size interval (Figure G in Appendices). The morphology of the cross-section is similar to other P(3HB) water emulsion templated scaffolds (Bergstrand et al. 2012, 2014).

Concerning P(HBHV), the scaffolds showed a thickness of 264 ± 23 µm and a similar white opaque colour (Figure 3.10, g), though, in contrast to P(3HB), the samples did not tend to curl, as chloroform evaporation was more gradual. SEM images proved that there was some porosity on the surface (Figure 3.10, h), and as well in the cross-section (Figure 3.10, i), the pores seemed interconnected and their size was mostly in the 1.35-5.0 µm range (Figure H in Appendices), exhibiting pores with slightly larger dimensions than P(3HB) and comparable size to other P(HBHV) scaffolds produced by emulsion templating reported in the literature (3-7 µm) (Ruiz et al., 2011).

In hopes to improve porosity, higher concentrations of water were implemented, maintaining P(HBHV) concentration, but increasing the water ratio (Figure 3.11), yet, the scaffolds displayed increased heterogeneity and mesh-like macrostructures that would not be suitable for this type of work, since scaffolds require homogeneity.

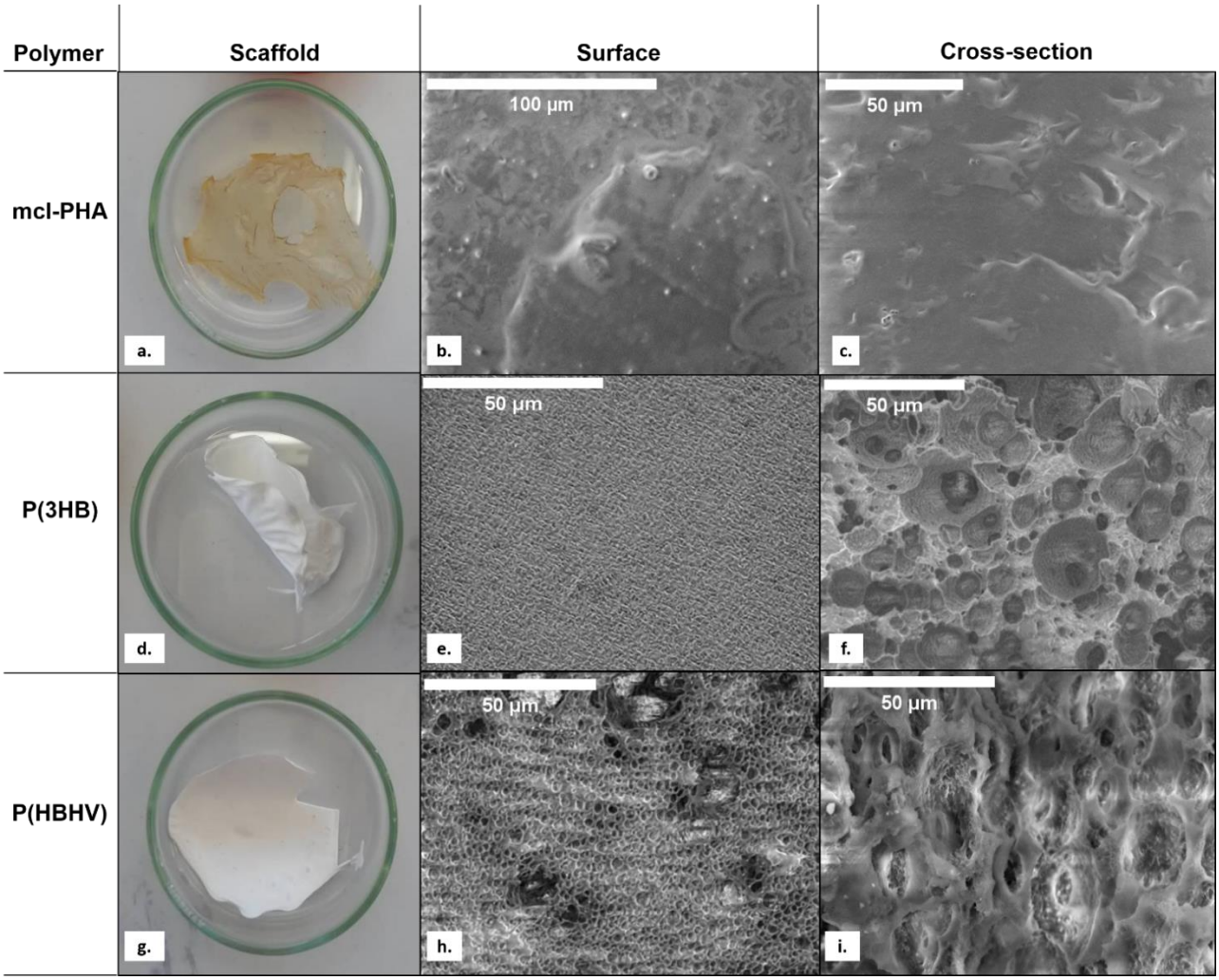

Figure 3.10- Macroscopic images of mcl-PHA (a.), P(3HB) (d.) and P(HBHV) (g.) scaffolds produced with emulsion templating; Surface (b, e, h) and cross-section (c, f, i) amplified 1500x images obtained by Scanning Electron Microscopy (SEM) analysis of the prepared PHA based scaffolds.

Figure 3.11- P(HBHV) scaffolds with different polymer solution: water ratios (2:20; 3:20 and 5:20).

3.3.4.2. Water Contact Angle and Swelling in Water

Regarding the water contact angle, the scaffolds produced with all three polymers demonstrated to have values under 90˚, with measurements of 65.7˚ ± 2.2, 79.7˚± 0.7 and 48.6˚± 2.7 for mcl-PHA, P(3HB) and P(HBHV), respectively. This proves that the emulsion template technique produces somewhat hydrophilic surfaces, with P(HBHV) suffering the biggest decrease in contact angle comparatively to non-porous P(HBHV) films.

Water uptake for mcl-PHA was negligible (2.9%), suggesting that the elastomer film did not acquire porosity with this technique. However, it is important to note that the emulsion template technique employed in this work was very simplified, its effectiveness can be improved by the tailoring of the method to each type of polymer, since they may require different treatments due their distinguishable intrinsic physical and chemical properties. Adding surfactants could be a way to increase emulsion stability (Cameron, 2005), sorbitan monooleate (Span 80) for example, is a widely used surfactant that has been applied to P(3HB) emulsions before (Bergstrand et al., 2012). Moreover, introducing electrolyte content in the water phase, has shown to have an effect in average pore diameter (Cameron, 2005), for instance, increasing amounts of lithium sulphate monohydrate in the water phase of a P(3HB) emulsion templated scaffold led to higher pore diameter and porosity (Bergstrand et al., 2012). The addition of electrolyte prevents or limits the occurrence of Ostwald ripening, an event where large droplets grow at the expense of smaller ones that leads to coalescence and eventually emulsion break down (Cameron, 2005), which might have occurred during mcl-PHA emulsion formation.

Concerning the water uptake of P(3HB) and P(HBHV) films, they demonstrated swelling in water of 31.8% and 42.6%, respectively. This confirms that both polymer scaffolds offer a degree of porosity, allowing the penetration of water, with P(HBHV) exhibiting the most water uptake percentage. These values are higher that of what was showed by P(3HB) emulsion templated scaffold produced with Span 80 as a surfactant and without electrolyte addition (15%) but lower of what was reported for the same method but with the addition of lithium sulphate monohydrate as an electrolyte in the water phase (65-75%) , which implies that adding a electrolyte in the water phase in future work would be of added value (Bergstrand et al., 2012).

Furthermore, P(3HB) and P(HBHV) scaffolds produced by emulsion templating show promise as 3D-cell culture scaffold, thus, further characterization of the scaffolds was performed.

3.3.4.3. Physical and Thermal Properties

When transforming a raw PHA into a porous scaffold, using for example emulsion templating and solvent casting, polymer processing is performed, which can be defined as the manufacturing activity of converting raw polymeric materials into finished products that display desired shape, microstructure and properties (Vlachopoulos & Strutt, 2003). In order to assess the effect of the scaffold fabrication process on the unmodified polymers, thermal properties and molecular weight distribution were examined, since they are a result of the shape and the way in which molecules are organized in the solid-state (Jasso-Gastinel et al., 2016).

Melting temperature, T_m, and degradation temperature, T_{deg}, did not suffer major alterations for both polymers. P(3HB) maintained the same T_m (175 ˚C) (Table 3.3) and had a slight decrease in T_{deg} from 293 to 291 ˚C (Table 3.3). On the other hand, P(HBHV) maintained the same T_{deg} (292˚C) (Table 3.3) and had a minor reduction in T_m from 176 to 173 ˚C (Table 3.3). Moreover, melting enthalpy (ΔHm), as well as the crystalline fraction (X_c), lowered for both polymers. For P(3HB) ΔHm lowered from 60.3 to 56.2 J g^{-1} and X_c from 41.3 to 38.5% (Table 3.3). Concerning P(HBHV), there was a decrease in ΔHm to 24.7 J g^{-1} from the original 26 J g^{-1} and X_c lowered from 17.8 to 16.9% (Table 3.3). When thermoplastics, such as P(3HB) and P(HBHV), are heated above their glass transition, T_g, they soften and flow as viscous fluids, after shaping and rapid solidification by cooling and solvent evaporation, they develop specific microstructures with different degrees of crystallinity and/or molecular orientation (Vlachopoulos & Strutt, 2003). The decrease in crystallinity can be related to the quick solidification of the scaffolds, as the polymer molecules freeze quickly they may not be able to form as many crystals and therefore, maintain more of the disordered arrangement as they go into the solid-state (Jasso-Gastinel et al., 2016). In accordance, when analysing the x-ray diffractogram from raw P(HBHV) and the scaffold produced by the same polymer (Figure 3.12) it's possible to observe very similar profiles, with two peaks located at 2θ = 14 and 17˚, as well as an amorphous phase represented by a broad hump at around 2θ = 22˚ and 26˚, however, the peaks corresponding to the crystalline phase for raw P(HBHV) display slightly higher intensities, due the greater degree of crystallinity.

Concerning molecular weight (M_w), there was an accentuated decrease in this parameter for both polymers. P(3HB) exhibited a decrease from 5.2 x 10^5 Da to 3.8 x 10^5 Da (Table 3.3) and P(HBHV) lowered its M_w from 5.6 x 10^5 Da to 4 x 10^5 (Table 3.3). This can be related to degradation that the polymers could have undergone during the emulsion templating process. Polymer degradation includes any changes in both the chemical structure and physical properties of polymers that leads to the loss of properties, such as the reduction in M_w, under the influence of processing conditions, or environmental factors. It is likely that the PHAs suffered polymer abiotic degradation through hydrolysis of the ester bonds, where there is random hydrolytic cleavage of functional groups, leading to a decrease in M_w (Wu & Wang, 2001). The polydispersity index (PDI) of the scaffolds did not vary much from the values of the raw polymers, with P(3HB) having a decrease from 1.80 to 1.75, and P(HBHV) an increase from 1.60 to 1.69 (Table 3.3), indicating that polymer processing did not greatly affect the size dispersity of polymer molecules.

Table 3.3- Thermal properties, melting enthalpy, degree of crystallinity, Mw, M_n and PDI of raw P(3HB) and P(HBHV), as well as of the scaffolds produced using these polymers trough emulsion templating.

PHA	Identification	T_m (˚C)	T_{deg} (˚C)	X_c (%)	ΔH_m (J g^{-1})	M_W (x 10^5 Da)	M_N (x 10^5 Da)	PDI
P(3HB)	Unmodified	175	293	41.3	60.3	5.2	2.9	1.80
	Emulsion Templated Scaffold	175	291	38.5	56.2	3.8	2.2	1.75
P(HBHV)	Unmodified	176	292	17.8	26.0	5.6	3.5	1.60
	Emulsion Templated Scaffold	173	292	16.9	24.7	4.0	2.8	1.69

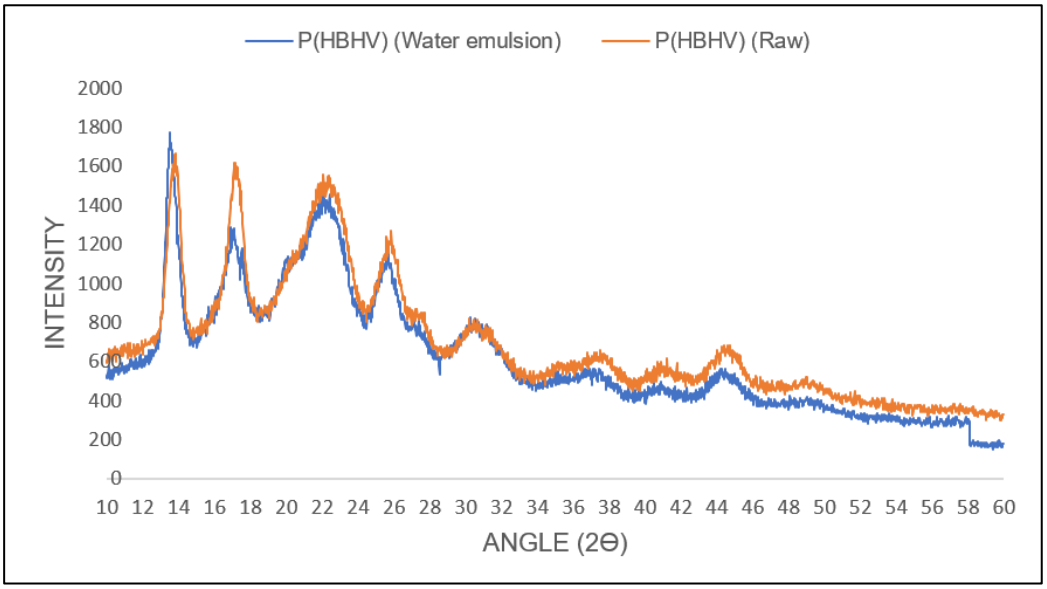

Figure 3.12- X-ray diffractogram for raw P(HBHV) and emulsion templated P(HBHV) scaffold.

3.3.4.4. Mechanical Properties

It is of great importance to be familiar with some basic mechanical properties of the scaffolds before its application, thus, mechanical tests were performed in order to study stress-strain behaviour and determinate tensile strength at break, deformation at break and Young Modulus.

As shown in Table 3.4, P(3HB) and P(HBHV) presented tensile strength at break values of 3.18 ± 0.19 MPa and 3.35 ± 0.54 MPa, respectively. Tensile strength is the stress required to break a sample by stretching it (Balani et al., 2015). The scaffolds values are quite similar, indicating that they require the same amount of stress until break. These values are much higher than emulsion templated acrylate scaffolds reported in the literature for bone tissue engineering (0.11±0.01-2.03±0.33 MPa) (Owen et al., 2016), but only slightly lower than the values presented by fibrin emulsion templated scaffolds for skin regeneration (4.25 ± 0.63-5.13 ± 0.51 MPa) (Lim et al., 2018). Furthermore, collagen emulsion templated scaffolds for skin regeneration present significant higher tensile strength at break with values in the range of 7.87 ± 1.45-9.65 ± 2.81 MPa (Lim et al., 2018). Tensile strength mainly depends on molecular weight, degree of cross-linking and crystallinity of a material (Balani et al., 2015), thus, the observed differences are linked to the difference in those properties between the various materials.

Deformation at break is a measure of ductility, being the percentage change in the length of the material before fracture (Balani et al., 2015). P(3HB) and P(HBHV) showed deformation at break values of 13.6 ± 0.44 % and 14.8 ± 1.74 %, respectively (Table 3.4). P(HBHV) presented a higher value than P(3HB) which is expected since it is slightly more elastic than P(3HB) due to its monomer composition, demonstrating to be more ductile and less resistant to deformation. These values are among the ones reported for emulsion templated acrylate-based scaffolds reported in the literature for bone tissue engineering (2.60 ± 0.61-21.86% ± 2.87) (Owen et al., 2016).

Young modulus is a measure of the stiffness of a material (Balani et al., 2015). P(3HB) presented a Young modulus of 0.07 ± 0.009 MPa and P(HBHV) a higher value of 0.11 ± 0.02 MPa (Table 3.4), suggesting superior stiffness than P(3HB), closer to the reported for polystyrene-based scaffolds produced trough emulsion templating (0.15 ± 0.01 MPa) (Naranda et al., 2016). However, both these values can be considered quite low when compared to other scaffolds intended for cell culture and tissue engineering. For example, fibrin and collagen scaffolds emulsion templated scaffolds for skin regeneration exhibited a Young modulus of 1.25 ± 0.74-2.14 ± 0.34 MPa and 1.12 ± 0.29-2.01 ± 0.11 MPa, respectively, and silk fibroin emulsion templated scaffolds for tissue engineering displayed values of 0.228-0.364 MPa (Wen et al., 2018).

Table 3.4- Mechanical properties of scaffolds prepared by emulsion templating and comparison with other scaffolds of different materials produced by emulsion templating in the literature; n.a- non-available.

Material	Tensile Strength at Break (MPa)	Deformation at break (%)	Young Modulus (MPa)	Reference
P(3HB)	3.18 ± 0.19	13.6 ± 0.44	0.07 ± 0.009	This Study
P(HBHV)	3.35 ± 0.54	14.8 ± 1.74	0.11 ± 0.02	This Study
Polystyrene-Based	n.a	n.a	0.15 ± 0.01	(Naranda et al., 2016)
EHA/IBOA*	0.11 ± 0.01-2.03 ± 0.33	2.60 ± 0.61-21.86 ± 2.87	0.36 ± 0.04-63.01 ± 9.13	(Owen et al., 2016)
Collagen	7.87 ± 1.45-9.65 ± 2.81	n.a	1.25 ± 0.74- 2.14 ± 0.34	(Lim et al., 2018)
Fibrin	4.25 ± 0.63-5.13 ± 0.51	n.a	1.12 ± 0.29-2.01 ± 0.11	(Lim et al., 2018)
Silk Fibroin	n.a	n.a	0.228-0.364	(Wen et al., 2018)

***EHA- 2-ethylhexyl acrylate; IBOA- isobornyl acrylate**

3.3.5. Electrospinning for Fibrous Scaffold Fabrication

In order to produce porous fibrous scaffolds, electrospinning was employed using P(3HB), P(HBHV), mcl-PHA and polymer blends.

3.3.5.1. Electrospinning Parameter Optimization

The electrospinning process is conditioned by several factors, including the properties of the spinning solution (solvent, polymer concentration, viscosity and solution conductivity), process parameters (applied electric field, distance between the needle and collector, flow rate, and needle diameter) and environmental parameters (relativity humidity and temperature) (Haider et al., 2018). Therefore, it's crucial to optimize the electrospinning process for successful fabrication of smooth and bead-free electrospun fibres.

3.3.5.1.1 Spinning Solutions Optimization

In this work 4 wt% P(3HB) and P(HBHV) polymer solutions were used with chloroform as a solvent, both spinning solutions displayed satisfactory viscosity and were easily spun. More concentrated solutions tended to hamper the flow of the solution and to block the tip of the metallic needle. Chloroform demonstrated to be an appropriate solvent as its volatility allowed solvent evaporation during fibre jet flight, avoiding the collection of solvent-containing fibres that could cause fibre deformation. Unlike P(3HB) and P(HBHV), mcl-PHA was not able to smoothly produce fibres due its low viscosity. mcl-PHA solutions with concentrations of 12 wt% and 25 wt% were tested, however, both failed to produce fibres, when collected onto a microscope slide, dots of polymer solution can be observed instead of the intended fibres (Figure 3.13). Henceforth, as a strategy to improve spinnability of mcl-PHA, while still obtaining fibres that showcase some of mcl-PHA properties, blends of P(3HB) and P(HBHV) with mcl-PHA were studied. Different polymer solution blend ratios (50:50, 60:40 and 70:30) at a fixed polymeric concentration (4 wt%) and processing parameters were analysed by collecting fibres onto microscopic slides for observation under the optical microscope and by SEM, the obtained images are presented in Figure 3.14.

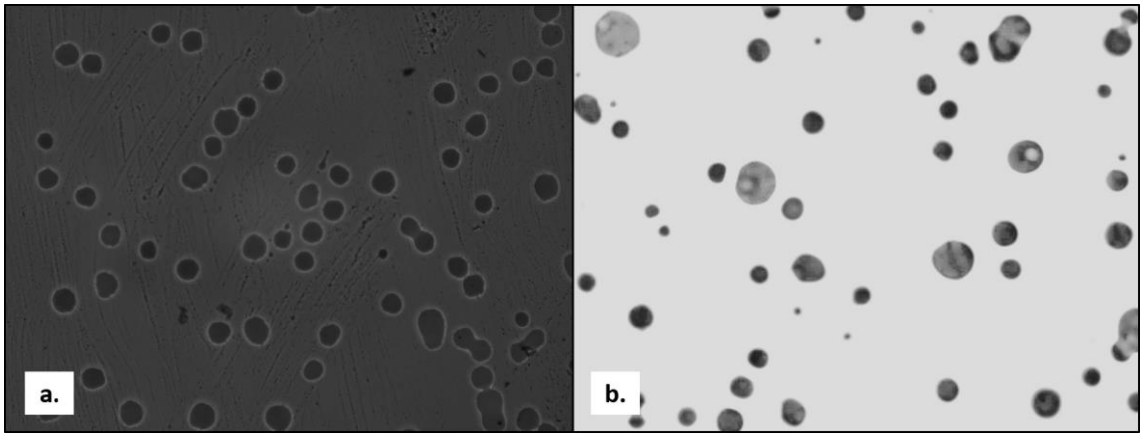

Figure 3.13- Optical microscope images of samples collected from mcl-PHA electrospinning amplified 40x; a- 12 wt% mcl-PHA; b-25 wt% mcl-PHA.

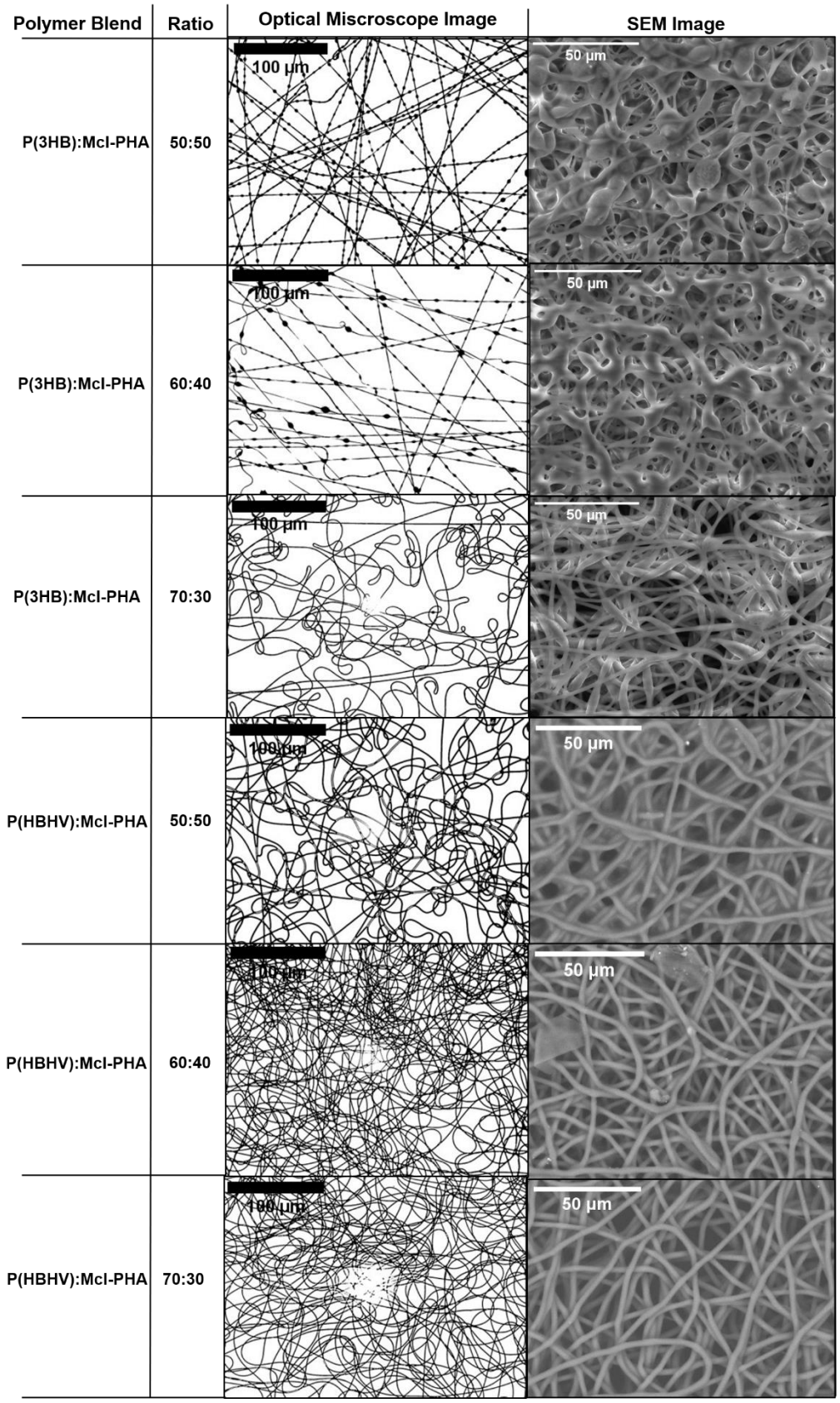

Figure 3.14- Optical microscope images amplified 40x (the black bar represents 100 µm) and scanning electron microscope images amplified 1500x of P(3HB)/P(HBHV):mcl-PHA blends at different ratios.

Microfibers morphology gradually changed as the ratios of P(3HB)/P(HBHV):mcl-PHA increased from 50:50 to 70:30, and fibrous features progressively became more stable. For P(3HB): mcl-PHA blends, ratios of 50:50 and 60:40 produced visible bead-fibres that can be observed in both optical microscope and SEM images (Figure 3.14), this can be attributed to lower viscosity of the spinning solution. As the ratio increased to 70:30, the microfibres were much more uniform and smooth fibres were achieved, though when observed under SEM, some bead-like structures and fibre fusing were identified. For P(HBHV): mcl-PHA blends, it was easier to obtain smooth bead-free microfibres at any ratio, however, the electrospun mats offered the greatest uniformity of microfibres at a ratio of 70:30, thus it was the solution chosen for subsequent experiments. These PHA blend spinning solution behaved similarly to previously reported studies, where P(HBV) : P(HOHHx) with P(HBHV) (25 wt% HV content) presented optimal fibre production at a 75:25 ratio (Li et al., 2018).

3.3.5.1.2 Processing Parameter Optimization

In order to further optimize the electrospinning process, processing parameters were assessed, specifically distance to the collector, flow rate and applied voltage.

The distance between the metallic needle tip and collector can affect fibre morphology, it largely depends on the polymer solution, as factors such as deposition time and evaporation play a huge role (Haider et al., 2018). For P(3HB) and P(HBHV) solutions, the critical distance needed for the fabrication of smooth and uniform fibres was of 20 cm, in contrast, for P(HBHV):mcl-PHA (70:30) blends, the distance needed to be increased to 25 cm for complete solvent evaporation, attributed to the slower evaporation rate of mcl-PHA present in the solution.

For the optimization of feeding rate and applied voltage, these parameters were varied while the distance to the collector was fixed at 20 cm for P(3HB) and P(HBHV), and at 25 cm for P(HBHV): mcl-PHA (70:30) blends. Fibres were deposited onto microscope slides and observed (Table 3.5), and the deposition stability was also assessed.

Four voltage levels were selected for investigation of the applied voltage effect on fibres fabrication, 8, 10, 12 and 15 kV. At 8 kV there were some bead formation for P(3HB) and P(HBHV): mcl-PHA (70:30) spinning solutions, which could be related to insufficient electric force to stretch the electrospinning jet, for P(HBHV) smoother fibres were obtained, however, there was some blockage of the metallic tip due to decreased jet velocity. As the tension increased to 10, 12 and 15 kV, smoother fibres were obtained for all three polymer solutions, however, the deposition of the fibres onto the collector was more stable at 12 kV for P(3HB) and P(HBHV) and at 15 kV for P(HBHV): mcl-PHA (70:30) related to the difference in viscosity.

Feeding rates of 0.5 mL/h and 1.0 mL/h were studied, at 0.5 mL/h there was a continuous electrospinning process, suggesting a balance between the rate of solutions consumption and the feeding rate, and only one electrospinning jet was observed. When increasing the flow rate to 1.0 mL/h, the electrospinning process becomes unstable and dual jets were observed, indicating that the feeding rate was higher than the consumption rate.

Table 3.5- Optical microscope images amplified 40x of different PHA fibres obtained at varying flow rate and tension, the white scale bar represents 100 µm.

Optical Microscope Image P(3HB)	Optical Microscope Image P(HBHV)	Optical Microscope Image P(HBHV):mcl-PHA	Flow Rate (ml/h)	Tension (kV)
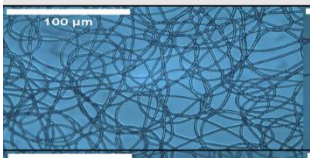		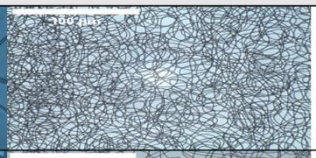	0.5	8.0
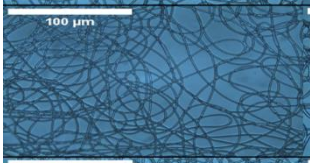	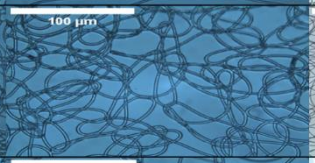	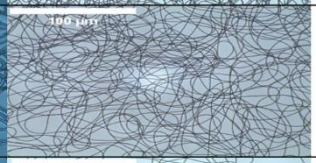	0.5	10
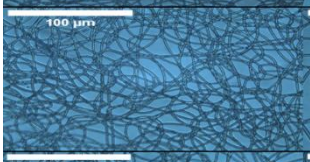			0.5	12
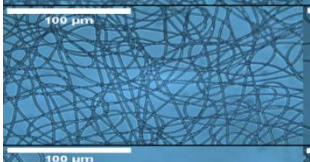		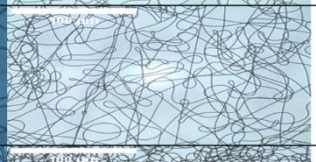	0.5	15
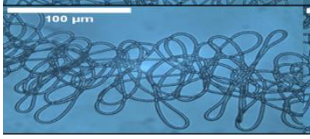	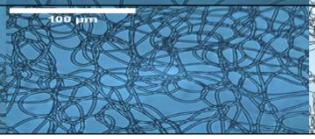	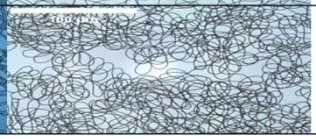	1.0	10

3.3.5.2. Scaffold Morphology

The SEM images of the resulting fibre meshes for P(3HB) and P(HBHV), as well as their diameter distribution, are illustrated in Figure 3.15. Both scaffolds present smooth, bead-less branched and randomly organized fibres with high void space interconnectivity (Figure 3.15, a, b, d and e). P(3HB) microfibres (84 ± 21 µm thick) presented fibre diameters ranging between 1.69-3.79 µm with a mean diameter of 2.56 ± 0.37 µm, dimensions somewhat lower than for other P(3HB) electrospun fibres, for instance, Sombatmankhong et al. (2006) reported a mean diameter of 3.7 ± 1.7 µm for P(3HB) microfibres. P(HBHV) exhibited similar results, with a thickness of 38 ± 10 µm, fibre diameters ranging between 2.08-3.76 µm and a mean diameter of 2.70 ± 0.37 µm, demonstrating fibres of slightly larger dimensions than P(3HB), and higher than the reported dimensions by Sombatmankhong et al. (2006) for P(HBHV) (2.3 ± 2.1 µm). However, both fibrous scaffolds present fibre dimensions higher than what is reported for other PHAs, for example, P(3HB-*co*-4HB) electrospun fibres presented an average diameter of 0.91 ± 0.24 µm (Sudesh et al., 2016), and P(3HB-4HB-3HV) terpolymers exhibited a mean diameter of 1.4 µm (Canadas et al., 2014).

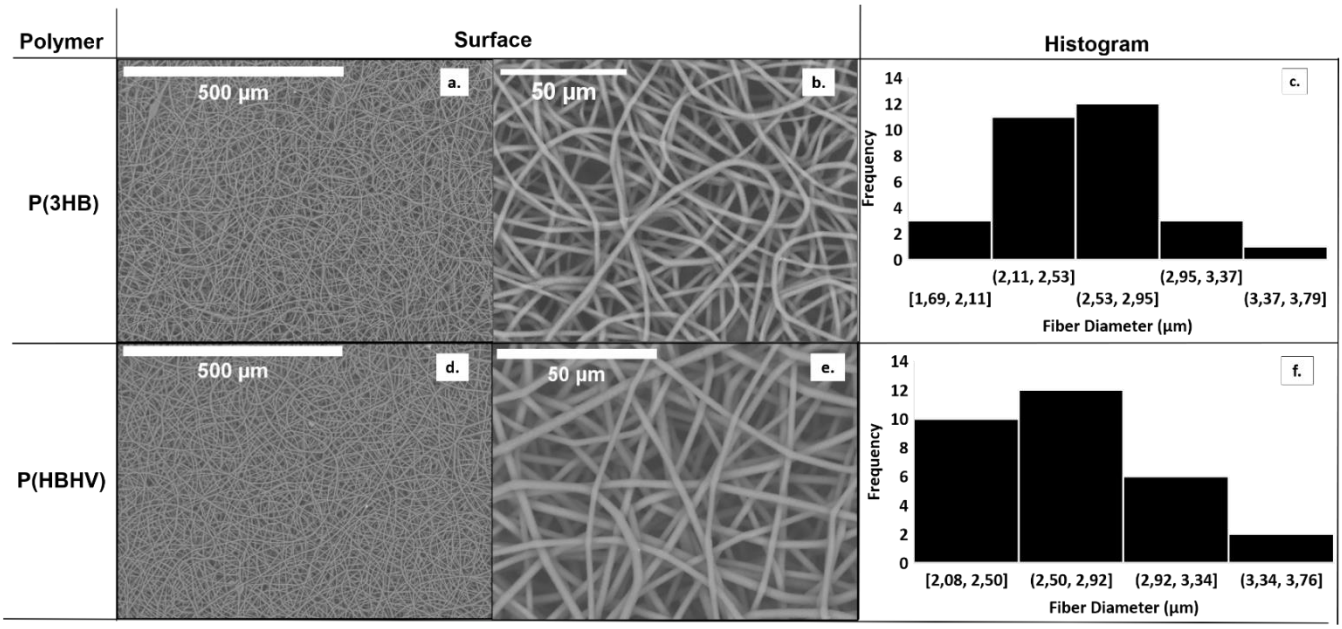

Figure 3.15- Surface images obtained by Scanning Electron Microscopy (SEM) analysis of the prepared P(3HB) and P(HBHV) based fibrous scaffolds amplified 200x (a and d) and amplified 1500x (b and e); Fibre diameter distribution of microfibre meshes obtained by electrospinning (c and f).

The SEM images of the resulting fibre for the P(HBHV): mcl-PHA (70:30) blend as well as its diameter distribution are illustrated in Figure 3.16. The scaffold was 39 ± 2 µm thick and exhibited homogenous, smooth, bead-less and randomly organized fibres with great void space interconnectivity, evident by the surface and cross-section of the fibrous scaffold (Figure 3.16, a and b). Concerning fibre diameter, the blend showed values ranging between 3.64-4.78 µm with a mean diameter of 4.0 ± 0.23 µm, which is considerably higher than P(3HB) and P(HBHV) fibre diameters. These values are among the demonstrated by Sombatmankhong et al. (2006) regarding P(3HB)/P(HBHV) blends, that exhibited mean fibre diameters in the 3.2-4 µm range,

and higher than the reported for another P(HBHV)/mcl-PHA blend, namely PHBHV/PHOHHx, with average fibre diameters in the 0.48-0.76 µm range.

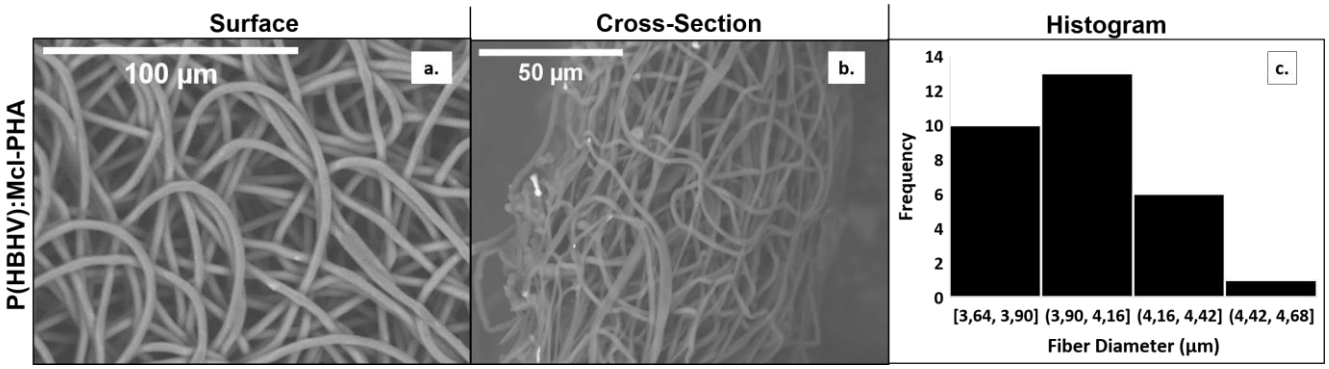

Figure 3.16- Surface (a) and cross-section (b) images obtained by Scanning Electron Microscopy (SEM) analysis of the prepared P(HBHV): mcl-PHA (70:30) blend based fibrous scaffolds amplified 1500x; Fibre diameter distribution of the microfibre mesh obtained by electrospinning (c).

3.3.5.3. Water Contact Angle and Swelling in Water

Water contact angle and swelling in water were assessed for all electrospun scaffolds on the air contacting side. P(3HB) demonstrated to have the most hydrophilic surface, with a water contact angle of 84.3 ± 1.85˚ (Table 3.6), this value is lower than the reported in the literature for other P(3HB) mesh scaffolds. For instance, P(3HB) nanofibers fabricated for drug delivery showed water contact angles of 126 ± 3˚ (Sudesh et al., 2016), and P(3HB) microfibres produced by Sombatmankhong et al. (2006) presented water contact angle of 115 ± 3.4˚. In terms of water uptake, P(3HB) displayed no swelling in water (0%) (Table 3.6), which suggests that water does not penetrate well in this scaffold.

For P(HBHV) there was an increase in water contact angle when compared to previous scaffold fabrication techniques, as well as non-porous PHA films, demonstrating a water contact angle of 96.8 ± 1.26˚ (Table 3.6), which makes the surface hydrophobic (Θ>90˚), this can be linked to the augmented surface roughness in microfibre meshes (Ferreira et al., 2014). However, it is a lower measurement than for the P(HBHV) fabricated by Sombatmankhong et al. (2006) (Θ=117.5 ± 2.5˚). This scaffold was the only one that proved to have some water uptake ability with a swelling degree of 77%, this value is superior to what is reported for PLA fibres (40%) (Hassan et al., 2016).

Concerning the P(HBHV)/mcl-PHA blend, it displayed the most hydrophobic surface between all fabricated scaffolds (113.5 ± 0.72˚) (Table 3.6), a value comparable to the exhibited by other PHA blends, namely P(3HB)/P(HBHV), with water contact angles in the 118.5 ± 2˚ – 121.6 ± 1.7˚ range (Sombatmankhong et al., 2006). Regarding water uptake, the PHA scaffold blend presented a swelling degree of 0% (Table 3.6), which indicated that the addition of mcl-PHA to the spinning solution of P(HBHV) in a 70:30 ratio (P(HBHV): mcl-PHA) causes a decrease in water affinity in the final scaffold.

When compared with other biopolymer-based electrospun fibres, all PHA based scaffolds fabricated in this work proved to be more hydrophilic than PLA (131.9 ± 0.21) (Hassan, Chong, & Sultana, 2016). Moreover, P(3HB) and P(HBHV) exhibited higher hydrophilicity than PLGA (105.5 ± 5.2) (Ajalloueian et al., 2014).

Table 3.6- Water contact angles for the PHA scaffolds fabricated with P(3HB), P(HBHV) and P(HBHV/mcl-PHA blends by electrospinning and comparison with values reported for different materials (PLA, polylactic acid; PCL and PLGA, poly(lactic-*co*-glycolic acid**)).**

Polymer	Water Contact Angle (Ɵ)	Swelling in Water (%)	References
P(3HB)	84.3 ± 1.85	0	This study
P(HBHV)	96.8 ± 1.26	77	
P(HBHV)/mcl-PHA	113.5 ± 0.72	0	
P(3HB)	126 ± 3	n.a	(Sudesh et al., 2016)
P(3HB)	115 ± 3.4	n.a	(Sombatmankhong et al., 2006)
P(HBHV)	117.5 ± 2.5	n.a	
P(3HB)/P(HBHV)	118.5 ± 2 – 121.6 ± 1.7	n.a	
PLA	131.9 ± 0.21	40	(Hassan, et al., 2016)
PLGA	105.5 ± 5.2	n.a	(Ajalloueian et al., 2014)

3.3.5.4. Physical and Thermal Properties

The transformation of raw PHA into microfibre meshes involves polymer processing in the form of shaping, an operation in which "structuring" occurs and the molecular orientation is modified to improve physical and mechanical properties (Vlachopoulos & Strutt, 2003). In order to evaluate the effect of the electrospinning process on the unmodified polymers, thermal properties and molecular weight distribution were examined.

Concerning molecular weight (M_w), there was a significant decrease from raw polymer to electrospun fibres. P(3HB) originally presented an M_w of 5.2 x 10^5 Da, this value decreased to 4.2 x 10^5 Da, with a 1 x 10^5 Da average molecular weight loss (Table 3.7). P(HBHV) also showed a similar decrease from 5.6 x 10^5 Da to 4.1 x 10^5 Da (Table 3.7). As previously mentioned, this is probably due to hydrolysis of the ester bonds of the polymers during the fabrication process. The P(HBHV)/mcl-PHA blend presented an M_w of 3.5 x 10^5 Da (Table 3.7), this value is lower than fibres with just P(HBHV), which is expected since mcl-PHA possesses a lower molecular weight. The polydispersity index didn't seem to be majorly affected during processing into P(3HB) and P(HBHV) fibres, with measurements of 1.63 and 1.68, respectively (Table 3.7). The value demonstrated to decrease from raw P(3HB) (1.8) and increase from raw P(HBHV) (1.6). In terms of the P(HBHV)/mcl-PHA fibres, PDI exhibited a significantly higher value of 2.79 (Table 3.7), because it is a polymer blend, it is anticipated that the size dispersity of polymer molecules is higher.

Concerning thermal properties, melting temperature for P(3HB) microfibres (172 ˚C) did not significantly deviate from the melting temperature of raw P(3HB) (175 ˚C) (Table 3.7), displaying only a slight decrease and a value close to other reported electrospun P(3HB) fibres by Sombatmankhong et al. (2006) (T_m = 173 ˚C). P(HBHV) electrospun fibres showed a melting temperature of 165 ˚C (Table 3.7), a lower measurement than for unprocessed P(HBHV) (176 ˚C), but among the value reported for P(HBHV) fibres reported by Sombatmankhong et al. (2006) (162 ˚C). The P(HBHV)/mcl-PHA blend showed a melting temperature of 129 ˚C (Table 3.7), demonstrating that adding mcl-PHA to the spinning solution leads to lower melting temperatures. Degradation temperatures did not show any substantial difference for both P(3HB) and P(HBHV), with T_{deg} values of 289 ˚C and 288 ˚C, respectively (Table 3.7), these parameters are higher than the reported by Sombatmankhong et al. (2006) for P(3HB) fibres (T_{deg} = 265 ˚C) and P(HBHV) fibres (T_{deg} = 265˚C), proving to have a higher upper limit for polymer manipulation. The P(HBHV)/mcl-PHA also showed the higher T_{deg} out of all the electrospun fibres (T_{deg} = 290 ˚C) (Table 3.7), confirming that the addition of mcl-PHA does not decrease degradation temperature.

P(3HB) and P(HBHV) fibres also proved to have higher melting enthalpy, and consequentially of crystallinity fraction. Unprocessed P(3HB) presented an ΔH of 60.3 J g^{-1} and an X_c of 41.3% (Table 3.7), whereas electrospun P(3HB) showed values of 64.1 J g^{-1} and 43.9% (Table 3.7). Likewise, P(HBHV) went from an ΔH of 26 J g^{-1} to 33.7 J g^{-1} after spinning, and increased its X_c to 23 % from 17.8% (Table 3.7), such results can be attributed to the orientation of macromolecular chains in the longitudinal fibre direction during the electrospinning process, that could have promoted crystallization (Mottin et al ., 2016). The P(HBHV)/mcl-PHA blend showed

an ΔH of 26.6 J g^{-1} and an X_c of 18.2% (Table 3.7), this value is among the reported for another scl-PHA/mcl-PHA blend, namely P(HBHV)/PHOHHx, with ΔH and X_c of 25 J g^{-1} and 16%, respectively (Li et al., 2018).

Table 3.7- Thermal properties, melting enthalpy, degree of crystallinity, Mw, M_n and PDI of raw P(3HB), P(HBHV) and mcl-PHA, and of the fibrous P(3HB), P(HBHV) and P(HBHV)/mcl-PHA scaffolds produced using these polymers through electrospinning, along as for some reported PHA electrospun fibres.

Material	T_m (˚C)	T_{deg} (˚C)	X_c (%)	ΔH_m (J g^{-1})	M_W (x 10^5 Da)	M_N (x 10^5 Da)	PDI	Reference
Raw P(3HB)	175	293	41.3	60.3	5.2	2.9	1.80	This study
Electrospun P(3HB)	172	289	43.9	64.1	4.2	2.6	1.63	
Raw P(HBHV)	176	292	17.8	26.0	5.6	3.5	1.60	This study
Electrospun P(HBHV)	165	288	23.0	33.7	4.1	2.5	1.68	
Raw mcl-PHA	n.o	292	3.7	5.3	0.69	0.46	1.50	This study
Electrospun P(HBHV)/mcl-PHA	129	290	18.2	26.6	3.5	1.2	2.79	
Electrospun P(3HB)	173	265	55.6	81.5	n.a	n.a	n.a	(Sombatmankhong et al., 2006)
Electrospun P(HBHV)	162	265	45.1	66.1	n.a	n.a	n.a	
Electrospun P(3HB)/P(HBHV)	167-172	264-265	48-55	71-81	n.a	n.a	n.a	
Electrospun P(HBHV)/PHOHHx	n.a	n.a	16	25	n.a	n.a	n.a	(Li et al., 2018)

For structural analysis, X-ray diffractograms were obtained for all three fibres (Figure 3.17). In terms of P(3HB) microfibres (Figure 3.17, a), they exhibited all main reflections of the X-ray diffraction pattern of crystalline P(3HB) with a similar pattern to its unprocessed counterpart, demonstrating two narrow humps located around 2θ = 14 and 17°, characteristic of the crystalline phase, the humps present a higher intensity than unprocessed P(3HB) characterized in Chapter 2, which is expected since X_c estimated by DSC is higher for the electrospun fibre. A broad hump at around 2θ = 22˚ and 25˚ is also displayed, typical for the amorphous phase.

The P(HBHV) diffractogram acquisition (Figure 3.17, a) seems to not have been completely successful, since the intensities of the peaks deviate greatly from unprocessed P(HBHV) and do not corroborate DSC results, however, it's possible to distinguish a similar pattern to the displayed by P(3HB) fibres.

Concerning the P(HBHV)/mcl-PHA blend (Figure 3.17, b), it demonstrated diffraction peaks at 14 and 17° due to the presence of P(HBHV), confirmed by the overlapping of the patterns of the blend with unprocessed P(HBHV) (Figure 3.17, b), and a broad hump located within the 2θ= 18, which coincides with the amorphous phase exhibited by unprocessed mcl-PHA (Figure 3.17, a), these results prove the successful fabrication of a blend of the different types of PHAs.

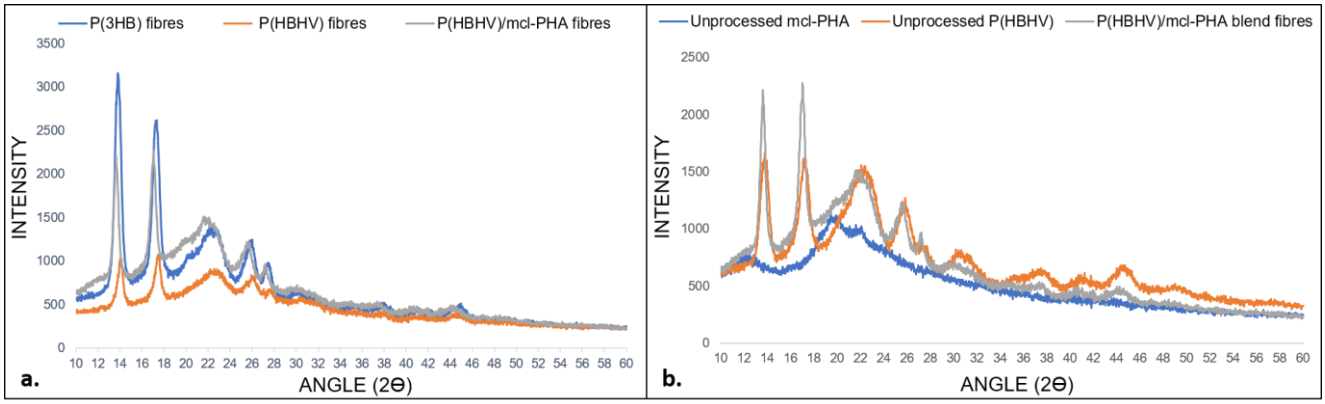

Figure 3.17- X-ray diffractogram of (a) electrospun P(3HB), P(HBHV) and P(HBHV)/mcl-PHA blend and (b) unprocessed P(HBHV) and mcl-PHA in comparison with their electrospun fibre blend.

3.3.5.5. Mechanical Properties

Mechanical tests were performed in order to study stress-strain behaviour and determinate tensile strength at break, deformation at break and Young Modulus of electrospun P(3HB), P(HBHV) and P(HBHV)/mcl-PHA fibres.

In terms of tensile strength, P(HBHV) required the most strength to break with a tensile strength of 1.51 ± 0.29 MPa, followed by P(3HB) with 1.07 ± 0.22 MPa and then by the P(HBHV)/mcl-PHA blend with 0.15 ± 0.003 MPa (Table 3.8) , proving that adding mcl-PHA to the spinning solution considerably decreased tensile strength at break. Reported values for other PHA fibres demonstrated to be higher, P(3HB) fibres produced by Fan et al. (2015) displayed a tensile strength of 48.46 ± 1.18 MPa, also, P(HBHV) fibres, as well as a P(HBHV)/PHOHxx blend fabricated by Li et al. (2018), exhibited tensile strengths of 2.90 ± 0.31 and 2.68 ± 0.05 MPa, respectively. On the other hand, the fibres produced in this study showed higher tensile strength than PLA/PCL blend fibres (0.10 MPa) (Kancheva et al., 2015). Moreover, P(3HB) and P(HBHV) emulsion templated scaffolds fabricated in this work displayed higher tensile strength at break than electrospun fibres (1.07 ± 0.22 and 3.35 ± 0.54, respectively) (Table 3.4), this is due to lower porosity of emulsion templated scaffolds when compared with electrospun fibrous scaffolds (Li et al., 2018).

Regarding deformation at break, P(3HB) and P(HBHV) showed similar values of 7.79 ± 1.05 and 7.33 ± 0.88 %, correspondingly (Table 3.8). These values are lower than what is reported for electrospun P(3HB) (94.15 ± 1.28 %) (Fan et al., 2015) and P(HBHV) (212 ± 42.2 %) (Li et al., 2018). Emulsion templated P(3HB) and P(HBHV) scaffolds also presented higher deformation measuring at 13.6 ± 0.44 and 14.8 ± 1.74 %, respectively (Table 3.4), proving to be more flexible than electrospun PHA fibres. When producing a P(HBHV)/mcl-PHA blend, flexibility was greatly improved with deformation at break of 42.75 ± 3.77 %, proving to be a successful strategy to enhance the fibres mechanical properties. This value was among the reported for a PLA/PCL blend (40-100%) (Kancheva et al., 2015).

In respect to Young modulus, P(3HB) and P(HBHV) fibres exhibited similar values (0.06 ± 0.02 and 0.08 ± 0.004 MPa, respectively) (Table 3.8), meaning that they possess similar ductility. These values are lower than the emulsion templated scaffolds produced with the same polymers (0.07 ± 0.009 MPa for P(3HB) and 0.11 ± 0.02 MPa for P(HBHV)) (Table 3.4), which similarly to the decrease in tensile strength can be correlated to the lower porosity of the emulsion templated scaffolds. For the P(HBHV)/mcl-PHA blend there was an accentuated decrease in Young modulus (0.006 ± 0.0005 MPa) (Table 3.8), characteristic for more amorphous materials (Li et al., 2018), which is the case of the blend due to the presence of mcl-PHA. Young modulus of the PHA microfibres fabricated in this study is much lower than the reported for other PHAs, such as P(HBHV) , 41.09 ± 3.69 MPa (Li et al., 2018) and P(HBHV)/PHOHHx, 34.46 ± 3.19 MPa (Li et al., 2018), as well as for other materials like PLA/PCL, 15 MPa (Kancheva et al., 2015), PLGA, 4.29 ± 1.79 MPa (Foraida et al., 2017) and PLGA/elastin, 0.59 ± 0.356 (Foraida et al., 2017).

Table 3.8- Mechanical properties of scaffolds prepared by electrospinning and comparison with other scaffolds of different materials produced by electrospinning in the literature; n.a- non-available.

Material	Tensile Strength at Break (MPa)	Deformation at break (%)	Young Modulus (MPa)	Reference
P(3HB)	1.07 ± 0.22	7.79 ± 1.05	0.06 ± 0.02	This Study
P(HBHV)	1.51 ± 0.29	7.33 ± 0.88	0.08 ± 0.004	This Study
P(HBHV)/mcl-PHA	0.15 ± 0.003	42.75 ± 3.77	0.006 ± 0.0005	This Study
P(3HB)	48.46 ± 1.18	94.15 ± 1.28	n.a	(Fan et al., 2015)
P(HBHV)	2.90 ± 0.31	212 ± 42.2	41.09 ± 3.69	(Li et al., 2018)
P(HBHV)/PHOHHx	2.68 ± 0.05	291 ± 51.3	34.46 ± 3.19	(Li et al., 2018)
PLA/PCL	0.10	40-100	15.0	(Kancheva et al., 2015)
PLGA	n.a	n.a	4.29 ± 1.79	(Foraida et al., 2017)
PLGA/Elastin	n.a	n.a	0.59 ± 0.356	(Foraida et al., 2017)

3.3.6. Scaffold Surface Modification

Since PHA scaffolds possess intrinsically hydrophobic surfaces, surface modification treatments, namely ultraviolet/ozone and oxygen plasma, were employed in order to increase hydrophilicity.

3.6.1. UV/Ozone

P(3HB) and P(HBHV) non-porous films were submitted to the different UV/ozone treatment times offered by the apparatus system (30, 60 and 120 minutes) in order to study changes in hydrophilicity. The water contact angle for each sample was measured before and after treatment to take into account the variability between films. As we can see in Figure 3.18, longer treatment time leads to the lower water contact angles, since the lengthier the exposure time, the more carboxyl groups can be created at the surface of the films. For both P(3HB) and P(HBHV), 120 minutes of treatment showed the highest decrease in water contact angle, with a decrease of 54 ± 0.3 % for P(3HB) and of 40 ± 0.82 % for P(HBHV). P(3HB) also showed a higher decrease in water contact angle than P(HBHV), independently of treatment time, showing a bigger response to the UV/ozone treatment. The effect of UV/ozone in decreasing water contact angle has previously been reported for many polymers, such as PCL, PCL/PLA and polystyrene (Mobasseri et al., 2014; Samsudin et al., 2017; Teare et al., 2000).

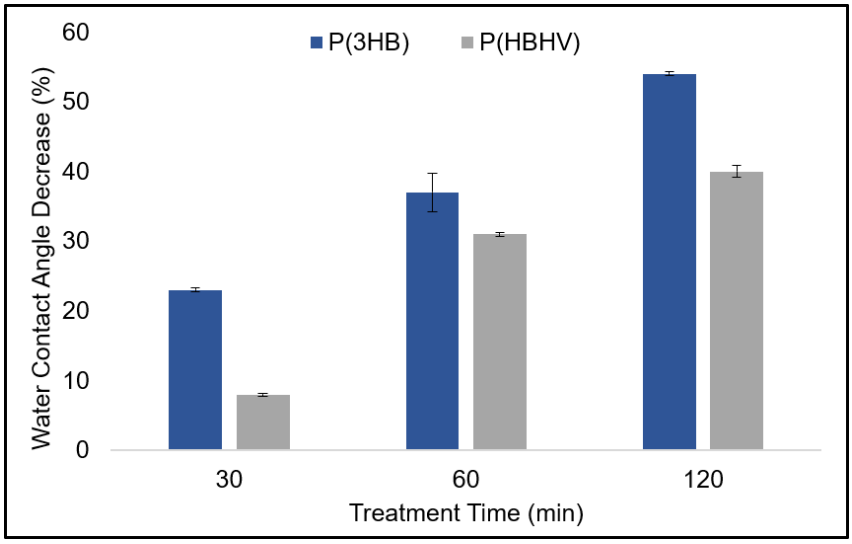

Figure 3.18- Water contact angle decreases for P(3HB) and P(HBHV) after 30,60 and 120 min of UV/ozone exposure.

Furthermore, when handling the samples after treatment, particularly after longer exposure to UV/ozone, the films become brittle and fragile, easily breaking upon touch, thus, emulsion templated P(3HB) and P(HBHV) scaffolds were exposed to 120 minutes of treatment and observed under SEM, before and after exposure, to further examine possible changes in polymer morphology.

In Figure 3.19 we can observe that there are notable differences before and after UV/ozone, for both P(3HB) and P(HBHV) distinguishable cracks can be observed in the microstructure. Such changes were also reported for PCL/PLA films where besides the damage to the films, there was

also a negative effect on mechanical properties, such as decreased toughness and increased brittleness, as well as poor stability of treatment, with increase of the water contact angle to the original value (before treatment) within 24 hours (Mobasseri et al., 2014). Hence, this treatment was eliminated as a possible tool to enhance scaffold hydrophilicity.

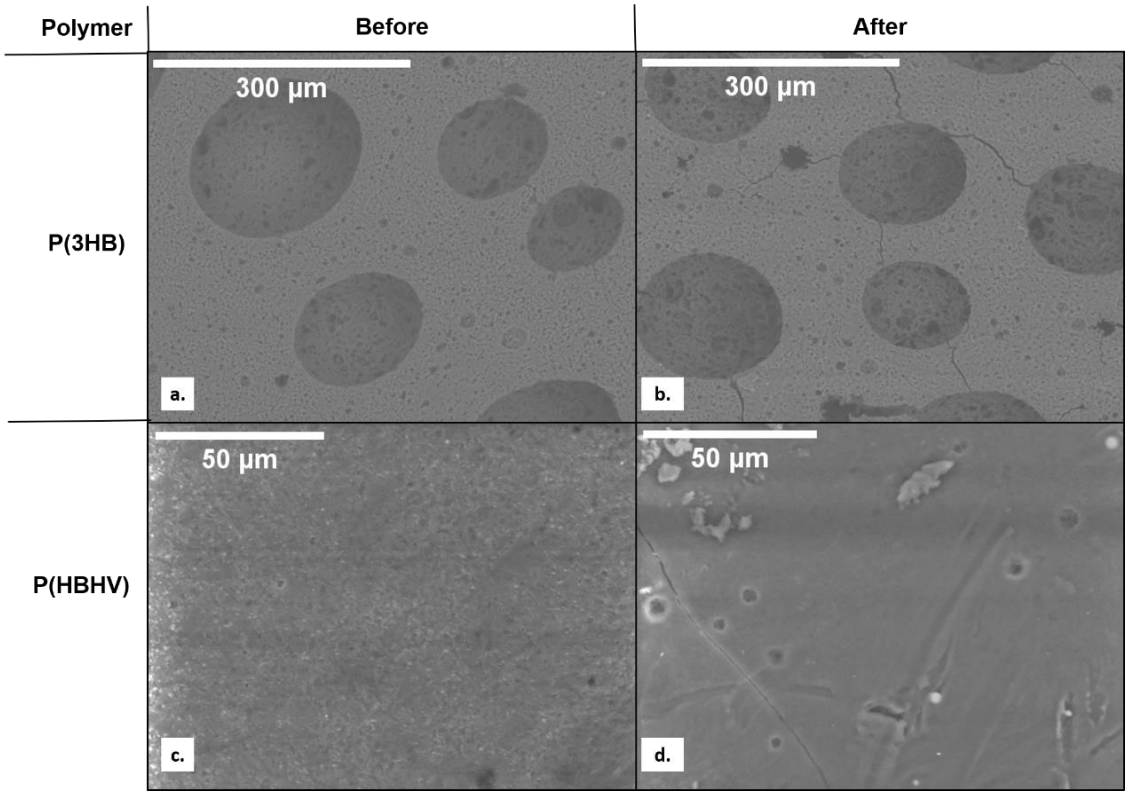

Figure 3.19- Emulsion templated P(3HB) and P(HBHV) scaffolds SEM imaging before and after 120 minutes of UV/ozone exposure amplified 300x (a. and b.) and 1200 x (c. and d.).

3.3.6.2. Oxygen Plasma

Oxygen plasma was tested as a surface modification method to increase scaffold hydrophilicity. To evaluate optimum exposure time emulsion templated P(3HB) and P(HBHV) were submitted to 5,8 and 12 minutes of oxygen plasma treatment. Regardless of treatment time, the surface of the scaffolds experienced complete wetting after treatment, making water contact angle an unfit method to study hydrophilicity, thus, swelling in water (or water uptake) was measured for both scaffolds at the different treatment times, the results are represented in Figure 3.20.

For P(3HB), water uptake demonstrated to increase with treatment time, however, 8 and 12 minutes of treatment showed similar water uptake, which may indicate that 8 minutes of exposure to plasma treatment is enough to reach maximum water uptake ability. Compared to untreated scaffolds, where the swelling was of 32%, with oxygen plasma it was possible to obtain swelling up to 143%. For P(HBHV) up to 8 minutes of treatment did not yield a significant increase in water uptake, however, at 12 minutes of treatment it was possible to increase swelling to 204%. These results indicate that 12 minutes of treatment is enough to ensure considerable enhancement of water uptake ability of the emulsion templated scaffolds.

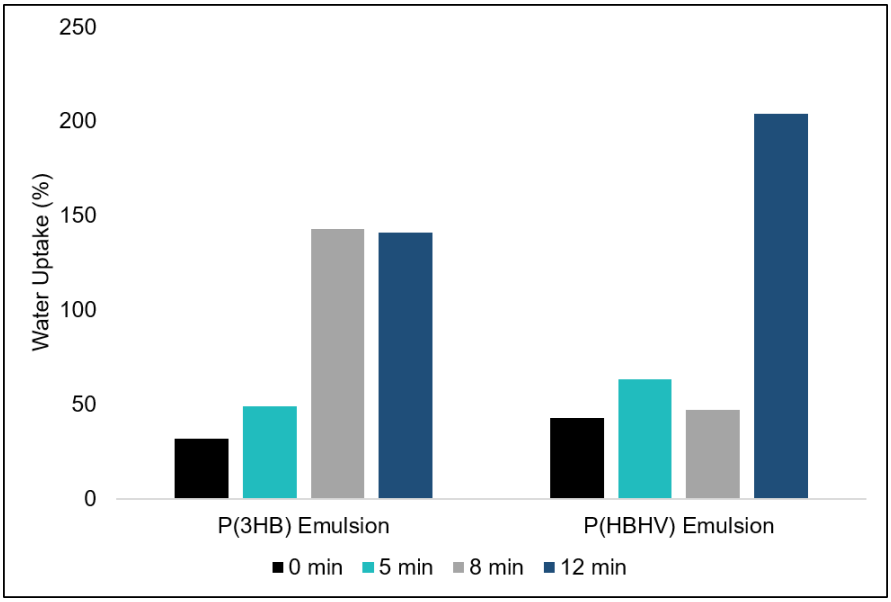

Figure 3.20- Water uptake for P(3HB) and P(HBHV) emulsion templated scaffolds after 0,5,8 and 12 min of oxygen plasma exposure.

Electrospun P(3HB), P(HBHV) and P(HBHV)/mcl-PHA fibrous scaffolds were also submitted to 12 minutes of treatment to investigate the effect on water uptake. Untreated P(3HB) and P(HBHV)/mcl-PHA did not experience any water uptake (0%), however, after 12 minutes of oxygen plasma treatment water uptake increased to 294% for P(3HB) and to 17% for the P(HBHV)/mcl-PHA blend, being more resistant to treatment. P(HBHV) also increased its original water uptake of 70% to 205%. Overall, oxygen plasma proved to not only enhance surface hydrophilicity but also to greatly improve water penetrability, which is of great importance when it comes to 3D-cell culture scaffolds.

3.3.6.2.1. Morphology of Oxygen Plasma Treated Scaffolds

To investigate changes in morphology emulsion templated P(3HB) and P(HBHV) scaffolds were examined before and after oxygen plasma treatment under SEM, the obtained images of surface and cross-section are represented in Figure 3.21.

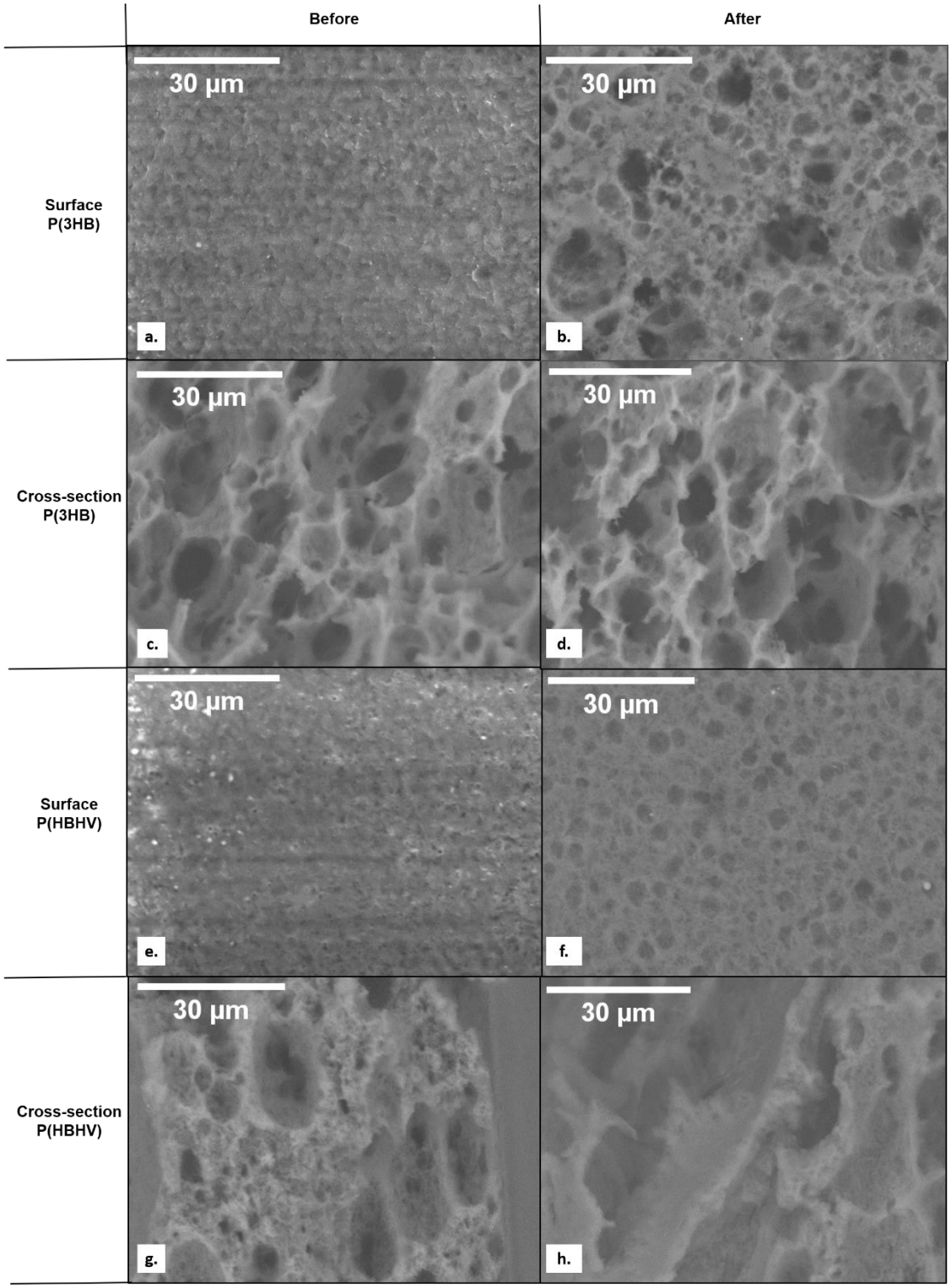

Figure 3.21- Emulsion templated P(3HB) and P(HBHV) scaffolds SEM imaging of their surface (a,b,e and f) and cross-section (c,d,g and h) before and after 8 minutes of oxygen plasma exposure, amplified 2000 x.

The SEM images show that the surfaces of both P(3HB) and P(HBHV) display some differences before and after treatment, after oxygen plasma exposure the scaffolds exhibit bigger pore size on the surface, this behaviour might be due to physical erosion by ions in plasma, sometimes designated as physical etching (Mirmohammadi et al., 2012). The cross-section of both scaffolds seems unmodified after treatment, which is expected, as it is only a surface treatment.

Electrospun P(3HB), P(HBHV) and P(HBHV)/mcl-PHA were also examined by SEM after oxygen plasma exposure (Figure 3.22). All fibres displayed some degree of modification in morphology. P(3HB) and P(HBHV) suffered some fracturing along the fibres, although P(HBHV) presented a higher number of said fractures. The P(HBHV)/mcl-PHA blend, on the other hand, did not seem to display much fracturing, however, it showed thinning of some fibres. Once again, this can be explained by the etching phenomena.

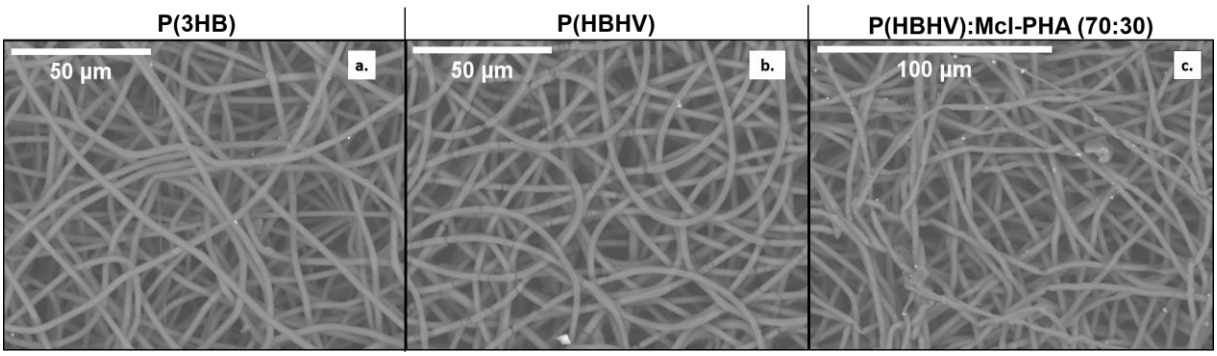

Figure 3.22- Electrospun P(3HB), P(HBHV) and P(HBHV)/mcl-PHA fibrous scaffolds SEM imaging of their surface after 12 minutes of oxygen plasma exposure, amplified (a) 1200 x (b) 1200 x and (c) 1000 x.

3.3.6.2.2. Molecular Mass Distribution of Oxygen Plasma Treated Scaffolds

To assess the effect of oxygen plasma on the molecular weight of the polymers, SEC analysis was performed on emulsion templated P(3HB) and P(HBHV) scaffolds, as well as electrospun P(3HB), P(HBHV) and P(HBHV)/mcl-PHA fibres after oxygen plasma exposure.

Overall, oxygen plasma seems to provoke a decrease in molecular weight and an increase in polydispersity index, this may be due to the treatment making the polymer more susceptible to hydrolysis leading to a lower M_w and an increase in the size dispersity of the polymer molecules.

For emulsion templated scaffolds, the difference before and after treatment is not as significant as for electrospun fibres. Emulsion templated P(3HB) scaffold decreased its M_w from 3.8 x 10^5 Da to 3.6 x 10^5 Da, and increased its polydispersity index from 1.8 to 1.9, while electrospun P(3HB) fibres reduced its M_w from 4.2 x 10^5 Da to 3.5 x 10^5 Da and increased its polydispersity index from 1.6 to 1.9 (Table 3.9).

For P(HBHV), emulsion templated scaffolds went from an M_w of 4.0 x 10^5 Da to 3.9 x 10^5 Da, which is almost negligible, and PDI increased from 1.7 to 1.9, on the other hand, electrospun fibres decreased their M_w from 4.1 x 10^5 Da to 3.5 x 10^5 Da, which is a much more considerable shift, and increased the PDI from 1.7 to 2.0 (Table 3.9).

Finally, the P(HBHV)/mcl-PHA blend electrospun fibres displayed the same M_w before and after oxygen plasma exposure, and only slightly increased its PDI from 2.8 to 2.9 (Table 3.9), confirming that the PHA blend was much more resistant to oxygen plasma than the other PHA materials.

Table 3.9- Mw, M_n and PDI of P(3HB), P(HBHV) emulsion templated scaffolds, and of the fibrous P(3HB), P(HBHV) and P(HBHV)/mcl-PHA scaffolds, before and after oxygen plasma exposure.

Polymer	Fabrication	Treatment	M_W (x 10^5 Da)	M_N (x 10^5 Da)	PDI
P(3HB)	Emulsion	No	3.8	2.2	1.8
P(3HB)		Yes	3.6	1.9	1.9
P(HBHV)	Emulsion	No	4.0	2.8	1.7
P(HBHV)		Yes	3.9	2.0	1.9
P(3HB)	Electrospinning	No	4.2	2.6	1.6
P(3HB)		Yes	3.5	1.8	1.9
P(HBHV)	Electrospinning	No	4.1	2.5	1.7
P(HBHV)		Yes	3.4	1.7	2.0
P(HBHV)/mcl-PHA	Electrospinning	No	3.5	1.2	2.8
P(HBHV)/mcl-PHA		Yes	3.5	1.2	2.9

3.4. Conclusions

PHAs, namely mcl-PHA, P(3HB) and P(HBHV) produced in the previous chapter, were used for the development of PHA based porous and fibrous scaffolds for 3D-cell culture. Several techniques were employed, including solvent casting with particulate leaching, supercritical CO_2 foaming, water emulsion templating and electrospinning.

Solvent casting with particulate leaching proved to be an acceptable method to introduce porosity in P(3HB) and P(HBHV), however, it failed to produce a porous mcl-PHA scaffold. In terms of surface hydrophilicity, it was possible to produce scaffolds with water contact angles inferior to 90˚ for P(3HB) and P(HBHV), implying hydrophilic surfaces. On the other hand, mcl-PHA presented a more hydrophobic surface with water contact angles close or superior to 90˚. Concerning swelling in water, values up to 54.5%, 175% and 181% were obtained for mcl-PHA, P(3HB) and P(HBHV), respectively. Although these scaffolds displayed some positive qualities, they did not gather the required properties for a 3D-scaffold, such as pore size and interconnectivity, as well as scaffold physical integrity.

Supercritical CO_2 was tested as an alternative to harmful solvent using methods, P(HBHV) porous scaffolds were produced with this technique, however, pore size was incredibly small and there was lack of pore interconnectivity. Water contact angle and swelling in water were studied for scaffolds produced in harsh conditions (pressure= 280 bar; soaking time= 6 hours) as well as for milder conditions (pressure= 200 bar; soaking time= 1 hour), water contact angle was similar for both scaffolds with values of 96.4 ± 2.13˚ (mild conditions) and 96.5 ± 0.18˚ (harsh conditions). Swelling in water however was higher for scaffolds processed under harsher conditions (18.5%) than of milder conditions (4.84%). Although promising, this method needs further optimizing to fit 3D scaffold requirements.

Emulsion templated scaffolds were produced using mcl-PHA, P(3HB) and P(HBHV). For mcl-PHA, this method proved ineffective with no discernible porosity presented by the scaffolds. For P(3HB) and P(HBHV) porosity was successfully implemented, with pore size concentrated in the 0.78-6.38 µm size interval for P(3HB) and in the 1.35-7.45 µm range for P(HBHV). Water contact angle showed hydrophilic surfaces for all polymers, with measurements of 65.7˚ ± 2.2, 79.7˚± 0.7 and 48.6˚± 2.7 for mcl-PHA, P(3HB) and P(HBHV), respectively. Swelling in water was negligible for mcl-PHA (2.9 %), on the other hand, P(3HB) displayed a swelling of 31.8% and P(HBHV) of 42.6%, demonstrating water uptake ability for the scl-PHA emulsion templated scaffolds. DSC and TGA analysis revealed that thermal properties such as T_m and T_{deg} did not suffer major alteration after processing, however, SEC analysis showed that there was a decrease in M_w. XRD confirmed that the crystallinity of the polymers was not greatly affected, besides a slight decrease in X_c. Furthermore, mechanical characteristics were also studied, P(3HB) emulsion templated scaffolds displayed a tensile strength at break of 3.18 ± 0.19 MPa, deformation at break of 13.6 ± 0.44 % and a Young modulus of 0.07 ± 0.009 MPa, while P(HBHV) emulsion templated scaffolds presented a tensile strength at break of 3.35 ± 0.54 MPa, deformation at break of 14.8 ± 1.74 % and a Young modulus of 0.11 ± 0.02 MPa. This porous scaffold fabrication method produced

good candidates for 3D-cell culture, that exhibited porosity, pore interconnectivity, surface hydrophilicity and water uptake ability, as well as acceptable mechanical properties.

The last fabrication method that was tested was electrospinning, P(3HB) and P(HBHV) fibres were fabricated using 4 wt% spinning solutions, however, mcl-PHA did not produce any fibres with concentrations up to 25 wt% by itself, but produced smooth bead-free fibres when blended with P(HBHV) in a 70:30 (P(HBHV)/mcl-PHA) ratio. After process parameter optimization, P(3HB) and P(HBHV) produced a fibrous scaffold with mean fibre diameters of 2.56 ± 0.37 µm and 2.70 ± 0.37 µm, respectively, using a distance to the collector of 20 cm, an applied voltage of 12 kV and a flow rate of 0.5 mL/h. The P(HBHV)/mcl-PHA blend produced electrospun microfibres with a mean fibre diameter of 4.0 ± 0.23 µm using a distance to collector of 25 cm, an applied voltage of 15 kV and a flow rate of 0.5 mL/h. T_m and T_{deg} of P(3HB) and P(HBHV) microfibres did not demonstrate major differences from unprocessed P(3HB) and P(HBHV). The P(HBHV)/mcl-PHA presented a lower T_m (129 ˚C), due to the presence of mcl-PHA and a T_{deg} of 290˚ C. SEC analysis revealed a decrease in M_w, in a similar way to emulsion templated scaffolds, related to the degradation of the polymers upon processing. Crystallinity proved to be higher for electrospun fibres than for unprocessed polymer or emulsion templated scaffolds. In terms of mechanical properties, P(HBHV) microfibres displayed the highest tensile strength at break measuring 1.51 ± 0.29 MPa, followed by P(3HB) with 1.07 ± 0.22 MPa, and then P(HBHV)/mcl-PHA with 0.15 ± 0.003 MPa. Deformation at break was similar for P(3HB) and P(HBHV) (7.79 ± 1.95 % and 7.33 ± 0.88 %, respectively), yet, the P(HBHV)/mcl-PHA revealed enhancement of this mechanical property with 42.75±3.77 % deformation. Young modulus was the highest for P(HBHV) fibres, 0.08 ± 0.004 MPa, followed by P(3HB) with 0.06 ± 0.02 MPa, and then P(HBHV)/mcl-PHA with 0.006 ± 0.0005 MPa. Overall, these fibrous scaffold present attractive properties that make them suitable for 3D-cell culture.

Surface modification treatments were employed, namely UV/ozone and oxygen plasma. UV/ozone showed a decrease in water contact angle for P(3HB) and P(HBHV) films, however, it also demonstrated to inflict damage to the scaffold's microstructure and integrity, being discarded as possible surface treatment for increased hydrophilicity. Moreover, oxygen plasma also increased surface hydrophilicity, providing complete wetting of emulsion templated P(3HB) and P(HBHV) scaffolds, as well as increasing water uptake ability of emulsion templated P(3HB) and P(HBHV) scaffolds, and fibrous P(3HB), P(HBHV) and P(HBHV)/mcl-PHA electrospun scaffolds. The surface of the scaffolds proved to undergo some degree of physical etching on the surface, increasing pore size on emulsion templated scaffolds and causing fracturing/thinning of electrospun fibres. Still, oxygen plasma demonstrated to be a favourable method to increase surface hydrophilicity, and thus improve cellular attachment to the PHA based scaffolds.

Chapter 4- PHA-based Scaffolds for Dermis Reconstitution

4.1. Introduction

There are a few essential features that a biomaterial must present, like biodegradability, non-cytotoxicity and biocompatibility. PHAs have been reported to have such characteristics, emerging as potentially useful materials in the biomedical field (Ali & Jamil, 2016).

Biodegradability is the first property that makes PHAs compatible with living cells. P(3HB) with various geometries (films, plates and microspheres) has been studied regarding biodegradation using several cell lines. It has been reported that in contrast to other widely used bioplastics (e.g. polyglycolic acid (PGA) and poly(lactic-*co*-glycolic acid) (PLGA)), P(3HB) shows little resistance to *in vitro* and *in vivo* degradation (Freier et al., 2002; Kunze et al., 2006; Saito et al., 1991). When implanted in the mandibular region of rats, it was found to degrade in six months. P(HBHV) and P(HBHHx) were also shown to be completely resorbed after three months in the subcutaneous region of rabbits (Jones et al., 2008; Kostopoulos & Karring, 1994; Philip, Keshavarz et al., 2007).

Furthermore, the effects of PHAs monomers on growth and cytotoxicity of target and surrounding cells have also been investigated. It has been demonstrated that 3HB, 3HB-*co*-3HHx and 3HHx had no adverse effects on murine fibroblast L929 cells if presented at a concentration of less than 20 mg/L (J. Sun et al., 2007). In addition, PHA monomeric units (3HB, 4HB and 3HV) have been proven to be less dangerous than other standard scaffolding polymers (e.g. PLA and PGA) thanks to their low acidity and bioactivity (Taylor et al., 1994).

Besides their non-toxic degradation, PHAs biocompatibility, their capacity to support cell adhesion and growth, is crucial for their commercialization. P(3HB) has been tested in various cell types, including osteoblasts, fibroblasts and chondrocytes, and it proved excellent biocompatibility with no side effects (Ali & Jamil, 2016). Moreover, mcl-PHA reported to shown to have a considerable biocompatible performance with human mesenchymal stromal cells (Naveen et al., 2015).

All these properties grant PHAs useful in many applications on the biomedical field, some examples include nerve regeneration, tissue-engineered heart valves, drug-carriers and medical sutures(Ali & Jamil, 2016).

The following work is focused on the study of the use of different PHA-based scaffolds as platforms for skin cell adhesion and growth, with the goal of skin reconstitution.

4.2. Materials and Methods

4.2.1. Animal Cell Culture Methods

4.2.1.1. Fibroblasts Defrosting

A cryovial containing human dermal fibroblasts (HFDn) (Neonate, P10875) was transferred from liquid nitrogen into a 37˚C water bath. In a 15 mL falcon, 500 µl of warm HDFn culture medium (IMDM Glutamax,10% Fetal Bovine Serum (FBS) and 0.1% Penstrep) and 500 µl of cell suspension were added alternatively until all cell suspension was in the falcon. The number of viable cells per mL was determined using a haemocytometer and the following equation:

$$\text{Number of Viable Cells: } \frac{X1 + X2 + X3 + X4}{4} \times \text{Dilution} \times 10^3 \quad (8)$$

Where X1, X2, X3 and X4 are the number of cells in each quadrant. The remaining cell suspension was distributed in a T-75 culture flask and incubated in a 37°C, 5% CO_2/ 95 % air, humidified cell culture incubator. The medium was changed once a week.

4.2.1.2. Fibroblasts Subculture

Culture medium was removed from the T-75 flask. 5 mL of PBS 1x was added and removed for washing. Trypsin-EDTA solution (5 mL) was added, and the flask was rocked to ensure coverage of the entire surface. The flask was incubated at room temperature for approximately 1 minute or until around 90% of cells are detached. 10 mL of HDFn culture medium was added to block trypsin-EDTA and the cell suspension was transferred to a sterile 50 mL falcon. The number of cells was determined as previously described and the cells were diluted in culture medium for a concentration of 4.0 x 10^3 cells/cm^2. The cells were seeded in a new culture vessel and incubated in a 37 °C, 5% CO_2/95% air, humidified cell culture incubator.

4.2.1.3. MTT Assay

Scaffolds produced by emulsion (P(3HB), P(HBHV)) and by electrospinning (P(3HB), P(HBHV) and P(HBHV)/mcl blend) untreated and treated by O_2 plasma were cut into circles of 1.5 cm in diameter to fit wells of 24 well plates. All scaffolds were sterilized under a 22-Watt UV lamp.

Fibroblasts were incubated after subculture until 90% confluent. Trypsin-EDTA solution (5 mL) was added, and the flask was rocked to ensure coverage of the entire surface. The flask was incubated at room temperature for approximately 1 minute or until around 90% of cells are detached. 10 mL of HDFn culture medium was added to block trypsin-EDTA and the cell suspension was transferred to a sterile 50 mL falcon. The cell suspension was centrifuged for 5 minutes (6000 rpm), the pellet was resuspended in 2 mL of HDFn culture medium and viable cells were counted. The cells were diluted for a concentration of 2 x 10^4 for each scaffold and plated in a 24 well plate, to use as a control, cells were seeded in wells with no scaffolds. Alvatex™ was also used as a positive control. The plates were incubated in a 37 °C, 5% CO_2/95% air, humidified cell culture incubator for 48 hours.

Following incubation, the culture medium was removed, and the scaffolds were transferred to new plates to discard any cells attached to the bottom of the well. The cells were washed with PBS 1x and 400 µm of fresh culture medium was added to each well and to well with no cells to use as white. 40 µm of MTT 5 mg/ml was added to each well and the plates were incubated for 4 hours, at 37 ˚C. After incubation, 200 µm of the extraction solution (89% isopropanol, 10% Trition-X, 1% HCL 0.37%) was added and the plates were agitated in an orbital shaker for 10 minutes (150 rpm), in the absence of light. The plates were then incubated for 2 hours, at room temperature, in the absence of light. The content of each well was homogenised and 200 µm was transferred to a 96-well plate. Absorbance was measured at 570 nm. Cells of 5th, 6th and 7th passage were used to assess reproducibility and triplicates of each type of scaffold were used in every assay. MTT assays were performed three times, in the same conditions, for statistical relevance. The results were submitted to statistical analysis with ordinary one-way ANOVA (GraphPad Prism 8.2.0).

4.2.1.4. Dermal Construct

Scaffolds produced by emulsion (P(3HB), P(HBHV)) and by electrospinning (P(3HB), P(HBHV) and P(HBHV)/mcl blend) untreated and treated by O_2 plasma were cut into circles of 1.5 cm in diameter to fit commercial inserts that fit 6 well plates. All scaffolds were sterilized under a 22-Watt UV lamp.

Fibroblasts were incubated after subculture until 90% confluent. Trypsin-EDTA solution (5 mL) was added, and the flask was rocked to ensure coverage of the entire surface. The flask was incubated at room temperature for approximately 1 minute or until around 90% of cells are detached. 10 mL of HDFn culture medium was added to block trypsin-EDTA and the cell suspension was transferred to a sterile 50 mL falcon. The cell suspension was centrifuged for 5 minutes (6000 rpm), the pellet was resuspended in 2 mL of HDFn culture medium and viable cells were counted. The cells were diluted for a concentration of 1 x 10^5 for each scaffold and seeded, one hour after seeding the scaffolds were completely submerged in dermal medium (HDFn culture medium supplemented with ascorbic acid (7.5 mg/mL) and incubated for 2 weeks in a 37 °C, 5% CO_2/95% air, humidified cell culture incubator. The medium was exchanged every 3 days. After the incubation period, each scaffold was preserved in 10% formalin and sent for histological processing and haematoxylin and eosin staining. Figure 4.1. shows a schematic representation of the dermal construct process.

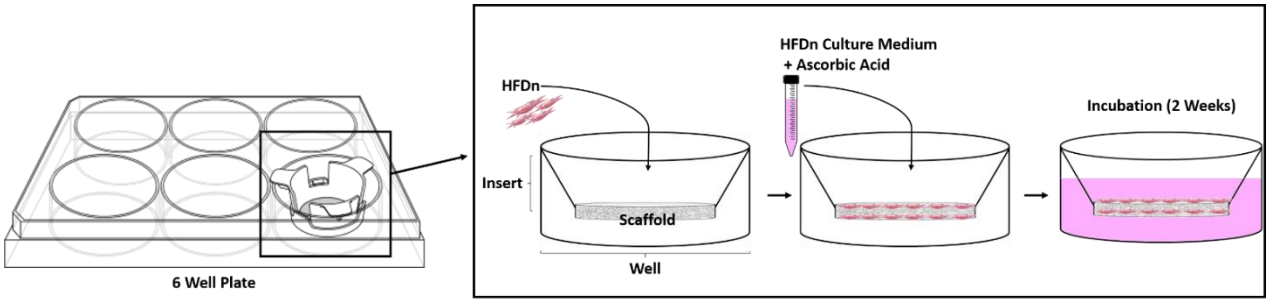

Figure 4.1 – Schematic representation of the dermal construct procedure.

4.1.5. Cell Fixation for SEM

Scaffolds produced by emulsion (P(3HB), P(HBHV)) and by electrospinning (P(3HB), P(HBHV) and P(HBHV)/mcl blend) untreated and treated by O_2 plasma were cut into circles of 1.5 cm and mounted as previously described for dermal constructs. All scaffolds were sterilized under a 22-Watt UV lamp. 2 x 10^4 cells were seeded, one hour after seeding the scaffolds were completely submerged in HDFn culture medium and incubated for 48 hours in a 37 °C, 5% CO_2/95% air, humidified cell culture incubator.

Following incubation, the cells were fixed with 2.5% glutaraldehyde for one hour, at room temperature. The scaffolds were subsequently washed with PBS 1x for 2 minutes followed with 2x dH_2O for 2 minutes. The scaffolds were then dehydrated with a graded ethanol series by subsequent exchanged of dilutions in deionized water (25% ETOH, 50% ETOH, 75% ETOH,95% ETOH and 100% ETOH). Each exchange had a duration of 5 minutes until 100% ETOH where the solution was exchanged twice and had a duration of 10 minutes. The scaffolds were left to air dry in a fume hood until completely dry and stored in a desiccator until observation.

4.3. Results and Discussion

4.3.1. MTT assay

In order to assess the scaffolds bioactivity, attachment and viability of human dermal fibroblasts was studied using the MTT assay on the most promising scaffolds, namely, emulsion templated P(3HB) and P(HBHV), as well as electrospun fibres of P(3HB), P(HBHV) and P(HBHV)/mcl-PHA blends. Oxygen plasma treatment's effect on bioactivity was also evaluated. For positive control, a commercial polystyrene scaffold (Alvatex™) was used as a reference.

Three independent trials were performed with cells of different passage for reproducibility purposes and empty wells were used as control and considered as 100% attachment. A ratio between the absorbance of each scaffold and the control was calculated for every trial, and then the average between all trials, as well as standard deviation was calculated (Figure 4.2). One-way ANOVA statistical method was utilized to compare the viability of cells cultured onto the different scaffolds and the results proved to be statistically significant ($p<0.05$) with a p-value of 0.01.

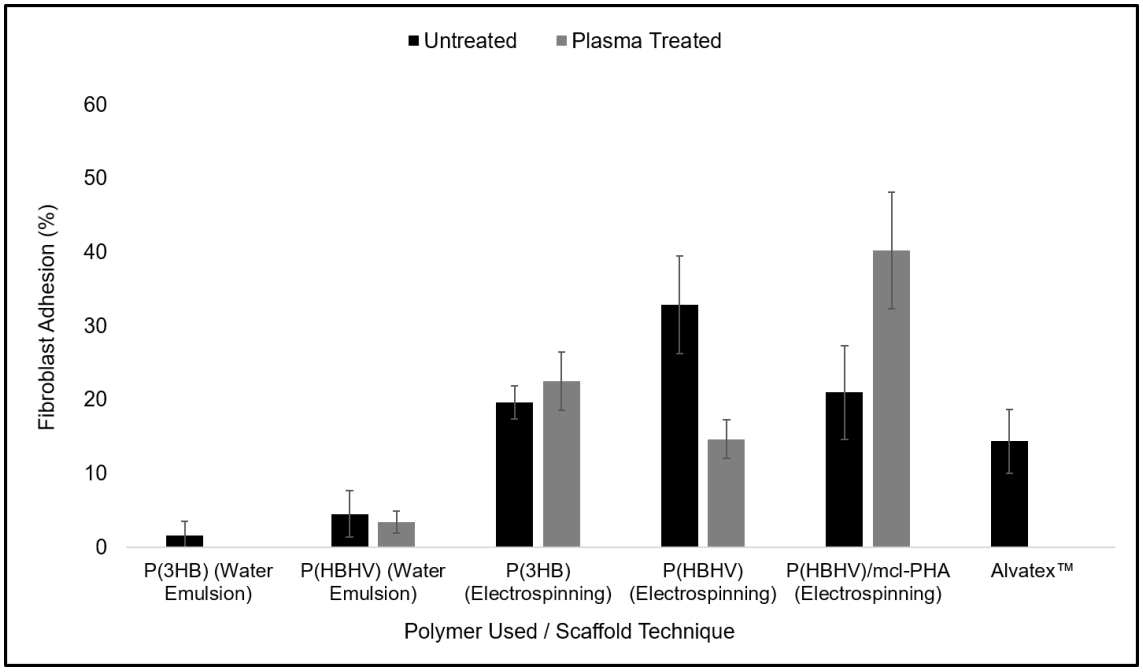

Figure 4.2- MTT assay results for human dermal fibroblast adhesion on different types of PHA based scaffolds with and without oxygen plasma treatment, as well as for commercial Alvatex™.

Emulsion templated scaffolds demonstrated a low percentage of fibroblasts attachment, P(3HB) emulsion templated scaffolds showed little attachment without treatment (1.6 ± 1.9%) and no attachment after plasma treatment, while P(HBHV) scaffolds demonstrated a 4.5 ± 3.1% attachment when untreated and 3.4 ± 1.5% after oxygen plasma treatment, presenting superior attachment than P(3HB) based scaffolds of the same fabrication technique. These results indicate that these scaffolds do not accommodate high fibroblast attachment, and that plasma treatment does not enhance cell adhesion. This can be correlated to the pore size being too small or be related to possible absorption of the dissolved MTT formazan onto the porous scaffolds, leading

to a false-negative result of the cell viability assay (Qi et al., 2011). For instance, an image of the scaffolds after MTT addition shows a more intense purple colour for treated P(HBHV) than for untreated scaffolds, but the absorbance indicates otherwise (Figure 4.3). This occurrence has been previously reported for other materials using the MTT assay, such as PLGA-based composite nanofibrous scaffolds (Qi et al., 2011), suggesting that alternative bioactivity assays could be considered.

Electrospun PHA microfibres showed more promising results. P(3HB) fibres presented an attachment superior to Alvatex™ scaffolds (14.4 ± 4.3%), with attachments of 19.6 ± 2.3% for untreated scaffolds and of 22.5 ± 4.0% for oxygen plasma-treated fibres, showing that plasma greatly improved cell attachment. In previous studies, P(3HB) plasma-treated materials also displayed improved cell attachment, examples include L-929 fibroblasts attachment and growth in solvent cast P(3HB) (Mirmohammadi et al., 2012) and mouse embryonic fibroblasts (NIH 3T3) attachment in P(3HB) foils (Slepička et al., 2014).

Regarding P(HBHV) electrospun scaffolds, untreated fibrous scaffolds exhibited attachment of 32.9 ± 6.6%, whereas treated fibres displayed a lower attachment of 14.6 ± 2.6%, comparable to the value presented by Alvatex™ scaffolds, this may be due to possible defects generated on P(HBHV) fibres, such as fractures, after plasma treatment (see section 3.3.6.1.2). In contrast to the observed in this study, previously reported studies proved that oxygen plasma treatment improved cell attachment onto P(HBHV) materials, such as osteoblasts attachment onto solvent cast with particulate leaching P(HBHV) (Köse et al., 2003b), and human retinal pigment epithelium (D407) attachment onto solvent cast P(HBHV) (Tezcaner et al., 2003). However, different cell lines may present different surface preferences, and electrospun P(HBHV) oxygen plasma-treated scaffolds could not have presented a favourable surface environment for human dermal fibroblast adhesion.

Finally, P(HBHV)/mcl-PHA scaffolds exhibited an adhesion of 20.9 ± 6.3% for untreated fibres and of 40.2 ± 7.9% for oxygen plasma-treated scaffolds, offering the best results in terms of attachment with a value almost three times superior to what is displayed for commercial Alvatex™ scaffolds. These results prove that electrospun P(HBHV)/mcl-PHA blends are great contenders for 3D-cell culture and that oxygen plasma can have a positive effect on attachment depending on the type of PHA that is employed.

Although MTT assay is the gold standard for the assessment of bioactivity, other tests could be performed to increase the reliability of these results, such as other colorimetric assays (XTT, LDH SRB, etc), fluorometric assays (alamarBlue and CFDA-AM), or luminometric assays like ATP assay (Aslantürk, 2018).

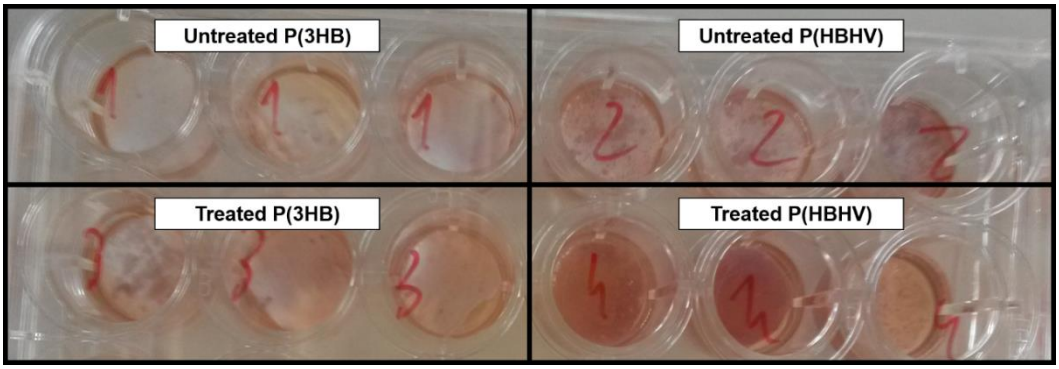

Figure 4.3- Emulsion templated PHA scaffolds after the formation of MTT purple formazan crystals.

4.3.2. Dermal Construct

To study cell proliferation and organization on PHA-based scaffolds into a dermis-like structure, fibroblasts were cultured onto emulsion templated P(3HB) and P(HBHV) untreated and oxygen plasma-treated scaffolds, as well as untreated and oxygen plasma-treated electrospun fibres of P(3HB), P(HBHV) and P(HBHV)/mcl-PHA blends. Ascorbic acid was supplemented to the HDFn culture medium since it has been reported to stimulate collagen production (Chojkier et al., 1989). After 2 weeks of cell culture, the scaffolds were fixed in formalin and sent for histological processing, where they were cut into sections and stained with haematoxylin and eosin (H&E staining).

Unfortunately, H&E staining revealed that there were no observable cells within any of the scaffolds that were investigated. These results can be linked to human error, or to lack of optimization of dermal construct parameters since the protocol that was employed was one intended for fibroblast culture onto Alvatex™ and not specific for PHA-based scaffolds. Therefore, a starting point for future experiments is the optimization of parameters of cell culture onto each type of PHA-based scaffold (electrospun and emulsion templated), such as concentration of seeded cells, ascorbic acid concentration, medium exchange necessities and culture duration.

4.3.3. Morphology of Cells Cultured onto PHA Scaffolds

In order to better investigate the cell morphology and their effect on the different scaffolds, cells were seeded onto emulsion templated P(3HB) and P(HBHV), as well as electrospun P(3HB), P(HBHV) and P(HBHV)/mcl-PHA fibre meshes and cultured for 48 hours, after which cells were immobilized and observed under SEM.

For emulsion templated scaffolds, it is difficult to distinguish between possible cell proliferation and just simple scaffold morphology, because they possess a very heterogeneous microstructure and since there is no biological marker. For untreated scaffolds, P(3HB) presented some areas that might exhibit a certain degree of cell attachment that show to be an opaquer film over the scaffold pores (Figure 4.4, a), emulsion templated P(HBHV) also showed some structures of what could be adhered fibroblasts (Figure 4.4, b). Oxygen plasma treated P(3HB) shows a more filled-in scaffold of what could be accounted as cell proliferation (Figure 4.4, c), treated P(HBHV) scaffolds, however, don't demonstrate any perceptible adhered cells (Figure 4.4, d). The degree of observed cell attachment may be lower because of poor attachment of cells or dislodgement during the immobilization process for SEM observation. As an alternative method for visualization of cells attached to the emulsion templated scaffolds, other appropriate types of microscopy reported in the literature for fibroblasts in 3D-environments could be performed, such as fluorescent microscopy with cell staining (Slepička et al., 2014) or confocal microscopy with cell labelling (Lin et al., 2011).

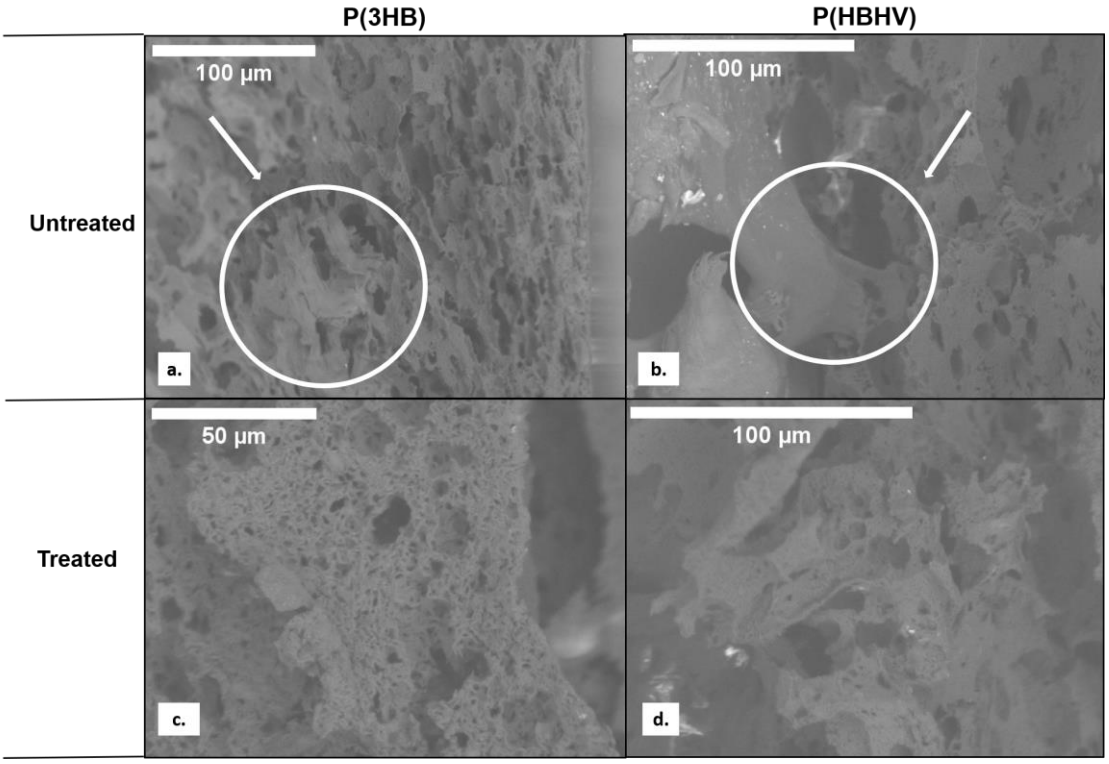

Figure 4.4- SEM images of human dermal fibroblasts attached to PHA-based emulsion templated scaffolds; (a) cross-section of untreated P(3HB) amplified 600x; (b) cross-section of untreated P(HBHV) amplified 800 x; (c) cross-section of oxygen plasma treated P(3HB) amplified 1200 x; (d) cross-section of oxygen plasma treated P(HBHV) amplified 1000x.

For electrospun fibres, it was possible to see cell attachment for all fibrous scaffolds in a much more obvious manner due to the morphology of the scaffolds (Figure 4.5), however, it was only possible to observe cells on plasma-treated scaffolds, which may imply that oxygen plasma produces a stronger attachment that is able to withstand immobilization without cell dislodgement, proving to be a favourable environment for cell adhesion and proliferation. The fibroblasts seem to elongate over the fibre's axis stretching to adhesion points on adjacent fibres in a similar way to other studies involving fibroblast culture onto electrospun fibres, for example as the reported for mouse fibroblast cells (L929) morphology onto a P(3HB)/silk fibroin composite nanofiber mats (Karahaliloğlu, 2017).

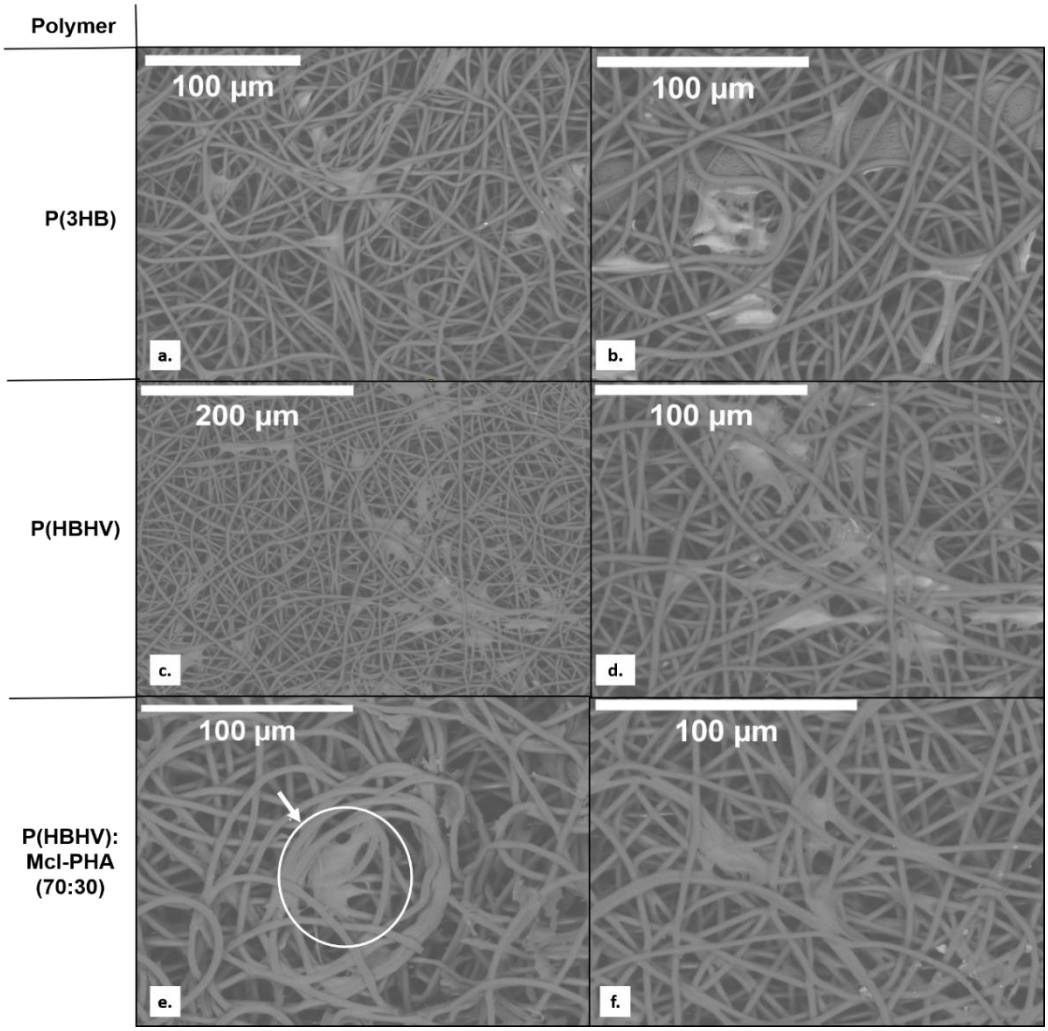

Figure 4.5- SEM images of human dermal fibroblasts attached to PHA-based electrospun scaffolds; (a) P(3HB) amplified 600x; (b) P(3HB) amplified 800 x; (c) P(HBHV) amplified 400 x; (d) P(HBHV) amplified 800x; (e) P(HBHV)/mcl-PHA amplified 800 x; (f) P(HBHV)/mcl-PHA amplified 1000x.

4.4. Conclusions

The bioactivity of PHA-based scaffolds, specifically emulsion templated P(3HB) and P(HBHV), as well as electrospun fibres of P(3HB), P(HBHV) and P(HBHV)/mcl-PHA blends, was assessed by the MTT assay and cell visualization through SEM. The effect of oxygen plasma on bioactivity was also determined.

The MTT assay showed statistically significant results ($p<0.05$) with a p-value of 0.01. Emulsion templated scaffolds did not offer a great degree of fibroblast adhesion with the higher attachment percentages being 1.6% for untreated P(3HB) and 4.5% for untreated P(HBHV) since oxygen plasma did not enhance attachment for these types of scaffolds. These results may indicate that emulsion templated scaffolds still need to be optimized (increase pore size and interconnectivity) or that alternative bioactivity assays need to be performed to confirm the validity of the MTT assay. Electrospun PHA fibres demonstrated more positive results, most untreated and oxygen plasma-treated scaffolds showed superior attachments to the commercial Alvatex™. The electrospun fibres that exhibited higher attachment were oxygen treated P(3HB) (22.5%), untreated P(HBHV) (32.9%) and finally oxygen treated P(HBHV)/mcl-PHA blend with a fibroblast adhesion of 40.2%, proving to be great contenders for 3D-cell culture. Furthermore, oxygen plasma seemed to have different effects depending on the type of PHA or scaffold fabrication techniques.

The dermal constructs using PHA-based scaffolds proved to be unsuccessful revealing a need for parameter optimization, namely, the concentration of seeded cells, ascorbic acid concentration, medium exchange necessities and culture duration.

SEM visualization of seeded fibroblasts onto the porous and fibrous PHA-based scaffolds permitted the observation of cell morphology. Cell distinction onto emulsion templated scaffolds demonstrated to be difficult since there are no biological markers and due to the heterogenicity of the scaffolds, suggesting that an alternative mode of visualization would be of benefit. Electrospun PHA-based fibres showed to be favourable environments for cell attachment and growth, although cell visualization was only possible on oxygen plasma treated scaffolds.

Overall, electrospun PHA fibres seem to be the most promising contenders for 3D-cell culture, and oxygen plasma proved to be a valuable surface modification treatment to enhance bioactivity of 3D-scaffolds.

Chapter 5- Conclusions and Future Perspectives

5.1. Conclusions and Future Perspectives

In this work, PHAs were obtained by microbial cultivation using glycerol or used cooking oil as carbon sources to produce mcl-PHA and P(3HB) polymers, respectively, and used cooking oil with levulinic acid co-substrate to produce P(HBHV). The resulting polymers offered different physical and chemical properties, demonstrating the versatility of PHA production by just changing the bacterial strain and/or carbon source.

Many different techniques were employed for scaffold fabrication using the polymers that were obtained from bioreactor experiments. Methods such as solvent casting with particulate leaching and supercritical CO_2 showed some promising results, however, it was clear the need for optimization in future work such as testing different porogens with SCPL, or tuning process parameters in $scCO_2$, like pressure, soaking time, temperature and even the use of other PHAs. Emulsion templating displayed positive results when it came to implementing porosity while maintaining the physical properties of the polymers, however, future work should focus on developing strategies to better tune pore size, as well as fabricate mcl-PHA porous scaffolds with this technique, which was not possible in this study. Some possibilities include the use of surfactants or the addition of electrolyte content in the water phase. Electrospinning proved to be a successful process to produce fibrous scaffolds with P(3HB) and P(HBHV) and allowed the fabrication of a polymer blend with P(HBHV) and mcl-PHA that displayed improved mechanical properties. Subsequent studies should further explore PHA blends, using mixtures of different PHAs, or even PHAs with other biopolymers, in hopes to enhance mechanical properties and biocompatibility.

Surface modification trough oxygen plasma increased the scaffolds hydrophilicity water uptake ability and biocompatibility. Scaffolds produced trough electrospinning offered fibroblast adhesion up to 40% for plasma-treated P(HBHV)/mcl-blends, although promising, future work should aim to increase these values and to enhance biocompatibility, a possible strategy is the immobilization of bio-macromolecules onto the surface of the scaffolds.

Additionally, proposed studies include the optimization of the dermal construct procedure for the investigation of fibroblast proliferation and ability to form a dermis-like structure using the scaffolds produced in this work, in hopes to then add keratinocytes for an epidermis layer to finally obtain a 3D-model that morphologically and physiologically resembles human skin.

References

Abd, E., Yousef, S. A., Pastore, M. N., Telaprolu, K., Mohammed, Y. H., Namjoshi, S., Roberts, M. S. (2016). Skin models for the testing of transdermal drugs. Clinical Pharmacology: Advances and Applications, 8, 163–176.

Ajalloueian, F., Tavanai, H., Hilborn, J., Donzel-Gargand, O., Leifer, K., Wickham, A., & Arpanaei, A. (2014). Emulsion electrospinning as an approach to fabricate PLGA/chitosan nanofibers for biomedical applications. BioMed Research International, vol. 2014, Article ID 475280, 13 pages.

Ali, I., & Jamil, N. (2016). Polyhydroxyalkanoates: Current applications in the medical field. Frontiers in Biology, 11(1), 19–27.

Anjum, A., Zuber, M., Zia, K. M., Noreen, A., Anjum, M. N., & Tabasum, S. (2016). Microbial production of polyhydroxyalkanoates (PHAs) and its copolymers: A review of recent advancements. International Journal of Biological Macromolecules, 89, 161–174.

Aslantürk, Ö. S. (2018). In vitro cytotoxicity and cell viability assays: principles, advantages, and disadvantages. Genotoxicity - A predictable risk to our actual world; IntechOpen limited, London; pp. 1-17.

Baker, B. M., & Mauck, R. L. (2007). The effect of nanofiber alignment on the maturation of engineered meniscus constructs. Biomaterials, 28(11), 1967–1977.

Balani, K., Verma, V., Agarwal, A., & Narayan, R. (2015). Physical, thermal, and mechanical properties of polymers. In Biosurfaces: A Materials Science and Engineering Perspective; John Wiley & Sons, Inc: Hoboken, NJ, USA; pp. 329–344.

Basnett, P., Lukasiewicz, B., Marcello, E., Gura, H. K., Knowles, J. C., & Roy, I. (2017). Production of a novel medium chain length poly(3-hydroxyalkanoate) using unprocessed biodiesel waste and its evaluation as a tissue engineering scaffold. Microbial Biotechnology, 10(6), 1384–1399.

Bell, E., Ehrlich, H. P., Buttle, D. J., & Nakatsuji, T. (1981). Living tissue formed in vitro and accepted as skin-equivalent tissue of full thickness. Science, 211(4486), 1052-4.

Bergstrand, A., Andersson, H., Cramby, J., Sott, K., & Larsson, A. (2012). Preparation of porous poly(3-Hydroxybutyrate) films by water-droplet templating. Journal of Biomaterials and Nanobiotechnology, 3(4), 431–439.

Bergstrand, A., Uppström, S., & Larsson, A. (2014). Permeability of porous poly(3-hydroxybutyrate) barriers of single and bilayer type for implant applications. International Journal of Polymer Science, 9, 1 - 8.

Bertrand, J. L., Ramsay, B. A., & Chavarie, C. (1990). Biosynthesis of poly-β-hydroxyalkanoates from pentoses by *Pseudomonas pseudoflava*. Applied and Environmental Microbiology, 56(10), 3133-8.

Bohmert, K., Balbo, I., Steinbüchel, A., Tischendorf, G., & Willmitzer, L. (2002). Constitutive xxpression of the β-Ketothiolase gene in transgenic plants. A major obstacle for obtaining polyhydroxybutyrate-producing plants. Plant Physiology, 128(4), 1282–1290.

Böttcher-Haberzeth, S., Biedermann, T., & Ernest, R. (2010). Tissue engineering of skin. Burns, 36, 450–460.

Brohem, C. A., Da Silva Cardeal, L. B., Tiago, M., Soengas, M. S., De Moraes Barros, S. B., & Maria-Engler, S. S. (2011). Artificial skin in perspective: Concepts and applications. Pigment Cell and Melanoma Research, 24(1), 35-50.

Burton, Z., & Bhushan, B. (2005). Hydrophobicity, adhesion, and friction properties of nanopatterned polymers and scale dependence for micro- and nanoelectromechanical systems. Nano Letters, 5(8), 1607-13.

Bustamante, D., Tortajada, M., Ramon, D., & Rojas, A. (2019). Camelina oil as a promising substrate for mcl-PHA production in *Pseudomonas* sp. cultures. Applied Food Biotechnology, 6(1), 61–70.

Cameron, N. R. (2005). High internal phase emulsion templating as a route to well-defined porous polymers. Polymer, 46(5), 1439–1449.

Canadas, R. F., Cavalheiro, J. M. B. T., Guerreiro, J. D. T., de Almeida, M. C. M. D., Pollet, E., da Silva, C. L., & Ferreira, F. C. (2014). Polyhydroxyalkanoates: Waste glycerol upgrade into electrospun fibrous scaffolds for stem cells culture. International Journal of Biological Macromolecules, 71, 131–140.

Carlson, M. W., Alt-Holland, A., Egles, C., & Garlick, J. A. (2008). Three-dimensional tissue models of normal and diseased skin. Current Protocols in Cell Biology, 19, 19.9.

Cavalheiro, J. M. B. T., de Almeida, M. C. M. D., Grandfils, C., & da Fonseca, M. M. R. (2009). Poly(3-hydroxybutyrate) production by *Cupriavidus necator* using waste glycerol. Process Biochemistry, 44(5), 509–515.

Chen, G. Q. (2009). A microbial polyhydroxyalkanoates (PHA) based bio- and materials industry. Chemical Society Reviews, 38(8), 2434-46.

Chen, G. Q., Wu, Q., Wang, Y. W., & Zheng, Z. (2009). Application of microbial polyesters-polyhydroxyalkanoates as tissue engineering materials. Key Engineering Materials, 26(33), 6565-78.

Chojkier, M., Houglum, K., Solis-Herruzo, J., & Brenner, D. A. (1989). Stimulation of collagen gene expression by ascorbic acid in cultured human fibroblasts. A role for lipid peroxidation? Journal of Biological Chemistry, 264(28), 16957–16962.

Choudhury, M., Mohanty, S., & Nayak, S. (2015). Effect of different solvents in solvent casting of porous PLA scaffolds—In biomedical and tissue engineering applications. Journal of Biomaterials and Tissue Engineering, 5(1), 1–9.

Ciesielski, S., Mozejko, J., & Przybyłek, G. (2010). The influence of nitrogen limitation on mcl-PHA synthesis by two newly isolated strains of *Pseudomonas* sp. Journal of Industrial Microbiology and Biotechnology, 37(5), 511–520.

Cooper, T. A. (2013). Developments in bioplastic materials for packaging food, beverages and other fast-moving consumer goods. In Trends in Packaging of Food, Beverages and Other Fast-Moving Consumer Goods (FMCG) , 1, 4 – 5.

Cromwick, A. M., Foglia, T., & Lenz, R. W. (1996). The microbial production of poly(hydroxyalkanoates) from tallow. Applied Microbiology and Biotechnology, 46(5), 464-469.

Cruz, M. V., Freitas, F., Paiva, A., Mano, F., Dionísio, M., Ramos, A. M., & Reis, M. A. M. (2016). Valorization of fatty acids-containing wastes and byproducts into short- and medium-chain length polyhydroxyalkanoates.New Biotechnology, 33(1), 206–215.

Cruz, M. V., Paiva, A., Lisboa, P., Freitas, F., Alves, V. D., Simões, P., Reis, M. A. M. (2014). Production of polyhydroxyalkanoates from spent coffee grounds oil obtained by supercritical fluid extraction technology. Bioresource Technology, 157, 360–363.

Cruz, M. V., Sarraguça, M. C., Freitas, F., Lopes, J. A., & Reis, M. A. M. (2015). Online monitoring of P(3HB) produced from used cooking oil with near-infrared spectroscopy. Journal of Biotechnology, 194, 1–9.

Degeratu, C. N., Zaharia, C., Tudora, M. R., Tucureanu, C., & Hubca, G. (2010). Influence of Porosity Upon Cells Adhesion on Polyhydroxyalkanoates Films, 55(69), 189–192.

Del Gaudio, C., Fioravanzo, L., Folin, M., Marchi, F., Ercolani, E., & Bianco, A. (2012). Electrospun tubular scaffolds: On the effectiveness of blending poly(ε-caprolactone) with poly(3-hydroxybutyrate-*co*-3-hydroxyvalerate). Journal of Biomedical Materials Research - Part B Applied Biomaterials, 100(7), 1883-98.

Denes, F. S., & Manolache, S. (2004). Macromolecular plasma-chemistry: An emerging field of polymer science. Progress in Polymer Science (Oxford). 29(8), 815-885.

Duarte, A. R. C., Mano, J. F., & Reis, R. L. (2009). Supercritical fluids in biomedical and tissue engineering applications: A review. International Materials Reviews, 54(4), 214–222.

Duval, K., Grover, H., Han, L. H., Mou, Y., Pegoraro, A. F., Fredberg, J., & Chen, Z. (2017). Modeling physiological events in 2D vs. 3D cell culture. Physiology, 32(4), 266-277.

Dwivedi, C., Pandey, I., Pandey, H., Ramteke, P. W., Pandey, A. C., Mishra, S. B., & Patil, S. (2017). Electrospun nanofibrous scaffold as a potential carrier of antimicrobial therapeutics for diabetic wound healing and tissue regeneration. In Nano- and Microscale Drug Delivery Systems: Design and Fabrication; Elsevier; pp 147-164.

Engler, A. J., Sen, S., Sweeney, H. L., & Discher, D. E. (2006). Matrix elasticity directs stem cell lineage specification. Cell, 126(4), 677-89.

European Bioplastics. (2017a). Bioplastic market data 2016, Available at: http://www.european-bioplastics.org/news/publications/, 4. Retrieved from http://docs.european-bioplastics.org/publications/EUBP_Bioplastics_market_data_report_2016.pdf

European Bioplastics. (2017b). Report - Bioplastics market data (www.european-bioplastics.org/market), 3. Retrieved from http://docs.european-bioplastics.org/publications/market_data/2017/Report_Bioplastics_Market_Data_2017.pdf

European Bioplastics. (2018). Bioplastics market data 2018. https://www.european-bioplastics.org/new-market-data-the-positive-trend-for-the-bioplastics-industry-remains-stable/. Retrieved from https://www.european-bioplastics.org/new-market-data-the-positive-trend-for-the-bioplastics-industry-remains-stable/

Fan, X., Jiang, Q., Sun, Z., Li, G., Ren, X., Liang, J., & Huang, T. S. (2015). Preparation and characterization of electrospun antimicrobial fibrous membranes based on polyhydroxybutyrate (PHB), 16(8), 1751–1758.

Ferreira, C. C., Botelho, G., Correia, D. M., & Ribeiro, C. (2014). Influence of electrospinning parameters on poly (hydroxybutyrate) electrospun membranes fiber size and distribution. Polymer Engineering and Science, 54(7), 1608–1617.

Flores-Sánchez, A., López-Cuellar, M. D. R., Pérez-Guevara, F., Figueroa López, U., Martín-Bufájer, J. M., & Vergara-Porras, B. (2017). Synthesis of poly-(R-hydroxyalkanoates) by *Cupriavidus necator* ATCC 17699 using mexican avocado (*Persea americana*) oil as a carbon source. International Journal of Polymer Science, 3, 1-10.

Foraida, Z. I., Kamaldinov, T., Nelson, D. A., Larsen, M., & Castracane, J. (2017). Elastin-PLGA hybrid electrospun nanofiber scaffolds for salivary epithelial cell self-organization and polarization. Acta Biomaterialia, 62, 116-127.

Freier, T., Kunze, C., Nischan, C., Kramer, S., Sternberg, K., Saß, M., Schmitz, K. P. (2002). In vitro and in vivo degradation studies for development of a biodegradable patch based on poly(3-hydroxybutyrate). Biomaterials, 23(13), 2649-2657.

Gahlawat, G., & Soni, S. K. (2017). Bioresource Technology Valorization of waste glycerol for the production of poly copolymer by *Cupriavidus necator* and extraction in a sustainable manner. Bioresource Technology, 243, 492–501.

Gao, X., Jian, J., Li, W. J., Yang, Y. C., Shen, X. W., Sun, Z. R., Chen, G. Q. (2013). Genomic study of polyhydroxyalkanoates producing *Aeromonas hydrophila* 4AK4. Applied Microbiology and Biotechnology, 97(20), 9099-109.

Gerard, T., & Budtova, T. (2012). Morphology and molten-state rheology of polylactide and polyhydroxyalkanoate blends. European Polymer Journal, 48(6), 1110-1117.

Godbole, S., Gote, S., Latkar, M., & Chakrabarti, T. (2003). Preparation and characterization of biodegradable poly-3-hydroxybutyrate-starch blend films. Bioresource Technology, 86(1), 33-37.

H. G. Schlegel, G. Gottschalk. & R. V. B. (1961). Formation and utilization of poly-β-hydroxybutyric acid by Knallgas bacteria (*Hydrogenomonas*). Nature, (191), 463–465.

Haider, A., Haider, S., & Kang, I. K. (2018). A comprehensive review summarizing the effect of electrospinning parameters and potential applications of nanofibers in biomedical and biotechnology. Arabian Journal of Chemistry, 11(8), 1165–1188.

Hassan, M. I., Chong, L. H., & Sultana, N. (2016). Wettability and water uptake properties of PLA and PCL/Gelatin-based electrospun fibers. ARPN Journal of Engineering and Applied Sciences, 11(23), 13604–13607.

Hayward, A. S., Sano, N., Przyborski, S. A., & Cameron, N. R. (2013). Acrylic-acid-functionalized polyhipe scaffolds for use in 3d cell culture. Macromolecular Rapid Communications, 34, 23-24.

Heywood, H. K., Sembi, P. K., Lee, D. A., & Bader, D. L. (2004). Cellular utilization determines viability and matrix distribution profiles in chondrocyte-seeded alginate constructs. Tissue Engineering, 10(9-10), 1467-79.

Huh, D., Hamilton, G. A., & Ingber, D. E. (2011). From 3D cell culture to organs-on-chips. Trends in Cell Biology, 21(12), 745–754.

Jasso-Gastinel, C. F., Soltero-Martínez, J. F. A., & Mendizábal, E. (2016). Introduction: Modifiable characteristics and applications. In Modification of Polymer Properties; Elsevier; pp 1–21.

Jones, N., Cooper, J., Waters, R., & Williams, D. (2008). Resorption profile and biological response of calcium phosphate filled PLLA and PHB7V. In Synthetic Bioabsorbable Polymers for Implants, ed. C. Agrawal, J. Parr, and S. Lin; ASTM international; pp 69-82.

Jongpaiboonkit, L., King, W. J., Lyons, G. E., Paguirigan, A. L., Warrick, J. W., Beebe, D. J., & Murphy, W. L. (2008). An adaptable hydrogel array format for 3-dimensional cell culture and analysis. Biomaterials, 29(23), 3346-56.

Jung, Y. C., & Bhushan, B. (2006). Contact angle, adhesion and friction properties of micro-and nanopatterned polymers for superhydrophobicity. Nanotechnology, 17(19), 4970.

Kancheva, M., Toncheva, A., Manolova, N., & Rashkov, I. (2015). Enhancing the mechanical properties of electrospun polyester mats by heat treatment. Express Polymer Letters, 9(1), 49–65.

Karahaliloğlu, Z. (2017). Cell-compatible PHB/silk fibroin composite nanofiber mat for tissue engineering applications. Turkish Journal of Biology, 41(3), 503–513.

Kaur, L., Khajuria, R., Parihar, L., & Singh, G. D. (2017). Polyhydroxyalkanoates: Biosynthesis to pommercial production: a review. Journal of Microbiology, Biotechnology and Food Sciences, 6(4), 1098–1106.

Ke, Y., Liu, C., Zhang, X., Xiao, M., & Wu, G. (2017). Surface modification of polyhydroxyalkanoates toward enhancing cell compatibility and antibacterial activity. Macromolecular Materials and Engineering. Wiley-VCH Verlag, 302(11), 1700258.

Keller, G. M. (1995). In vitro differentiation of embryonic stem cells. Current Opinion in Cell Biology, 7(6), 862-9.

Khanna, S., & Srivastava, A. K. (2005). Recent advances in microbial polyhydroxyalkanoates. Process Biochemistry, 40(2), 607-619.

Knight, E., & Przyborski, S. (2015). Advances in 3D cell culture technologies enabling tissue-like structures to be created in vitro. Journal of Anatomy, 227(6), 746–756.

Koller, M., & Marsalek, L. (2015). Principles of glycerol-based polyhydroxyalkanoate production. Applied Food Biotechnology, 2(4), 3–10.

Köse, G. T., Ber, S., Korkusuz, F., & Hasirci, V. (2003). Poly(3-hydroxybutyric acid-co-3-hydroxyvaleric acid) based tissue engineering matrices. In Journal of Materials Science: Materials in Medicine, 14(2), 121-6.

Kostopoulos, L., & Karring, T. (1994). Guided bone regeneration in mandibular defects in rats using a bioresorbable polymer. Clinical Oral Implants Research, 5(2), 66-74.

Kunze, C., Bernd, H. E., Androsch, R., Nischan, C., Freier, T., Kramer, S., & Schmitz, K. P. (2006). In vitro and in vivo studies on blends of isotactic and atactic poly (3-hydroxybutyrate) for development of a dura substitute material. Biomaterials, 27(2), 192-201.

Laursen, J. B., & Nielsen, J. (2004). Phenazine natural products: Biosynthesis, synthetic analogues, and biological activity. Chemical Reviews, 104(3), 1663-86.

Lee, S. Y. (1996a). Bacterial polyhydroxyalkanoates. Biotechnology and Bioengineering, 49(1),

1–14.

Lee, S. Y. (1996b). Plastic bacteria? Progress and prospects for polyhydroxyalkanoate production in bacteria. Trends in Biotechnology, 14(11), 431–438.

Lemechko, P., Le Fellic, M., & Bruzaud, S. (2019). Production of poly(3-hydroxybutyrate-co-3-hydroxyvalerate) using agro-industrial effluents with tunable proportion of 3-hydroxyvalerate monomer units. International Journal of Biological Macromolecules, 128, 429–434.

Levenberg, S., Huang, N. F., Lavik, E., Rogers, A. B., Itskovitz-Eldor, J., & Langer, R. (2003). Differentiation of human embryonic stem cells on three-dimensional polymer scaffolds. Proceedings of the National Academy of Sciences of the United States of America, 100(22), 12741-6.

Li, W., Cicek, N., Levin, D. B., & Liu, S. (2018). Enabling electrospinning of medium-chain length polyhydroxyalkanoates (PHAs) by blending with short-chain length PHAs. International Journal of Polymeric Materials and Polymeric Biomaterials, 68(9), 1–11.

Li, Z., Yang, J., & Loh, X. J. (2016). Polyhydroxyalkanoates: Opening doors for a sustainable future. NPG Asia Materials, 8(4), e265-20.

Lim, X., Potter, M., Cui, Z., & Dye, J. F. (2018). Manufacture and characterisation of EmDerm—novel hierarchically structured bio-active scaffolds for tissue regeneration. Journal of Materials Science: Materials in Medicine, 29(6), 79.

Lin, J. Y., Lin, W. J., Hong, W. H., Hung, W. C., Nowotarski, S. H., Gouveia, S. M., & Lin, K. H. (2011). Morphology and organization of tissue cells in 3D microenvironment of monodisperse foam scaffolds. Soft Matter, 7(21), 10010–10016.

Liu, C., Xia, Z., & Czernuszka, J. T. (2007). Design and development of three-dimensional scaffolds for tissue engineering. Chemical Engineering Research and Design, 85(7), 1051–1064.

Ma, P. X., & Choi, J. W. (2001). Biodegradable polymer scaffolds with well-defined interconnected spherical pore network. Tissue Engineering, 7(1), 23-33.

Madigan, M. T., Martinko, J. M., & Parker, J. (2000). Brock - biology of microorganisms, 9, 135–162.

Martino, L., Cruz, M. V., Scoma, A., Freitas, F., Bertin, L., Scandola, M., & Reis, M. A. M. (2014). Recovery of amorphous polyhydroxybutyrate granules from *Cupriavidus necator* cells grown on used cooking oil. International Journal of Biological Macromolecules, 71, 117–123.

Martins, M., Craveiro, R., Paiva, A., Duarte, A. R. C., & Reis, R. L. (2014). Supercritical fluid processing of natural based polymers doped with ionic liquids. Chemical Engineering Journal, 241, 122–130.

Mas, A., Jaaba, H., Schue, F., Belu, A. M., Kassis, C., Linton, R. W., & Desimone, J. M. (1997). Poly(hydroxybutyrate-co-9% hydroxyvalerate) film surface modification by Ar, O_2, H_2O/O_2, H_2O, and H_2O_2 plasma treatment. Journal of Macromolecular Science - Pure and Applied Chemistry, 34(1), 67-69.

Mauclaire, L., Brombacher, E., Bünger, J. D., & Zinn, M. (2010). Factors controlling bacterial attachment and biofilm formation on medium-chain-length polyhydroxyalkanoates (mcl-

PHAs). Colloids and Surfaces B: Biointerfaces, 76(1), 104-11.

Mirmohammadi, S. A., Khorasani, M. T., Mirzadeh, H., & Irani, S. (2012). Investigation of plasma treatment on poly(3-hydroxybutyrate) film surface: Characterization and invitro assay. Polymer - Plastics Technology and Engineering, 51(13), 1319–1326.

Misra, S. K., Valappil, S. P., Roy, I., & Boccaccini, A. R. (2006). Polyhydroxyalkanoate (PHA)/inorganic phase composites for tissue engineering applications. Biomacromolecules, 7(8), 2249-58.

Mobasseri, S. A., Terenghi, G., & Downes, S. (2014). Schwann cell interactions with polymer films are affected by groove geometry and film hydrophilicity. Biomedical Materials, 9(5), 055004.

Monteiro-Riviere, N. (2006). Structure and Function of Skin. In Toxicology of the skin-target organ series, 29, 1–19.

Morais, C., Freitas, F., Cruz, M. V., Paiva, A., Dionísio, M., & Reis, M. A. M. (2014). Conversion of fat-containing waste from the margarine manufacturing process into bacterial polyhydroxyalkanoates. International Journal of Biological Macromolecules, 71, 68-73.

Mottin, A. C., Ayres, E., Preto, O., & Horizonte, B. (2016). What changes in poly (3-Hydroxybutyrate) (PHB) when processed as electrospun nanofibers or thermo-compression molded film ?. Materials Research, 19(1), 57–66.

Możejko-Ciesielska, J., & Kiewisz, R. (2016). Bacterial polyhydroxyalkanoates: Still fabulous? Microbiological Research, 192(2016), 271–282.

Muhr, A., Rechberger, E. M., Salerno, A., Reiterer, A., Malli, K., Strohmeier, K., & Koller, M. (2013). Novel Description of mcl-PHA Biosynthesis by *Pseudomonas chlororaphis* from Animal-Derived Waste. Journal of Biotechnology, 165(1), 45-51.

Muhr, A., Rechberger, E. M., Salerno, A., Reiterer, A., Schiller, M., Kwiecień, M., & Koller, M. (2013). Biodegradable latexes from animal-derived waste: Biosynthesis and characterization of mcl-PHA accumulated by *Ps. citronellolis*. Reactive and Functional Polymers, 73(10), 1391–1398.

Naranda, J., Sušec, M., Maver, U., Gradišnik, L., Gorenjak, M., Vukasović, A., & Krajnc, P. (2016). Polyester type polyHIPE scaffolds with an interconnected porous structure for cartilage regeneration. Scientific Reports, 6, 1–11.

Naveen, S. V., Tan, I. K. P., Goh, Y. S., Balaji Raghavendran, H. R., Murali, M. R., & Kamarul, T. (2015). Unmodified medium chain length polyhydroxyalkanoate (uMCL-PHA) as a thin film for tissue engineering application - Characterization and in vitro biocompatibility. Materials Letters, 141, 55-58.

Ng, K. S., Ooi, W. Y., Goh, L. K., Shenbagarathai, R., & Sudesh, K. (2010). Evaluation of jatropha oil to produce poly(3-hydroxybutyrate) by *Cupriavidus necator* H16. In Polymer Degradation and Stability, 95(8), 1365-1369.

Obruca, S., Marova, I., Snajdar, O., Mravcova, L., & Svoboda, Z. (2010a). Production of poly(3-hydroxybutyrate-co-3-hydroxyvalerate) by *Cupriavidus necator* from waste rapeseed oil using propanol as a precursor of 3-hydroxyvalerate. Biotechnology Letters, 32(12), 1925–1932.

Okochi, M., Matsumura, T., Yamamoto, S., Nakayama, E., Jimbow, K., & Honda, H. (2013). Cell behavior observation and gene expression analysis of melanoma associated with stromal fibroblasts in a three-dimensional magnetic cell culture array. Biotechnology Progress, 29(1), 135-42.

Ouyang, H. W., Goh, J. C. H., Thambyah, A., Teoh, S. H., & Lee, E. H. (2003). Knitted poly-lactide-co-glycolide scaffold loaded with bone marrow stromal cells in repair and regeneration of rabbit achilles tendon. Tissue Engineering, 9(3), 431-9.

Owen, R., Sherborne, C., Paterson, T., Green, N. H., Reilly, G. C., & Claeyssens, F. (2016). Emulsion templated scaffolds with tunable mechanical properties for bone tissue engineering. Journal of the Mechanical Behavior of Biomedical Materials, 54, 159–172.

Pais, J., Serafim, L. S., Freitas, F., & Reis, M. A. M. (2016). Conversion of cheese whey into poly(3-hydroxybutyrate-co-3-hydroxyvalerate) by *Haloferax mediterranei*. New Biotechnology, 33(1), 224–230.

Pamua, E., Ba, M., Czajkowska, B., Dobrzyñski, P., Bero, M., & Kasperczyk, J. (2004). Elaboration and characterization of biodegradable scaffolds from poly(L-lactide-*co*-glycolide) copolymer synthesized with low-toxic zirconium acetylacetonate. Ann Transplant, 9(1), 64–67.

Philip, S., Keshavarz, T., & Roy, I. (2007). Polyhydroxyalkanoates: Biodegradable polymers with a range of applications. Journal of Chemical Technology and Biotechnology, 82(3), 233-247.

Phung, Y. T., Barbone, D., Broaddus, V. C., & Ho, M. (2011). Rapid generation of in vitro multicellular spheroids for the study of monoclonal antibody therapy. Journal of Cancer, 2, 507-14.

Qi, R., Shen, M., Cao, X., Guo, R., Tian, X., Yu, J., & Shi, X. (2011). Exploring the dark side of MTT viability assay of cells cultured onto electrospun PLGA-based composite nanofibrous scaffolding materials. Analyst, 136(14), 2897–2903.

Rathbone, S., Furrer, P., Lübben, J., Zinn, M., & Cartmell, S. (2010). Biocompatibility of polyhydroxyalkanoate as a potential material for ligament and tendon scaffold material. Journal of Biomedical Materials Research - Part A, 93(4), 1391–1403.

Rebocho, A. T., Pereira, J. R., Freitas, F., Neves, L. A., Alves, V. D., Sevrin, C., & Reis, M. A. M. (2019). Production of medium-chain length polyhydroxyalkanoates by *Pseudomonas citronellolis* grown in apple pulp waste. Applied Food Biotechnology, 6(1), 71–82.

Rebocho, A. T. (2018). Development of films based on bacterial biopolyesters produced from apple pulp waste. Masters in Biotechnology by FCT/UNL

Reis, M., Albuquerque, M., Villano, M., & Majone, M. (2011). Mixed Culture Processes for Polyhydroxyalkanoate Production from Agro-Industrial Surplus/Wastes as Feedstocks. Comprehensive Biotechnology, 6(2), 670-682.

Rudin, A., & Choi, P. (2013). Biopolymers. In The Elements of Polymer Science & Engineering; Elsevier: Amsterdam, The Netherlands; pp. 521–535.

Ruiz, I., Hermida, É. B., & Baldessari, A. (2011). Fabrication and characterization of porous PHBV

scaffolds for tissue engineering. Journal of Physics: Conference Series, 332(1).

Saito, T., Tomita, K., Juni, K., & Ooba, K. (1991). In vivo and in vitro degradation of poly(3-hydroxybutyrate) in rat. Biomaterials, 12(3), 309-12.

Salehizadeh, H., & Van Loosdrecht, M. C. M. (2004). Production of polyhydroxyalkanoates by mixed culture: Recent trends and biotechnological importance. Biotechnology Advances, 22(3), 261–279.

Samsudin, N., Hashim, Y. Z. H. Y., Arifin, M. A., Mel, M., Salleh, H. M., Sopyan, I., & Jimat, D. N. (2017). Optimization of ultraviolet ozone treatment process for improvement of polycaprolactone (PCL) microcarrier performance. Cytotechnology, 69(4), 601–616.

Sánchez, R. J., Schripsema, J., Da Silva, L. F., Taciro, M. K., Pradella, J. G. C., & Gomez, J. G. C. (2003). Medium-chain-length polyhydroxyalkanoic acids (PHA mcl) produced by *Pseudomonas putida* IPT 046 from renewable sources. European Polymer Journal, 39, 1385–1394.

Sankhla, I. S., Bhati, R., Singh, A. K., & Mallick, N. (2010). Poly(3-hydroxybutyrate-co-3-hydroxyvalerate) co-polymer production from a local isolate, *Brevibacillus invocatus* MTCC 9039. Bioresource Technology, 101(6), 1947–1953.

Saraf, A., Baggett, L. S., Raphael, R. M., Kasper, F. K., & Mikos, A. G. (2010). Regulated non-viral gene delivery from coaxial electrospun fiber mesh scaffolds. Journal of Controlled Release, 143(1), 95-103.

Serafim, L. S., Lemos, P. C., Albuquerque, M. G. E., & Reis, M. A. M. (2008). Strategies for PHA production by mixed cultures and renewable waste materials. Applied Microbiology and Biotechnology, 81(4), 615-28.

Sharma, P. K., Fu, J., Cicek, N., Sparling, R., & Levin, D. B. (2012). Kinetics of medium-chain-length polyhydroxyalkanoate production by a novel isolate of *pseudomonas putida* LS46. Canadian Journal of Microbiology, 58(8), 982–989.

Singh, L., Kumar, V., & Ratner, B. D. (2004). Generation of porous microcellular 85/15 poly (DL-lactide-*co*-glycolide) foams for biomedical applications. Biomaterials, 25(13), 2611-7.

Singh, M., Kumar, P., Ray, S., & Kalia, V. C. (2015). Challenges and opportunities for customizing polyhydroxyalkanoates. Indian Journal of Microbiology, 55(3), 235–249.

Slepička, P., Stýblová, S., Kasálková, N. S., Rimpelová, S., & Švorčík, V. (2014). Cytocompatibility of polyhydroxybutyrate modified by plasma discharge. Polymer Engineering and Science, 54(6), 1231-1238.

Soboleva, A. G., Mezentsev, A., Zolotorenko, A., Bruskin, S., & Pirusian, E. (2014). Three-dimensional skin models of psoriasis. Cells Tissues Organs, 199(5-6), 301-10.

Sombatmankhong, K., Suwantong, O., Waleetorncheepsawat, S., & Supaphol, P. (2006). Electrospun fiber mats of poly(3-hydroxybutyrate), poly(3-hydroxybutyrate-co-3-hydroxyvalerate), and their blends. Journal of Polymer Science, Part B: Polymer Physics, 44(19), 2923 - 2933.

Steinbüchel, A., & Lütke-Eversloh, T. (2003). Metabolic engineering and pathway construction for biotechnological production of relevant polyhydroxyalkanoates in microorganisms.

Biochemical Engineering Journal, 16(2), 81–96.

Sudesh, K., Lee, Y.-F., Sridewi, N., & Ramanathan, S. (2016). The influence of electrospinning parameters and drug loading on polyhydroxyalkanoate (PHA) nanofibers for drug delivery. International Journal of Biotechnology for Wellness Industries, 4(4), 103–113.

Sun, J., Dai, Z., Zhao, Y., & Chen, G. Q. (2007). In vitro effect of oligo-hydroxyalkanoates on the growth of mouse fibroblast cell line L929. Biomaterials, 28(27), 3896-903.

Tai, H., Mather, M. L., Howard, D., Wang, W., White, L. J., Crowe, J. A., & Shakesheff, K. M. (2007). Control of pore size and structure of tissue engineering scaffolds produced by supercritical fluid processing. European Cells and Materials, 14, 64-77.

Tan, D.; Yin, J.; Chen, G.Q. (2017). Production of polyhydroxyalkanoates. In Current Developments in Biotechnology and Bioengineering, Production, Isolation and Purification of Industrial Products; Pandey, A., Negi, S., Soccol, C.R., Eds.; Elsevier: Amsterdam, The Netherlands; pp. 655–6.

Taylor, M. S., Daniels, A. U., Andriano, K. P., & Heller, J. (1994). Six bioabsorbable polymers: In vitro acute toxicity of accumulated degradation products. Journal of Applied Biomaterials, 5(2), 151-792.

Teare, D. O. H., Emmison, N., Ton-That, C., & Bradley, R. H. (2000). Cellular attachment to ultraviolet ozone modified polystyrene surfaces. Langmuir, 16(6), 2818–2824.

Teimouri, A.; Yeung, P.; Agu, R. (2018). 2D vs. 3D cell culture models for in vitro topical (dermatological) medication testing. In Cell Culture; Mehanna, R.A., Ed.; IntechOpen: London, UK; pp. 4–20

Terms, D. O. F. (2015). Chapter 1- Introduction. In Biopolymers: Processing and Products. Niaounakis. M.; Elsevier: Amsterdam, The Netherlands; pp. 1-77.

Tezcaner, A., Bugra, K., & Hasirci, V. (2003). Retinal pigment epithelium cell culture on surface modified poly(hydroxybutyrate-co-hydroxyvalerate) thin films. Biomaterials, 24(25), 4573–4583.

Tham, C. Y., Abdul Hamid, Z. A., Ahmad, Z., & Ismail, H. (2014). Surface modification of poly (lactic acid) (PLA) via alkaline hydrolysis degradation. Advanced Materials Research, 970, 324–327.

Tibbitt, M. W., & Anseth, K. S. (2009). Hydrogels as extracellular matrix mimics for 3D cell culture. Biotechnology and Bioengineering, 103(4):655-63.

Tobin, D. J. (2006). Biochemistry of human skin - Our brain on the outside. Chemical Society Reviews, 35(1), 52–67.

Topman, G., Shoham, N., Sharabani-Yosef, O., Lin, F. H., & Gefen, A. (2013). A new technique for studying directional cell migration in a hydrogel-based three-dimensional matrix for tissue engineering model systems. Micron, 51, 9-12.

van den Broek, L. J., Bergers, L. I. J. C., Reijnders, C. M. A., & Gibbs, S. (2017). Progress and future prospectives in skin-on-chip development with emphasis on the use of different cell types and technical challenges. Stem Cell Reviews and Reports, 13(3), 418–429.

Ventura, H., Laguna-Gutiérrez, E., Rodriguez-Perez, M. A., & Ardanuy, M. (2016). Effect of chain

extender and water-quenching on the properties of poly(3-hydroxybutyrate-co-4-hydroxybutyrate) foams for its production by extrusion foaming. European Polymer Journal, 85, 14–25.

Vlachopoulos, J., & Strutt, D. (2003). Polymer processing. Materials Science and Technology, 19(9), 1161–1169.

Walters, K. A. (2002). Dermatological and Transdermal Formulations; CRC Press: Boca Raton, FL, USA; pp. 436–438

Wang, C., Venditti, R. A., & Zhang, K. (2015). Tailor-made functional surfaces based on cellulose-derived materials. Applied Microbiology and Biotechnology, 99(14), 5791-9.

Ward, P. G., Roo, G. De, & Connor, K. E. O. (2005). Accumulation ofpPolyhydroxyalkanoate from styrene and phenylacetic acid by *Pseudomonas putida* CA-3, 71(4), 2046–2052.

Warren, H. S., Tompkins, R. G., Moldawer, L. L., Seok, J., Xu, W., Mindrinos, M. N., & Davis, R. W. (2015). Mice are not men. Proceedings of the National Academy of Sciences of the United States of America, 112(4), E345.

Wen, J., Yao, J., Chen, X., & Shao, Z. (2018). Silk fibroin acts as a self-emulsifier to prepare hierarchically porous silk fibroin scaffolds through emulsion-ice dual templates. ACS Omega, 3(3), 3396–3405.

Wu, X., & Wang, N. (2001). Synthesis, characterization, biodegradation, and drug delivery application of biodegradable lactic/glycolic acid polymers. Part II: biodegradation. Journal of Biomaterials Science, Polymer Edition, 32(4), 575–591.

Xia, Y., Zhou, P. Y., Cheng, X. S., Xie, Y., Liang, C., Li, C., & Xu, S. G. (2013). Selective laser sintering fabrication of nano-hydroxyapatite/poly-ε-caprolactone scaffolds for bone tissue engineering applications. International Journal of Nanomedicine, 8, 4197–4213.

Xu, C. Y., Inai, R., Kotaki, M., & Ramakrishna, S. (2004). Aligned biodegradable nanofibrous structure : a potential scaffold for blood vessel engineering, 25, 877–886.

Yan, C., Wang, Y., Shen, X. Y., Yang, G., Jian, J., Wang, H. S., & Wu, Q. (2011). MicroRNA regulation associated chondrogenesis of mouse MSCs grown on polyhydroxyalkanoates. Biomaterials, 32(27), 6435–6444.

Yun, H. S., Kim, D. Y., Chung, C. W., Kim, H. W., Yang, Y. K., & Rhee, Y. H. (2003). Characterization of a tacky poly(3-hydroxyalkanoate) produced by *Pseudomonas chlororaphis* HS21 from palm kernel oil. Journal of Microbiology and Biotechnology, 13(1), 64–69.

Zakaria, M. R., Ariffin, H., Abd-Aziz, S., Hassan, M. A., & Shirai, Y. (2013). Improved properties of poly(3-hydroxybutyrate- co -3-hydroxyvalerate) produced by *Comamonas sp*. EB172 utilizing volatile fatty acids by regulating the nitrogen source. BioMed Research International, vol. 2013, Article ID 237806, 7 pages.

Zhang, B., Korolj, A., Lai, B. F. L., & Radisic, M. (2018). Advances in organ-on-a-chip engineering. Nature Reviews Materials, 3(8), 257–278.

Zhang, D. ., Cui, F. ., Luo, Z. ., Lin, Y. ., Zhao, K., & Chen, G. . (2000). Wettability improvement of bacterial polyhydroxyalkanoates via ion implantation. Surface and Coatings Technology,

131 (1-3), 350-354.

Zhang, H., Obias, V., Gonyer, K., & Dennis, D. (1994). Production of polyhydroxyalkanoates in sucrose-utilizing recombinant *Escherichia coli* and *Klebsiella* strains. Applied and Environmental Microbiology, 60(4), 1198–1205.

Zhang, Q., Sito, L., Mao, M., He, J., Zhang, Y. S., & Zhao, X. (2018). Current advances in skin-on-a-chip models for drug testing. Microphysiological Systems, 1, 1–1.

Zhao, K., Deng, Y., Chen, J. C., & Chen, G. Q. (2003). Polyhydroxyalkanoate (PHA) scaffolds with good mechanical properties and biocompatibility. Biomaterials, 24(6), 1041–1045.

Zhu, X., Zhong, T., Huang, R., & Wan, A. (2015). Preparation of hydrophilic poly(lactic acid) tissue engineering scaffold via (PLA)-(PLA-b-PEG)-(PEG) solution casting and thermal-induced surface structural transformation. Journal of Biomaterials Science, Polymer Edition, 26(17), 1286–1296.

Zubairi, S. I. (2015). Porous three dimensional (3-D) scaffolds of poly (3-hydroxybutyric acid) (PHB) and poly (3- hydroxybutyric-*co*-3-hydroxyvaleric acid) (PHBV): Determination of salt leaching efficiency. Advances in Environmental Biology, 10, 925–932.

Zubairi, S. I., Mantalaris, A., Bismarck, A., & Aizad, S. (2016). Polyhydroxyalkanoates (PHAs) for tissue engineering applications: Biotransformation of palm oil mill effluent (POME) to value-added polymers. Jurnal Teknologi, 78(1), 13-29.

Appendices

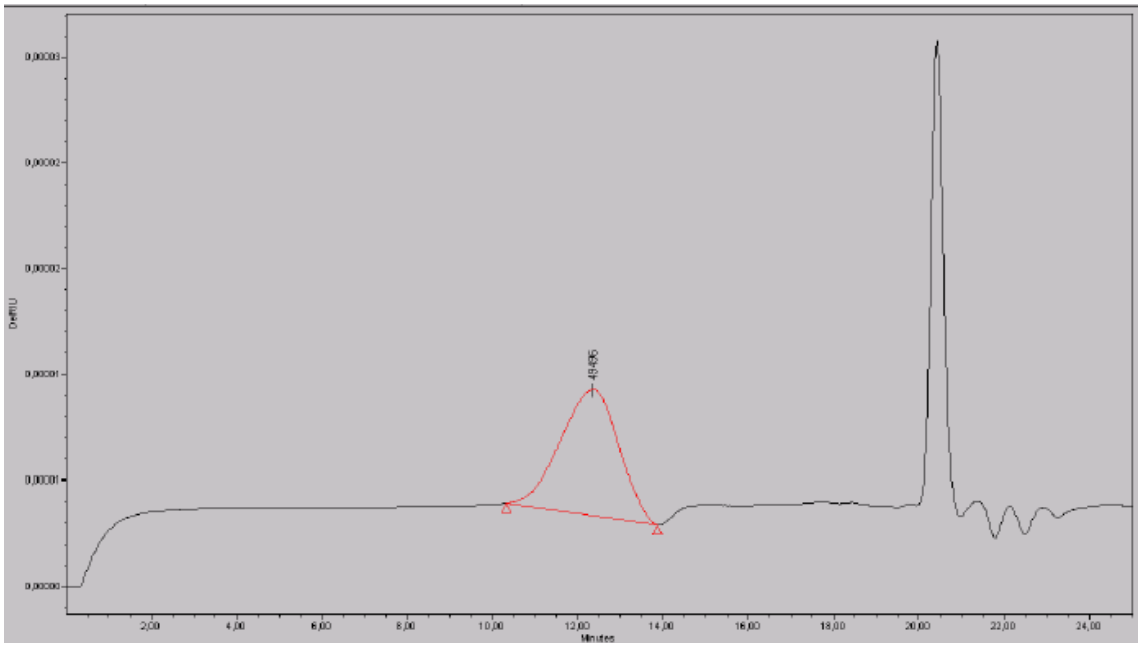

Figure A- Size exclusion chromatograms (SEC) of the mcl-PHA polymer produced by *P. chlororaphis* from glycerol.

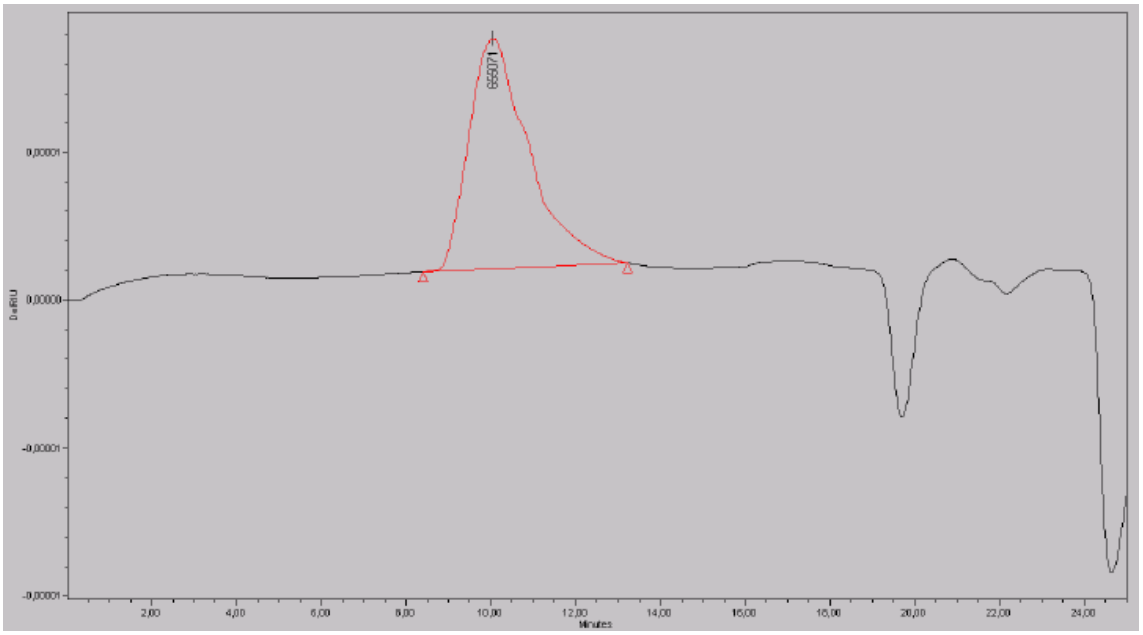

Figure B- Size exclusion chromatograms (SEC) of the P(3HB) polymer produced by *C. necator* from used cooking oil.

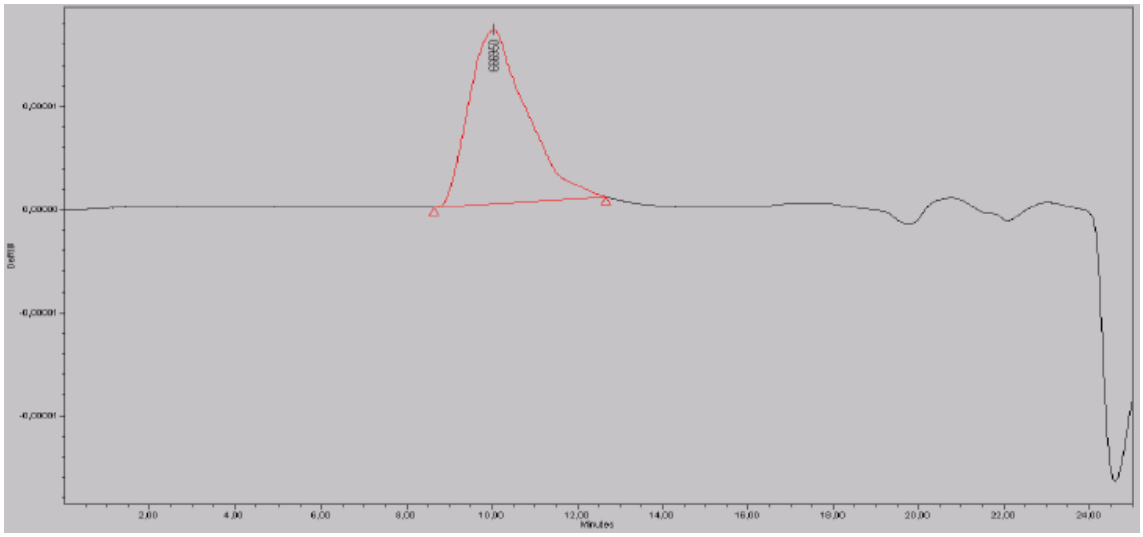

Figure C- Size exclusion chromatograms (SEC) of the P(HBHV) polymer produced by *C. necator* from used cooking oil and levulinic acid.

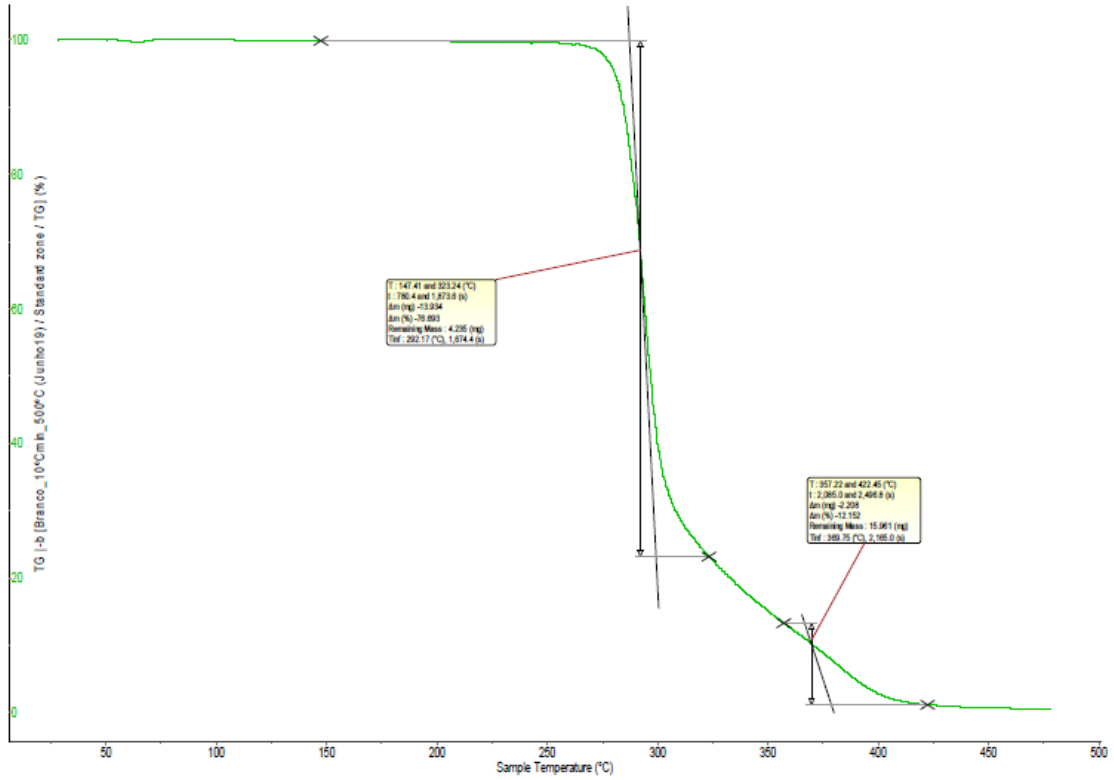

Figure D- Thermogravimetric curve of the mcl-PHA polymer produced by *P. chlororaphis* from glycerol.

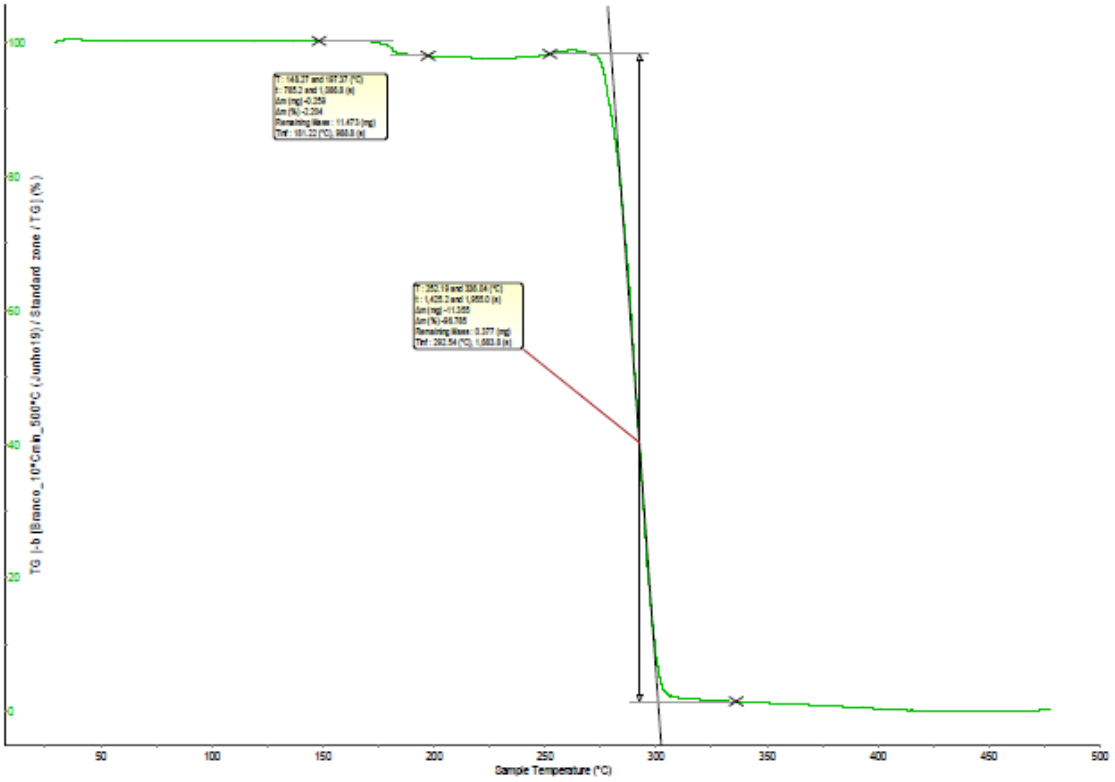

Figure E- Thermogravimetric curve of the P(3HB) polymer produced by *C.necator* from used cooking oil.

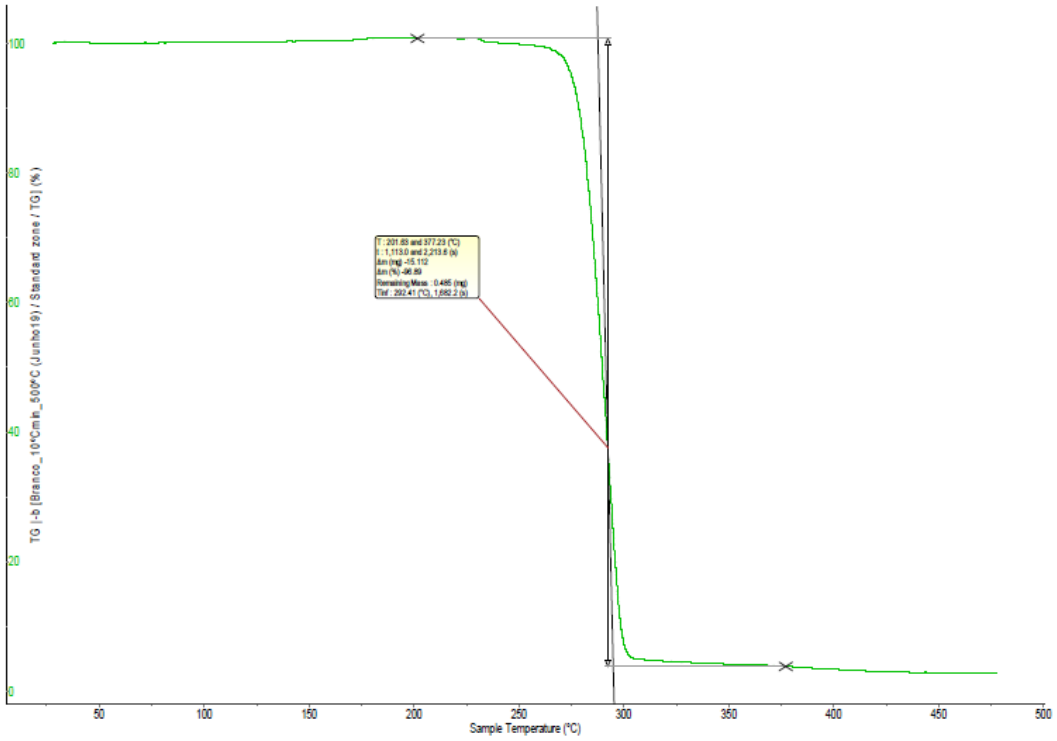

Figure F- Thermogravimetric curve of the P(HBHV) polymer produced by *C.necator* from used cooking oil and levulinic acid.

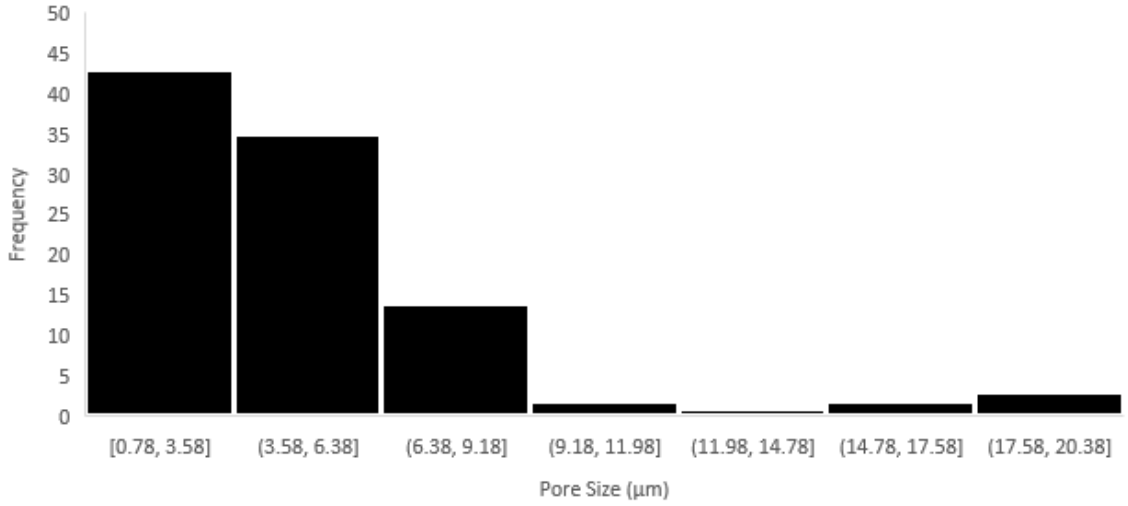

Figure G- Size distribution of pores from P(3HB) emulsion templated scaffolds.

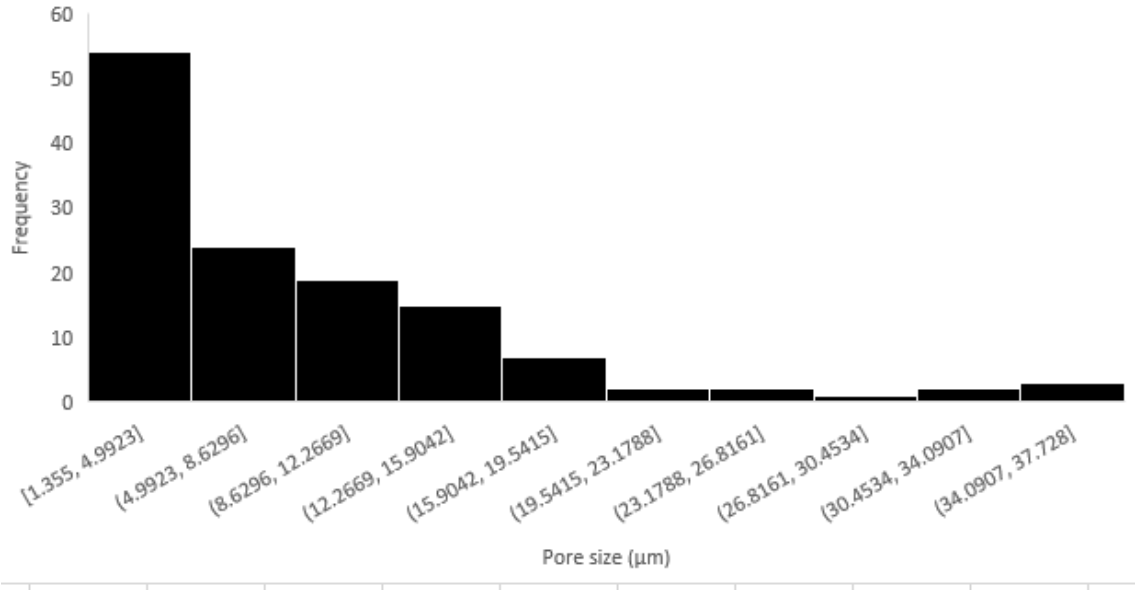

Figure H- Size distribution of pores from P(HBHV) emulsion templated scaffolds.